

Interfacial properties of water-in-water emulsions and their effect on dynamical behavior

Elke Scholten

Promotor: Prof. dr. E. van der Linden
Hoogleraar in de fysica en fysische chemie van
levensmiddelen, Wageningen Universiteit

Co-promotor: dr. ir. L.M.C. Sagis
Universitair docent bij de leerstoelgroep fysica en fysische
chemie van levensmiddelen, Wageningen Universiteit

Promotiecommissie:	Prof. dr. ir. P. van Puyvelde	(Universiteit Leuven, België)
	Prof. dr. ir. R. M. Boom	(Universiteit Wageningen)
	dr. ir. E. M. Blokhuis	(Universiteit Leiden)
	dr. P. Fischer	(Institute of Food Science and Nutrition, Zurich, Zwitserland)

Interfacial properties of water-in-water emulsions and their effect on dynamical behavior

Elke Scholten

Proefschrift
ter verkrijging van de graad van doctor
op gezag van de rector magnificus
van Wageningen Universiteit
Prof. dr. M. J. Kropff
in het openbaar te verdedigen
op vrijdag 3 maart 2006
des namiddags te vier uur in de Aula

Interfacial properties of water-in-water emulsions and their effect on dynamical
behavior

ISBN: 90-8504-366-2

Elke Scholten (2006)

Interfacial properties of water-in-water emulsions and their effect on
dynamical behavior

PhD Thesis, Wageningen University, The Netherlands

Keywords: biopolymer mixtures, water-in-water emulsions, phase separation, interfaces, interfacial tension, bending rigidity, permeability, droplet deformation, morphology.

Abstract

The objective of this work was to investigate interfacial properties of biopolymer-based water-in-water emulsions, and to determine the effect of these interfacial properties on the kinetics of phase separation and the deformation behavior of emulsions droplets in shear flow. Since the experimental determination of interfacial properties, such as interfacial thickness and bending rigidity is difficult, we have developed a model that determines these parameters from the experimentally accessible interfacial tension and the interaction potential of the dissolved biopolymers. From the results we could conclude that the thickness of these water/water interfaces is much larger than for oil/water interfaces. The bending rigidities for these interfaces were found to be very large compared to those of water/oil interfaces. The permeability of these interfaces was tested with the spinning drop and the droplet relaxation method. These water/water interfaces were found to be permeable to all ingredients in the system at long time scales (spinning drop experiments) and permeable to water for short time scales (droplet relaxation after cessation of a flow field). This permeability was incorporated into the description of the droplet relaxation time, from which the interfacial tension and the permeability can be deduced simultaneously. Due to the permeability, both the spinning drop method and the droplet relaxation method (without contribution of permeability) cannot be used to measure the interfacial tension accurately. Furthermore, both bending rigidity and permeability were incorporated into the description of coarsening of bicontinuous structures during phase separation. We found four different regimes for coarsening depending on whether the process is dominated by interfacial tension, bending rigidity or permeability.

Interfacial properties of water-in-water emulsions and their effect on dynamical behavior

Table of contents

Table of contents

1 Introduction	2
1.1 General introduction	2
1.2 Biopolymers	3
1.2.1 Gelatin	3
1.2.2 Dextran	4
1.2.3 Gum arabic	4
1.2.4 Biopolymers in solution	4
1.3 Phase separation	5
1.4 Interfaces	6
1.4.1 Interfacial energy	7
1.4.2 Interfacial parameters	8
1.5 Near-critical behavior	9
1.6 Structure	9
1.7 Permeability	12
1.8 Focus of thesis	12
2 Ultralow interfacial tensions in an aqueous phase-separated gelatin/dextran and gelatin/gum arabic system: A comparison	17
2.1 Introduction	18
2.2 Experimental section	20
2.2.1 Materials	20
2.2.2 Methods	21
2.2.2.1 Preparation of the protein/polysaccharide mixtures	21
2.2.2.2 Determination of the radius of biopolymers	21
2.2.2.3 Construction of phase diagram	22
2.2.2.4 Interfacial tension measurements	22
2.2.2.5 Density measurements	23
2.3 Results and discussion	24
2.3.1 Phase behavior of gelatin/dextran and gelatin/gum arabic mixtures	24

2.3.2 Determination of the radius of gyration	26
2.3.3 Interfacial tension	27
2.3.4 Distribution of molecules	31
2.4 Conclusion	33
 3 Bending rigidity of interfaces in aqueous phase-separated biopolymer mixtures	 39
3.1 Introduction	40
3.2 Theory	41
3.3 Materials	45
3.4 Results and discussion	47
3.4.1 Interfacial thickness, scaling behavior	49
3.4.2 Bending rigidity, scaling behavior	52
3.4.3 Influence of bending rigidity	54
3.5 Conclusion	55
 4 Coarsening rates of bicontinuous structures in polymer mixtures	 61
4.1 Introduction	62
4.1.1 Phase separation	63
4.1.2 Coarsening of domains	63
4.1.3 Coarsening mechanisms	65
4.2 Comparison with experimental data	66
4.3 Contribution of bending rigidity to hydrodynamic flow	67
4.4 Conclusion	70
 5 Effect of permeability on aqueous biopolymer interfaces in spinning drop experiments	 75
5.1 Introduction	76
5.2 Experimental section	78
5.2.1 Materials	78
5.2.2 Methods	78
5.2.2.1 Preparation of the biopolymer mixtures	78

5.2.2.2 Determination of the concentration of biopolymers in both phases	79
5.2.2.3 Determination of the densities of both phases	79
5.2.2.4 Spinning drop experiments	79
5.3 Results and discussion	80
5.3.1 Phase diagram and coexisting phases	80
5.3.2 Densities of the phases	81
5.3.3 Spinning drop experiments	81
5.3.3.1 Droplet volume measurements	82
5.3.3.2 Interfacial tension measurements	89
5.4 Conclusion	91
 6 Effect of interfacial permeability on droplet relaxation in biopolymer-based water-in-water emulsions	 95
6.1 Introduction	96
6.2 Experimental section	97
6.2.1 Materials and methods	97
6.2.1.1 Preparation of the biopolymer mixtures	97
6.2.1.2 Determination of concentration of biopolymers in both phases	98
6.2.1.3 Determination of viscosity of both coexisting phases	98
6.2.1.4 Relaxation experiments	99
6.3 Results and discussion	100
6.3.1 Phase behavior and distribution of biopolymers	100
6.3.2 Phase behavior and viscosities of separated phases	102
6.3.3 Relaxation behavior	102
6.4 Conclusion	116
 7 Discussion	 120
7.1 Biopolymer mixtures in daily life	120
7.1.1 Relevance of interfacial properties	120
7.2 Permeability	121

7.3 Bending rigidity	123
7.4 Effect of interfacial permeability and bending rigidity on kinetics of phase separation	124
7.5 Conclusion	129
Summary	134
Samenvatting	137
Dankwoord	142
List of publications	144
Curriculum Vitae	146
Educational part	147

Chapter 1

Chapter 1

Introduction

1.1 General introduction

In the food industry, a variety of ingredients, such as water, oils, biopolymers, and flavors are mixed together to create a wide range of products; examples are ice-cream, desserts, sweets, dressings, spreads, and low-calorie fat-free products.^{1,2} In these products you can find mixtures of biopolymers. The phase behavior of these mixtures is frequently used to create various structures that determine the food properties, such as stability, shelf life, texture, flavor and sensorial perception. By changing the concentration of the ingredients one can alter the interactions in the system, and subsequently the structure and the properties of the food products.

In this thesis we focus on aqueous biopolymer mixtures. At high concentrations of biopolymers (around 10%), depletion interactions are induced and the system will phase separate into two separate phases. One phase is enriched in one biopolymer, the other phase is enriched in the other biopolymer. Since the system consists of two liquids (aqueous biopolymer solutions) that are immiscible upon mixing, these systems are also known as water-in-water emulsions. Upon mixing, one phase will be dispersed as droplets (dispersed phase) in the other phase (continuous phase). Since their properties are comparable to normal oil/water emulsions, these mixtures are used in the food industry to create zero-fat products. By tuning the properties of both phases in terms of viscosity, gel strength, etc, one can control the properties of the food product. Hence, the properties of fat-containing products, such as creaminess, can be mimicked with the use of water-in-water emulsions. Using ingredients that have gelling properties, the emulsion droplets can be gelled, and the system will have solid-like or gel-like properties. Upon consuming, the temperature raise might decrease the gel strength of the droplets, and will change the sensorial perception of the system, such as mouth feel. In the gelled state of the emulsion droplets, ingredients such as flavor molecules might be enclosed. These compounds can be released after melting of the emulsion droplets. Using these droplets as delivery vehicles, one can control the flavor release in for example desserts, ice-cream and zero-fat spreads.

To be able to control the properties of these systems, the shape and the size of the dispersed phase play an important role, as well as the structures of that phase (droplet morphology, bicontinuous morphology). During the production of food products,

these systems are often subjected to a shear flow, which changes the size and the shape of the emulsion droplets and hence the morphologies of the system. The shape and size of these droplets are determined by the properties of the interface. In general, it is assumed that interfacial tension only is important to describe the evolution of these systems under shear. Other interfacial properties such as interfacial permeability and bending rigidity have not been addressed until now for these water-in-water emulsions.

This thesis will focus on several interfacial properties, such as interfacial tension, interfacial permeability and bending rigidity in order to gain insight in the interfaces of these biopolymer mixtures. Food products are often produced under the influence of a shear flow and the phase separation process is used in order to control the morphologies and the size of the dispersed droplets. Therefore, we will relate these interfacial properties to the kinetics of phase separation and the deformation behavior of emulsion droplets in shear flow.

1.2 Biopolymers

Looking at the ingredients list of food products, especially dairy products, reveals items such as polysaccharides and proteins, which are known as biopolymers. Polysaccharides and proteins are often added to food products as thickening agents, whose functionality relies on the viscosity enhancement, gel formation and water binding-ability. They improve the product texture and give body to liquid systems. In this thesis, the protein gelatin and the polysaccharides dextran and gum arabic have been used.

1.2.1 Gelatin

The protein gelatin is frequently used in products such as low-calorie reduced-fat products, desserts, soups and sauces. Two types of gelatin can be distinguished; fish gelatin and mammalian gelatin. The basic difference between the two types originates in a different chemical structure or configuration, which determines the gelation temperature. The gelation temperature of mammalian gelatin is approximately 30°C,

indicating that at room temperature this type is able to form a gel. The gelation temperature of fish gelatin is about 5°C, much lower than that of mammalian gelatin.

1.2.2 Dextran

The polysaccharide dextran is used in different types of food applications, such as ice-creams, candies and low-calorie, sugar-free beverages.³ Dextran can be formed from a sucrose solution containing the dextran-producing bacteria belonging to the *Leuconostoc* genus. Dextran is composed of α -D-glucopyranose monomeric units, interconnected through (1 → 6) and (1 → 3) linkages. The ratio of linkages determines the structure of the dextran in terms of degree of branching.

1.2.3 Gum Arabic

The polysaccharide gum arabic can be found in food products such as dry mix foods and soft drinks.⁴ Gum arabic is produced by the Acacia tree and is composed of β -1,3 and 1,6 linked D-galactopyranose monomeric units, which are connected to a common protein core.

1.2.4 Biopolymers in solution

All three biopolymers are regarded as random coils in solution with a specific radius, R . At low concentrations, the coils will be present as individual particles surrounded by the solvent (Figure 1.1A). This regime is known as the dilute regime. If more biopolymer particles are added to the solution, the particle density will increase and the particles will start to overlap (Figure 1.1B). This concentration is called the overlap concentration, c^* .⁵ Above the overlap concentration, the biopolymers will intersect, forming a network (Figure 1.1C). A solution with a concentration above the overlap concentration is called a semi-dilute solution. In this regime, the radius of gyration is no longer the most important length scale but the blob size of the network, ζ . As the overlap concentration is very low for the biopolymers described in this thesis, a network solution or semi-dilute solution is often present in food products containing these biopolymers.

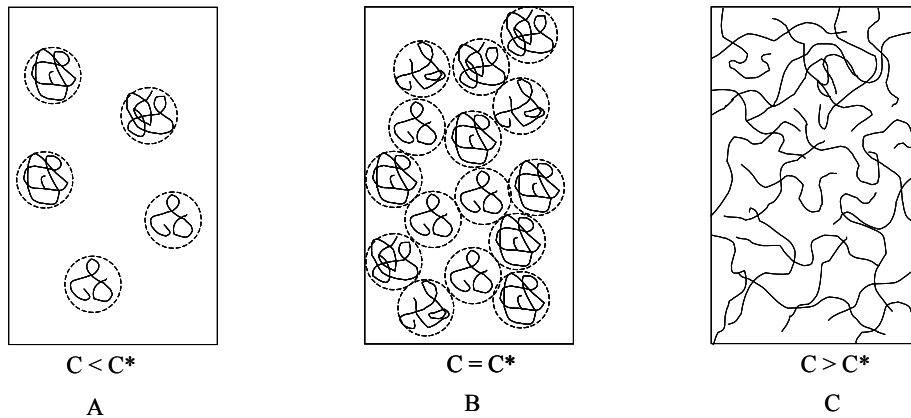


Figure 1.1 Conformation of biopolymers in solution. A) dilute regime. B) overlap concentration. C) semi-dilute regime.

1.3 Phase separation

When two different biopolymers, for example proteins and polysaccharides, are mixed in an aqueous environment at low concentrations, a homogeneous solution is formed, and the proteins and polysaccharides are distributed randomly. However, when these biopolymers are mixed at high concentrations, depletion interactions are present and the mixture often phase separates into two distinct phases, separated by a clear interface.⁶⁻¹⁰ One phase is rich in protein and poor in polysaccharide, while the other phase is concentrated in polysaccharide and depleted in protein. The two phases have their own bulk properties, such as concentration, viscosity etc. The phenomenon of phase separation can be illustrated by using a phase diagram.¹¹ For aqueous biopolymer systems, a two-dimensional phase diagram is often used, which shows both the miscible and the immiscible region. Figure 1.2 shows such a phase diagram.

On the axes, the concentrations of both biopolymers are plotted. The solid line shows the binodal. Below the binodal is the one-phase region; any overall concentration (point A) in this area will yield a miscible one-phase system. Above the binodal is the two-phase region; any overall concentration in that area, for example point B, will phase separate into a phase 1 and a phase 2. The line that connects these two phases is called a tie-line which goes through the overall concentration. Taking

the mid-points of the tie-lines and extrapolating through the binodal gives the critical point, denoted by the star.

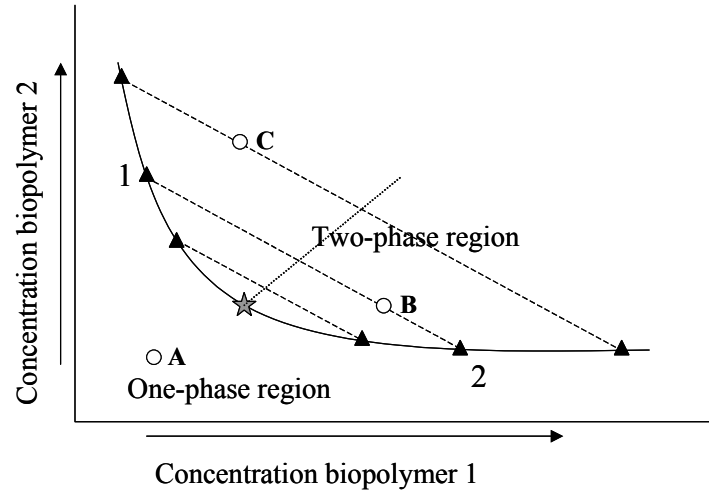


Figure 1.2 Phase diagram of a biopolymer mixture. The solid line is the binodal. The dashed line is the tie-line, which connects the two coexisting phases, denoted by the triangles. The dotted line represents the line going through the midpoints and the critical point, which is denoted by the star.

1.4 Interfaces

The interfaces formed as a result of the phase separation of biopolymers appear to be very sharp when observed by eye. Although they are very sharp at this macroscopic level, they are not always sharp at the mesoscopic level. The reason we observe an interface is because there is a difference in optical properties between the two phases. This optical property is a result of the difference in concentration of biopolymers in both phases. Figure 1.3 shows an impression of the distribution of both biopolymers. Biopolymer 1 (black line) is concentrated in the lower phase, while depleted in the upper phase, while biopolymer 2 (gray line) is concentrated in the upper phase and depleted in the lower phase. The region, in which the concentration changes from one bulk phase to the other, is known as the interfacial region. The thickness of this region, the interfacial thickness, ξ , depends on this concentration profile.

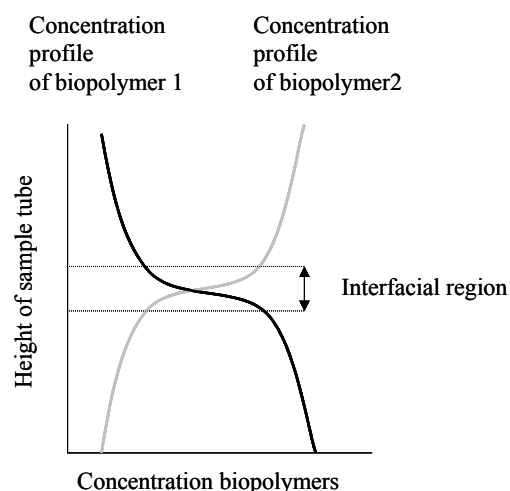


Figure 1.3 Concentration profile across the interface. The black line represents the concentration profile of biopolymer 1 and the gray line represents biopolymer 2.

In many gas-liquid, liquid-liquid or solid-liquid interfaces, this interfacial region is normally of the size of the particles, so on a mesoscopic level the interface is still very sharp. However, in the case of aqueous biopolymer mixtures, the thickness of the interfacial region is much wider (as described in chapter 3). This large interfacial region has an effect on the bending properties of the interface, and therefore influences the size and the shape of the emulsion droplets. This large interfacial thickness might therefore have an effect on both the phase separation process and formation of morphologies under shear flow.

1.4.1 Interfacial energy

When a system phase separates, the proteins and polysaccharides are not randomly distributed anymore, but are concentrated in either one of the phases. The molecules are mostly surrounded by like molecules and just a few dissimilar molecules. The molecules benefit from interactions with all its similar neighbors and find themselves in a favorable energy state. Molecules at the interface lose half their cohesive interactions and are in an unfavorable energy state. The interfacial tension, γ , is a

measure of this difference in energy, and is expressed in a force per length as N/m (or energy per surface area).¹²

When distorting an interface to create more surface area, molecules must be brought to the interface. Since they lose their favorable energy, energy needs to be provided in order to compensate this loss. Therefore, it will cost energy to create more surface/interface, and hence the system will always try to minimize its interfacial area. This is for example the reason why water droplets and soap bubbles are spherical. A spherical shape is the shape that has the least amount of area for a specific volume.

1.4.2 Interfacial parameters

The interfacial tension is related to the energy you need to deform a certain area of interface. However, the interfacial tension accounts only for the deformation in the tangential direction, the energy you need to stretch it. The energy that is related to the deformation in the perpendicular direction is what we call the bending energy. Helfrich¹³ showed already in 1973 to what extent these two parameters are related and proposed the following equation

$$\gamma(R) = \gamma_0 + \frac{2k}{R^2} \quad (1.1)$$

in which γ_0 is the interfacial tension of a flat interface, and k is the bending rigidity. $\gamma(R)$ is known as the curvature-dependent interfacial tension, which contains a stretching contribution and a bending contribution. Since the last term is curvature dependent, the total energy to deform a certain area is dependent on the curvature of the interface. For large curvature (small R), the bending contribution will be large, while for small curvature (large R) the bending contribution will be small. Thus, the formation of smaller droplets will cost more energy than the formation of larger droplets.

During phase separation, various sizes and shapes of droplets are present in the system, and different curvatures can be found. Therefore, the bending contributions to the interfacial energy may be of relevance in the phase separation process, depending on the ratio between the interfacial tension and the bending rigidity.

1.5 Near-critical behavior

As mentioned before, in a biopolymer system, there exists a point on the binodal that is called the critical point. Approaching the critical point from the two-phase region, the interfacial tension decreases to zero and the interfacial region, ξ , diverges. So, for samples close to a critical point, the interfacial region can be very large, which is also known as a diffuse interface. Depending on the system, you can define a near-critical regime, in which the interfaces are considered to be diffuse, i.e., have a large interfacial thickness. These systems show a universal scaling behavior,¹⁴⁻¹⁶ which describes the relation between different parameters of the system, such as interfacial tension, interfacial thickness, concentration, density, and pressure. For biopolymer mixtures, the interfacial tension, γ , is often related to the distance to the critical point. The distance to the critical point can either be given as the density difference between the two phases, $\Delta\rho$, or as the difference in concentration, Δc . The scaling relations can be given as

$$\gamma \propto \Delta\rho^{\mu/\beta} \quad (1.2)$$

$$\gamma \propto \Delta c^\mu \quad (1.3)$$

where μ and β are called the critical exponents, which have different values depending on the theory used for their calculation. Mean field theories predict values for μ and μ/β of 1.5 and 3 respectively, while the Ising model predicts values of 1.3 and 3.9, respectively. Systems that show these critical exponents can be considered to be near-critical. Systems that do not show these exponents are considered to be off-critical.

1.6 Structure

During the production of food products, biopolymer mixtures are often mixed vigorously or subjected to a shear flow. During this process, the emulsion droplets will break up into smaller droplets. The size and the shape of the droplets determine amongst others, the properties of the food product, such as the creaminess in mayonnaise, the white color in milk, and the spreading ability in margarines. The

phase separation process can be used to tune the size of the droplets. When the process starts, the sizes of the droplets in the systems are very small. Since the formation of interfacial area costs energy, the system will try to reduce its interfacial area by merging of the droplets. As soon as the droplets touch, they will merge together into bigger droplets. These droplets will meet other (bigger) droplets, and will merge again to form even bigger droplets, as depicted in Figure 1.4. Without the presence of a flow field, all dispersed droplets present will merge, which leads again to two macroscopically large phases. So, depending on the time the phase separation process has progressed, the size of the droplets changes.

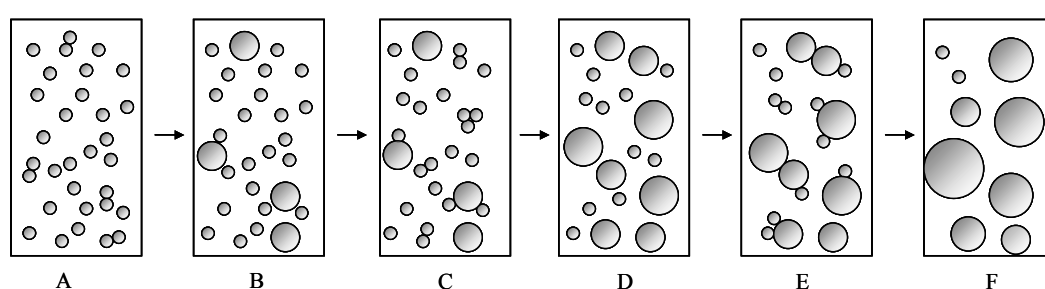


Figure 1.4 Length scale evolution in time. The small dispersed droplets (A) will merge as soon as they come into contact with another droplet (B). The newly formed droplets will move throughout the solution and will meet other droplets (C), which will merge again to even bigger droplets (D). The process of moving (E) and merging (F) is repeated till one big droplet/phase is formed.

When either the dispersed phase (the emulsion droplets) or the continuous phase contains a biopolymer that has gelling properties, one could “freeze” a specific size of the droplets at a specific time during the phase separation process. Hence, the properties of the food product (creaminess etc.) can be tuned in order to control sensorial perception (mouth feel). Since the properties of the food are influenced to a large extent by the morphologies and the size of the dispersed droplets, control over the phase separation process is essential in order to control the properties of the food product.

Since the sizes during the separation process change in time, the curvatures of the structures also change in time. Therefore, the sizes and the morphologies during the

phase separation process are influenced by the bending rigidity of the system. To be able to control the morphologies and the size of the droplets of the system, the bending rigidity has to be taken into account.

When this phase separation process is allowed to take place under the influence of shear, the shape of the droplets can also be altered. Due to the shear flow, bigger droplets will be broken up into smaller ones¹⁷ and therefore a better control of the size is possible. Depending on the shear flow that is used, the degree of deformation into an ellipsoidal shape will be different as well as the size of the droplets. The larger the shear flow, the larger is the ellipsoidal deformation, as depicted in Figure 1.5, but also the smaller are the droplets. When using a very viscous or gelling dispersed phase (the droplets), one could elongate these droplets to such an extent that fibrillar structures can be made. Once gelled, these long elongated structures are able to form a network.^{18,19} The properties of these networks can be very different than the properties in a system of separate droplets.

During the deformation of the droplets, the curvatures of the interface will change. Therefore, the bending rigidity might become important in the deformation behavior.

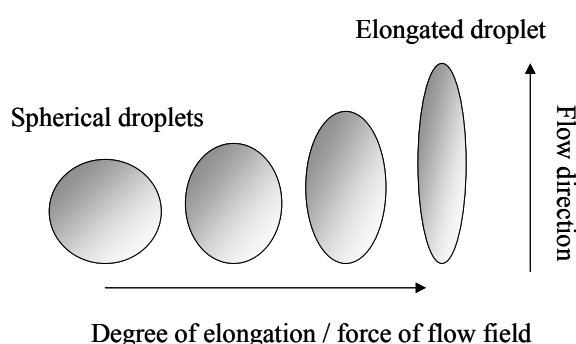


Figure 1.5 Degree of elongation of a dispersed droplet. The droplets will elongate in the direction of the flow field. The stronger the flow force, the larger is the degree of elongation.

1.7 Permeability

The deformation of the droplets is due to an external force field that is exerted on the droplet, which induces a pressure difference across the interface that deviates from its value at equilibrium. The main component in both phases of these aqueous biopolymer mixtures is water. Since water does not favor one of the phases, water could easily diffuse through the interface to the other bulk phase if a pressure gradient is present. When interfaces are permeable to certain ingredients, this will have a large effect on phenomena where pressure gradients play a role, such as the phase separation process and droplet deformation under shear flow. In this thesis we focus on the interfacial permeability of these aqueous biopolymer interfaces, relate this permeability to diffusion coefficients of the ingredients, and discuss its relevance in certain interfacial-related phenomena.

1.8 Focus of thesis

This thesis focuses on the interfacial properties of phase-separated biopolymer mixtures, known as water-in-water emulsions. The first part of this thesis is devoted to the interfacial properties of gelatin/dextran and gelatin/gum arabic systems, such as the interfacial tension, bending rigidity and interfacial thickness. Chapter 2 describes the phase separation of both biopolymer mixtures, and focuses on the measurement of interfacial tension that arises as a result of the formation of the interface. The interfacial tension is related to the distance from the critical point and used to determine the regime of phase separation: near-critical or off-critical. In chapter 3, a model is proposed to determine the bending rigidity and the interfacial thickness of the interface. This model uses the interactions between the biopolymers in both phases, and the concentration profile of the biopolymers. Using the experimentally accessible interfacial tension (determined in chapter 2), the remaining interfacial properties (bending rigidity and interfacial thickness) were calculated. These interfacial properties are determined for both systems and are related to the regime of phase separation described in chapter 2. The second part of the thesis describes the relation between the interfacial properties and physical phenomena that play a role in the food fabrication process, such as the phase separation process and deformation of droplets in a flow field. Chapter 4 describes the phase separation process and the

structure evolution in time. The change in length scales during the structural evolution is related to the interfacial properties. We derive a new coarsening mechanism, in which we have taken into account the bending rigidity for these systems. From the results we see that taking this bending rigidity into account, different regimes for the kinetics in phase separation can be found. The length scales for which the different regimes play a role are of practical relevance in the phase separation process.²⁰ Chapter 5 and 6 describe the effect of force fields on dispersed droplet, and discuss the effects of interfacial permeability in these systems. Chapter 5 describes the effect of a rotational force field on a single gelatin-concentrated droplet in a matrix of the dextran-concentrated phase. The shape and size of this droplet were followed in time and from these results we could conclude that the interfaces are permeable to all ingredients in the system. In chapter 6 we investigated the effect of permeability in the deformation behavior of droplets under the influence of a shear flow. From the relaxation behavior of droplets after the cessation of a shear flow, we concluded that the interfaces are permeable to the water molecules only. We included this permeability into the full description of the relaxation time of droplets. In chapter 7 we give a general discussion in which all interfacial properties, such as interfacial tension, interfacial permeability and bending rigidity are discussed. All interfacial properties are shown to influence the phase separation process and the length scales for which each property is important are discussed.

Understanding these interfacial properties and the relation with interfacial-related phenomena such as the phase separation process and the relaxation behavior of deformed droplets, contributes to a better understanding of the important parameters during processing of water-in-water emulsions. Since the relevance of the different parameters change as a function of length scale, the results of this thesis will help to distinguish between important and less important interfacial properties at different length scales. Taking into account all these interfacial properties, a better control of the structures is possible, and might lead to the development of novel food products.

References

- (1) Bot, A.; Mellema, M. and Reiffers-Magnani, C. K. *Industrial Proteins* **2003**, *11*, 11-13.
- (2) Goff, H. D. *Int. Dairy J.* **1997**, *7*, 363-373.
- (3) Glicksman, M. *Food Hydrocolloids*; CRC Press: New York, 1982.
- (4) Menzies, A. R.; Osman, M. E.; Malik, A. A. and Baldwin, T. C. *Food Add. Contam.* **1996**, *13*, 991-999.
- (5) de Gennes, P. G. *Scaling Concepts in Polymer Physics*; Cornell University Press: New York, 1979.
- (6) Norton, I. T. and Frith, W. J. *Food Hydrocolloids* **2001**, *15*, 543-553.
- (7) Tolstoguzov, V. B. *Food Hydrocolloids* **1991**, *4*, 429-468.
- (8) Grinberg, V. Y. and Tolstoguzov, V. B. *Food Hydrocolloids* **1997**, *11*, 145-158.
- (9) Tolstoguzov, V. *Nahrung* **2000**, *44*, 299-308.
- (10) Doublier, J. L.; Garnier, C.; Renard, D. and Sanchez, C. *Curr. Opin. Colloid Interface Sci.* **2000**, *5*, 202-214.
- (11) Albertsson, P. A. *Partition of Cell Particles and Macromolecules*; second edition, John Wiley & Sons Inc.: Stockholm, 1971.
- (12) de Gennes, P. G.; Brochard-Wyart, F. and Quere, D. *Capillarity and Wetting Phenomena*; Springer-Verlag: New York, 2002.
- (13) Helfrich, W. *Z. Naturforsch.* **1973**, *28c*, 693.
- (14) Widom, B. *J. Chem. Phys.* **1996**, *100*, 13190-13199.
- (15) Widom, B. *Chem. Soc. Rev.* **1985**, *14*, 121-140.
- (16) Rowlinson, J. S. and Widom, B. *Molecular Theory of Capillarity*; Clarendon Press: Oxford, 1984.
- (17) Clift, R.; Grace, J. R. and Weber, M. E. *Bubbles, Drops and Particles*; Academic Press: New York, 1978.
- (18) Wolf, B. and Frith, W. J. *J. Rheol.* **2003**, *47*, 1151-1170.
- (19) Wolf, B.; Scirocco, R.; Frith, W. J. and Norton, I. T. *Food Hydrocolloids* **2000**, *14*, 217-225.
- (20) Lorén, N.; Altskär, A. and Hermansson, A.-M. *Macromolecules* **2001**, *34*, 8117-8128.

Chapter 2

Ultralow interfacial tensions in an aqueous phase-separated gelatin/dextran and gelatin/gum arabic system: A comparison

Ultralow interfacial tensions in an aqueous phase-separated gelatin/dextran and gelatin/gum arabic system: A comparison

Abstract

Many protein/polysaccharide mixtures phase separate when the concentrations of these biopolymers are sufficiently high. One of the properties involved in this phenomenon is the interfacial tension. We present measurements of the interfacial tension of two different protein/polysaccharide mixtures. The protein gelatin was mixed with either dextran or gum arabic, all used in a variety of food products. The phase diagrams were constructed using optical rotation. Although both polysaccharides have the same molecular weight, the phase diagrams differed. The interfacial tension of samples, varying in the distance from the critical point, was determined using the spinning drop method. The interfacial tension was found to be in the range of $1\text{--}15\ \mu\text{N}/\text{m}$. For both systems, the scaling behavior of the interfacial tension was investigated. The investigated gelatin/dextran system gave critical exponents of 2.5 ± 0.1 and 1.4 ± 0.1 , in reasonable agreement with the mean-field values 3 and 1.5 respectively. The gelatin/gum arabic system did not show near-critical behavior. For this system, the interfacial tension shows a logarithmic dependence on the distribution of the gelatin and the gum arabic molecules in the separated phases.

2.1 Introduction

Phase separation in polymer and biopolymer systems is a well-known phenomenon, which has been studied extensively.¹⁻⁵ Phase separation results in two distinct phases, each enriched in either one of the polymers and depleted in the other. A clear interface is formed between the two phases, which has its own specific characteristics, such as interfacial tension. Phase separation occurs only when the driving force for decomposition overcomes the accompanying increase in interfacial free energy, which equals the product of interfacial tension and the interfacial area created by the separation. Therefore, interfacial tension is of fundamental interest. Phase separation of biopolymers can also occur under the influence of shear, and the interfacial tension affects the resulting morphologies and structures of the phase-separated system.⁶ Besides being of fundamental interest, interfacial tension is also of practical interest since, for optimal continuous polymer fractionation, it is necessary to know how the interfacial tension varies with the distance to the critical point.⁷

The order of magnitude of the interfacial tension in phase-separated colloidal systems can be estimated from the scaling relation $\gamma \propto (kT / \xi^2)$,^{8,9} where γ is the interfacial tension and ξ is the width of the interfacial region, that is, the region where material properties differ from their bulk values in the coexisting phases. Assuming that the width of the interfacial region is of the order of the size of the polymer (10-100 nm) the corresponding interfacial tension is expected to be of the order of 1-100 $\mu\text{N}/\text{m}$, which is indeed found for a large variety of ternary mixtures. This interfacial tension depends on the degree of phase separation and the distance from the critical point, where the interfacial tension vanishes.

For near-critical conditions, the interfacial tension as a function of $\Delta\rho$ and Δc is given by $\gamma = a(\Delta\rho)^{\mu/\beta}$ and $\gamma = b(\Delta c)^\mu$,¹⁰ in which $\Delta\rho$ is the difference in density between the two phases, and Δc is the difference between the polysaccharide concentration in the mixture and its concentration at the critical point. The exponents μ and β are critical exponents. Mean-field theory predicts $\mu = 1.5$ and $\beta = 0.5$, and the Ising model predicts $\mu = 1.26$ and $\beta = 0.32$.⁹ These exponents have been found in many systems. Schneider and Wolf¹¹ investigated the relation between the interfacial

tension and the length of the tie-lines for a copolymer system. They found values for μ/β in the range of 2.5 to 4.7. Similar values were also found for a mixture of poly(dimethylsiloxane) in toluene and ethanol.¹² Several studies have investigated mixtures of methylcyclohexane and polystyrene.^{7,13,14} For this system, the scaling of interfacial tension with critical temperature was investigated. This scaling is given by $\gamma \propto (1 - T/T_c)^\beta$. These studies found values between 1.2 and 1.6 for the critical exponent μ and values ranging from 0.45 to 0.60 for the critical exponent β .

Although these relations have been well studied in synthetic polymer systems, biopolymer systems have received little attention. Scholten et al.¹⁵ studied the interfacial tension of one particular aqueous phase-separated gelatin/dextran mixture with the spinning drop method. They found critical exponents μ , β , and μ/β equal to 1.5, 0.55, and 2.7 respectively, in agreement with mean-field theory. Ding et al.¹⁶ measured the interfacial tension of a gelatin/dextran system with a modified retracting drop method and found comparable scaling exponents of μ/β equal to 2.4, and μ equal to 2.0.

To investigate whether these exponents could be found in other biopolymer systems, we investigated the interfacial tension of the interface of two different phase-separated protein/polysaccharide systems: a gelatin/dextran and a gelatin/gum arabic system in 0.5 M sodium iodide, at pH 8.5. To be able to compare the results in terms of phase separation and interfacial tension, the molecular weight of the dextran and gum arabic was chosen to be equal.

The protein gelatin is frequently used in products such as low-calorie reduced-fat products and as a thickener in yogurts; it is also a material for encapsulating pharmaceutically active ingredients. Gelatin consists of linearly polymerized amino acids and is obtained from the fibrous protein collagen. It is able to undergo a coil/helix transition, where chains in the helix conformation can form thermo-reversible gels.^{17,18} Dextran is a polysaccharide produced by the bacterium *Leuconostoc mesenteroides* and is mainly composed of the monomeric units α -D-glucopyranose, linked primarily by (1 \rightarrow 6) bonds and in a small fraction by (1 \rightarrow 3) bonds. Dextran is often used as a stabilizer and thickening agent in a variety of products, such as creams,

syrups, candies, and low-calorie sugar free beverages. Gum arabic is a complex branched heteropolyelectrolyte with a backbone of 1,3-linked β -galactopyranose units and side-chains of 1,6-linked galactopyranose units. It also contains 2% protein, covalently linked to the carbohydrate through serine and hydroxyproline residues, resulting in a mixture of arabinogalactan-protein complexes, each containing several polysaccharide units linked to a common protein core.¹⁹ The most widely accepted structure for gum arabic is the so-called ‘wattle-blossom’ model.²⁰ Gum arabic is used as a flavor encapsulator in various dry mix foods and as a stabilizer/emulsifier in soft drinks.²¹

Sodium iodide was added to suppress the gelation of gelatin. The alkaline environment (pH 8.5) was used to obtain a negatively charged gelatin (pI = \pm 5.5) to prevent complex coacervation of gelatin with negatively charged gum arabic.

2.2 Experimental section

2.2.1 Materials

A purified low molecular weight gelatin fraction was obtained from DGF-Stoess, Germany. Dextran and gum arabic were purchased from Sigma-Aldrich. The molecular weight of the samples was determined using a combination of size-exclusion chromatography (SEC) and multiangle laser light scattering (MALLS) at NIZO Food Research (Ede, The Netherlands). All biopolymers were dissolved in a 0.1 M NaNO₃ solution and measured at a wavelength of 660 nm at room temperature (20°C). The dn/dc values of the biopolymers are 0.130 for both dextran samples and 0.159 for both gelatin and gum arabic. The gelatin had a weight-averaged mass, M_w , of 41 kDa and a polydispersity of 1.7 (M_w/M_n). Dextran A had a weight-averaged mass of 387 kDa. Dextran B and gum arabic had a M_w of 579 and 580 kDa respectively. All investigated polysaccharides had a polydispersity of 1.5. All components are relatively monodisperse.

2.2.2 Methods

2.2.2.1 Preparation of the protein/polysaccharide mixtures

Gelatin and dextran B were simultaneously dissolved in a 0.5 M sodium iodide solution at pH 8.5, and allowed to stand at room temperature for at least one hour. Then, the solution was heated at 60°C for one hour, and was frequently shaken to obtain a homogeneous mixture. After both biopolymers had been dissolved and the mixture had been cooled to room temperature, the pH was adjusted to 8.5 using a NaOH solution. Sodium azide (0.02%) was added as an antimicrobial agent. For the mixtures of gelatin and gum arabic a slightly different approach was used. Since gum arabic contains some impurities, which would give problems during the experiments, gelatin and gum arabic were dissolved separately in a 0.5 M sodium iodide solution at pH 8.5. Before these solutions were mixed, the gum arabic solutions were centrifuged at 1000 rpm to sediment the impurities. Approximately 5% of the sample was lost as a result of this procedure, and this was taken into account in further calculations. Sodium azide (0.02%) was added as an antimicrobial agent.

2.2.2.2 Determination of the radius of biopolymers

The hydrodynamic radii of polymers can be determined by viscosity measurements. For a dilute solution, with $\eta < 1.03\eta_0$, where η is the viscosity of the solution and η_0 is the viscosity of the solvent, the viscosity can be described by the Einstein formula as

$$\eta = \eta_0(1 + a\varphi) \quad (2.1)$$

Here φ is the volume fraction of polymer and a is a constant, equal to 2.5 in the case of spherical particles. The hydrodynamic radius of the particles, R_h , can thus be calculated from the volume fraction φ

$$\varphi = \frac{4\pi R_h^3 c_p N_{av}}{3M} \quad (2.2)$$

where c_p is the polymer concentration, N_{av} is Avogadro's number and M is the molecular weight. Using a theoretical value of 1.27 for the ratio R_g / R_h , obtained from Monte Carlo simulations performed by Freire et al.,²² the radius of gyration of the biopolymer can be calculated. The viscosity measurements were performed using a Ubbelohde capillary viscometer (Schott Geräte), with a diameter of 0.53 mm. All

experiments were performed with Ubbelohdes, situated in a water bath with a constant temperature of 20°C. The hydrodynamic radii of all components were determined by measuring the viscosity for at least seven samples in the dilute regime, with concentrations ranging from 0.1 to 1.5 g/L, where the Einstein relation is valid. The biopolymers were dissolved in the desired solvent (0.5 M NaI or 1 M NaI solution).

2.2.2.3 Construction of phase diagram

Phase diagrams are constructed by preparing samples that segregate and by then determining the concentrations of both biopolymers in the upper and lower phase. In the case of the gelatin/dextran and gelatin/gum arabic systems, this can easily be done by measuring the optical rotation of both phases²³ at two different wavelengths, λ_i . The measured optical rotation, α_{meas} , is given by

$$\alpha_{meas}(c_p, c_{pol}, \lambda_i) = \alpha_{sp,p}(\lambda_i)c_p + \alpha_{sp,pol}(\lambda_i)c_{pol} \quad i = 1, 2 \quad (2.3)$$

where c_p is the protein concentration and c_{pol} is the polysaccharide concentration. The specific optical rotations $\alpha_{sp,p}$ and $\alpha_{sp,pol}$ were obtained from calibration curves. This method is valid only if the optical rotation of a mixture is a simple addition of the contribution of each biopolymer. This relation was tested and proved to be valid in the concentration range of the samples. All measurements were performed at room temperature with a Perkin-Elmer polarimeter. For each system, we prepared five to six samples. These samples were centrifuged at 2000 rpm for 30 minutes to enhance the phase separation kinetics and were allowed to stand for at least one day to reach equilibrium. After separation, both phases were diluted 20-50 times before their optical rotation was measured. From these results the binodal could be determined.

2.2.2.4 Interfacial tension measurements

To measure the interfacial tension of the mixtures, a spinning drop tensiometer was used^{15,24} (van 't Hoff Laboratory, Debye Research Institute, Utrecht University, The Netherlands). A droplet of the low-density phase is inserted into a matrix of the high-density phase in a horizontally mounted capillary. The capillary is rotated around its length axis. As the speed of rotation is increased, the drop deforms along the axis of the capillary until equilibrium is achieved. Then deformation of the droplet, due to centrifugal forces, is balanced by the interfacial tension between the two phases.

When equilibrium is reached, and the length of the droplet exceeds four times the diameter of the droplet, the Vonnegut equation is valid^{25,26}

$$\gamma = \frac{\Delta\rho\omega^2 R^3}{4} \quad (2.4)$$

where $\Delta\rho$ is the difference in density between the two phases, ω is the spinning frequency, and R is the radius of the droplet. As a result of the curvature of the capillary, the dimensions of the droplet, measured with a micrometer, are slightly different from their actual size. The correction factor,²⁷ used to determine the actual size of the droplet, R_d , is given by the equation $R_d = R_{da} n_a / n_1$. Here R_{da} is the measured apparent droplet radius, and n_1 and n_a are the refractive indices of the high-density phase and the air phase outside the capillary, respectively. The refractive index of the high-density phase was determined using a refractometer. The droplet radius was determined for at least five different rotational speeds. For each measurement the system was allowed to reach equilibrium, and the radius of the droplet was determined only after the shape of the droplet no longer changed. All measurements were performed at room temperature (20°C). For each measurement we confirmed that the length of the droplet exceeded four times the diameter.

2.2.2.5 Density measurements

For the phase-separated biopolymer mixtures, the densities of both phases were determined with an Anton Paar DMA 5000 density meter. The densities are required for the calculations of the interfacial tensions, and are used to study the interfacial tension as a function of the density difference between the two phases. The densities were measured at least three times to estimate the error in the density measurements.

2.3 Results and discussion

2.3.1 Phase behavior of gelatin/dextran and gelatin/gum arabic mixtures

In Figure 2.1, we present the phase diagram of gelatin/dextran A (molecular weight of 387 *kDa*) in a 1 M NaI solution at pH 6. In this figure, the triangles represent the results of optical rotation measurements. The solid line through these points represents the binodal.

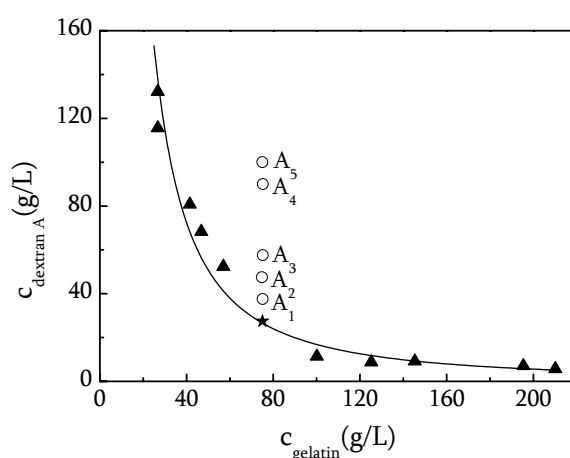


Figure 2.1 Phase diagram of gelatin/dextran A in a 1 M NaI solution at pH 6. The solid line represents the binodal, and the triangles refer to the composition of the phases. The star denotes the critical point.

Figures 2.2 and 2.3 show the phase diagrams of the gelatin/dextran B and the gelatin/gum arabic system. Although dextran B and gum arabic have the same molecular weight (approximately 500 *kDa*) the phase diagrams are substantially different. The gelatin concentration at the critical point has shifted to a lower concentration for the gelatin/gum arabic system, and the diagram is more symmetrical compared to the phase diagrams of the gelatin/dextran systems (Figures 2.1 and 2.2). In the next section we will show that the differences between the phase diagrams may be attributed to the difference in size and the structure of the polysaccharides.

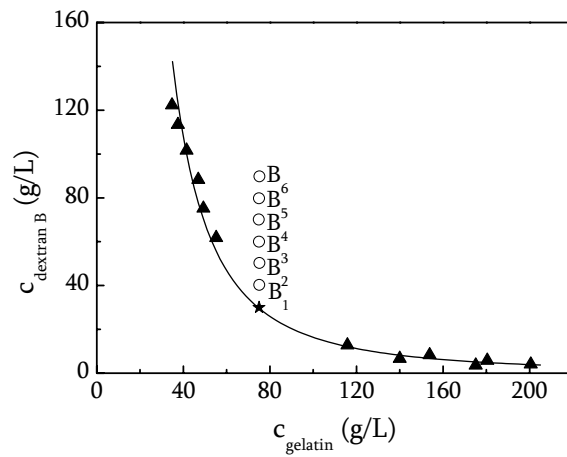


Figure 2.2 Phase diagram of the gelatin/dextran B system in a 0.5 M NaI solution at pH 8.5. The triangles represent the phases after phase separation of the samples B_1 to B_6 . The solid line represents the binodal through those points, and the star denotes the critical point. For the samples represented by the open circles, the interfacial tension was measured.

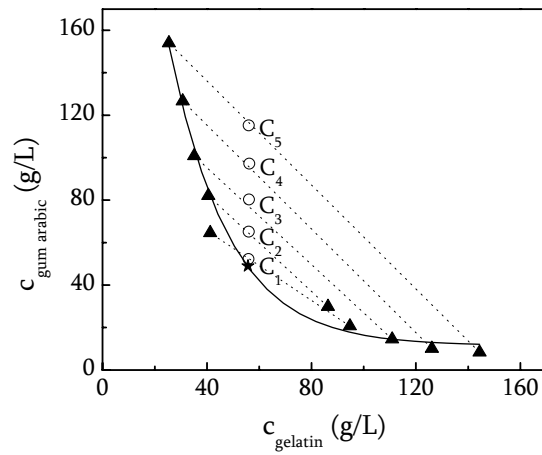


Figure 2.3 Phase diagram of the gelatin/gum arabic system in a 0.5 M NaI solution at pH 8.5. The triangles refer to the phases after phase separation of the samples C_1 to C_5 , for which the interfacial tension was measured. The solid line represents the binodal through the triangles, and the star denotes the critical point. The dotted lines represent the tie-lines.

2.3.2 Determination of the radius of gyration

Since there were differences in the phase diagrams, the radii of gyration were determined to obtain more insight into the structure of the biopolymers. To determine the hydrodynamic radii, we performed viscosity measurements of diluted biopolymer solutions. Equation (2.1) was used to determine the volume fraction of the components; inserting this volume fraction and the molecular weight of the biopolymers in equation (2.2), we could determine the hydrodynamic radii. These were converted into radii of gyration by multiplying by 1.27.²² Table 2.1 gives an overview of the biopolymers with accompanying molecular weight and the calculated radius of gyration.

Table 2.1 Molecular weight and radius of gyration of biopolymers.

Biopolymer	Solvent	Molecular weight (<i>kDa</i>)	Radius of gyration (<i>nm</i>)	Monomer weight* (<i>g/mol</i>)
gelatin	1 M NaI, pH 6	41	6.7	100
	0.5 M NaI, pH 8.5	41	7.0	
dextran A	1 M NaI, pH 6	387	17.5	180
dextran B	0.5 M NaI, pH 8.5	579	19.4	180
gum arabic	0.5 M NaI, pH 8.5	580	15.4	180

* The monomer weight is taken as the average weight of a basic unit.

(For gelatin, this has been taken as the weight averaged over the aminoacids present in the gelatin molecule. For gum arabic and dextran, this was taken as the weight of a galactopyranose and a glycopyranose molecule respectively.)

The radius of gyration of dextran A was equal to 17.5 *nm*. In a previous study,¹⁵ a value of 20 *nm* was found in pure water, when measured by multi-angle static light scattering. Comparing dextran B and gum arabic, which have approximately the same molecular weight, we see that the radius of gyration is significantly different. This might be explained by the difference in the structure of both biopolymers. Gum arabic is known to exist as a ‘wattle-blossom’ model, which is a relatively denser structure than a linear polymer such as dextran. This difference in structure could cause the difference in symmetry in the phase diagrams observed in Figures 2.2 and 2.3.

2.3.3 Interfacial tension

To determine the interfacial tension as a function of $\Delta\rho$ and Δc , we prepared samples ranging in quench depth. These samples are denoted by the open circles B₁-B₆ and C₁-C₅ in Figures 2.2 and 2.3. The gelatin concentration was kept constant at its value at the critical point, and the concentration of dextran B and gum arabic was varied. An overview of the interfacial tensions is given in Tables 2.2 and 2.3. These values are comparable to values previously found for gelatin/dextran systems.¹⁵

Table 2.2 Concentration, density difference between coexisting phases, and interfacial tension for the phase-separated gelatin/dextran B system (0.5 M NaI, pH 8.5) presented as open circles in Figure 2.2.

Number sample	Gelatin concentration (g/L)	Dextran B concentration (g/L)	$\Delta\rho$ (g/L)	γ ($\mu\text{N}/\text{m}$)
B ₁	75.1	40.3	1.6 ± 0.1	0.6 ± 0.2
B ₂	75.2	50.3	2.3 ± 0.1	1.9 ± 0.3
B ₃	75.0	60.0	3.1 ± 0.1	3.4 ± 0.3
B ₄	74.9	70.1	3.6 ± 0.1	5.3 ± 0.4
B ₅	75.0	79.8	4.0 ± 0.1	7.1 ± 0.4
B ₆	75.2	89.8	4.5 ± 0.1	9.1 ± 0.6

As can be seen in Tables 2.2 and 2.3, the interfacial tension for both systems is very small close to the critical point (samples B₁ and C₁). It increases when the concentration of polysaccharide is increased. The interfacial tension can be estimated from the scaling relation $\gamma \propto kT/\xi^2$, and, since the sizes of the biopolymers are comparable, we can expect the interfacial tension to have the same order of magnitude, as is indeed the case. Although the interfacial tensions are comparable, there is a large difference in the density difference. For the gelatin/dextran B system, the density difference far from the critical point, for sample B₆, is approximately 5 g/L. The density difference observed in the gelatin/gum arabic system is much higher and ranges from 5.6 to 28.3 g/L.

Table 2.3 Concentration, density difference between coexisting phases and interfacial tension for the phase-separated gelatin/gum arabic system (0.5 M NaI, pH 8.5) presented by the open circles in Figure 2.3.

Number sample	Gelatin concentration (g/L)	Gum arabic concentration (g/L)	$\Delta\rho$ (g/L)	γ ($\mu\text{N}/\text{m}$)
C ₁	55.9	52.2	5.6 ± 0.2	1.5 ± 0.2
C ₂	56.0	65.1	14.6 ± 0.4	6.7 ± 1.2
C ₃	56.1	80.3	18.4 ± 0.1	9.7 ± 1.5
C ₄	56.2	97.2	22.2 ± 0.6	12.9 ± 1.9
C ₅	56.0	115.2	28.3 ± 0.4	14.9 ± 2.4

To investigate the scaling behavior in both systems and to determine the critical exponents, the interfacial tension was plotted as a function of $\Delta\rho$ and Δc . Figure 2.4 shows the interfacial tension of the gelatin/dextran B system as a function of $\Delta\rho$. The data were fitted to the relation $\gamma = a(\Delta\rho)^{\mu/\beta}$, and we found that $a = 0.2 \pm 0.1$ and $\mu/\beta = 2.5 \pm 0.1$ gave the best fit. The scaling exponent 2.5 ± 0.1 agrees with exponents previously found^{11-13,15} and is closer to the scaling exponent $\mu/\beta = 3$, given by the mean-field model, than it is to the value from the Ising model of $\mu/\beta = 3.9$.

In Figure 2.5, the interfacial tension is plotted as a function of Δc . The data were fitted to the relation $\gamma = e(\Delta c)^\mu$, and the best fit was obtained for $e = 0.026 \pm 0.003$ and $\mu = 1.4 \pm 0.1$. The exponent 1.4 ± 0.1 agrees with the critical exponent $\mu = 1.5$ (mean-field), which was also found from density functional theory.¹⁰ Since the critical exponents for the gelatin/dextran B system are in reasonable agreement with the mean-field values, we can conclude that the concentration region for which these exponents have been determined is near-critical.

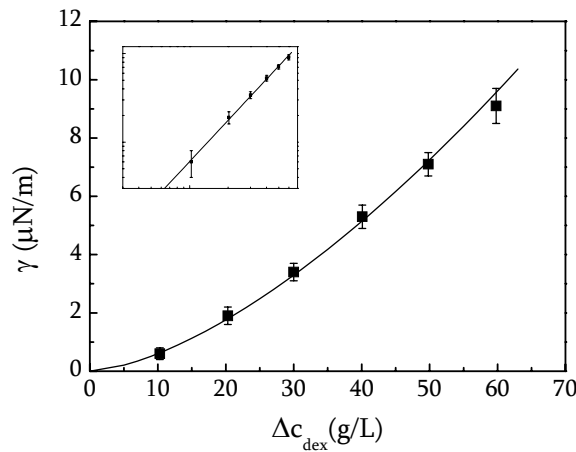


Figure 2.4 Interfacial tension of the gelatin/dextran B system as a function of the density difference between the two coexisting phases. The line represents the best fit to the scaling relation $\gamma = a(\Delta\rho)^{\mu/\beta}$, with $\mu/\beta = 2.5$. The inset shows the same plot on a logarithmic scale.

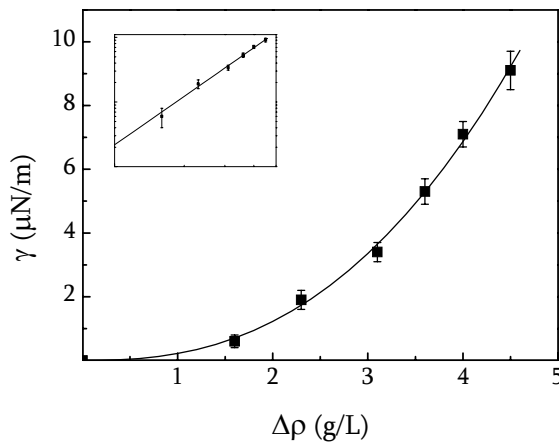


Figure 2.5 Interfacial tension of the gelatin/dextran B system as a function of the concentration difference of dextran. The line represents $\gamma = e(\Delta c)^\mu$, with $\mu = 1.4$. In the inset, the scaling relation is given on a logarithmic scale.

For the gelatin/gum arabic system we plotted the interfacial tension as a function of the density difference in Figure 2.6. We observe a linear relation in this case, instead of $\gamma \propto \Delta\rho^{\mu/\beta}$ with $\mu/\beta = 3$ or 3.9 . This linear relationship was also found by de Hoog

and Lekkerkerker,²⁴ who measured the interfacial tension in a colloid-polymer mixture. The interfacial tension as a function of Δc does not show a power law dependence either (Figure 2.7). From these results we can conclude that the region for which the scaling behavior has been investigated is not near-critical, but off-critical.

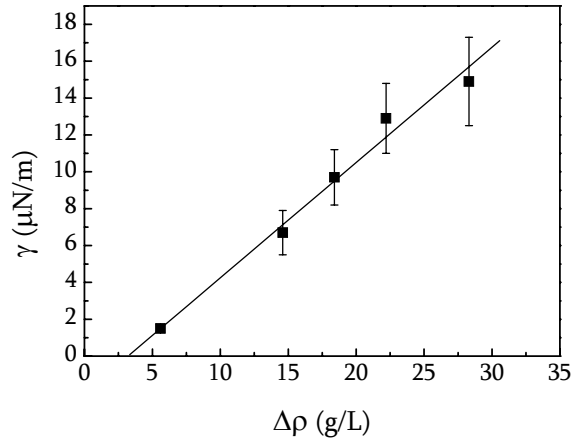


Figure 2.6 The interfacial tension γ , plotted as a function of the density difference between the two phases of the gelatin/gum arabic system.

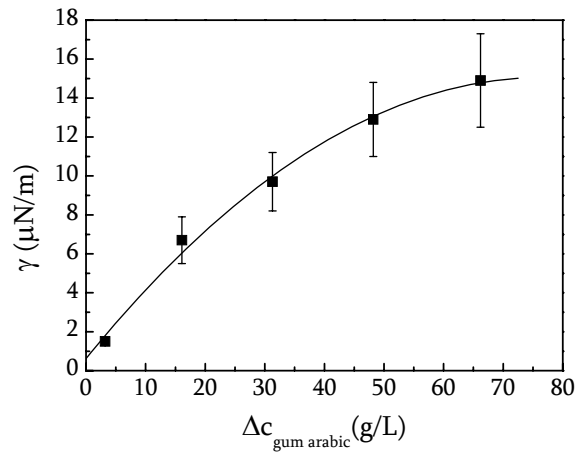


Figure 2.7 Interfacial tension of the gelatin/gum arabic system as a function of the concentration difference of gum arabic. The line is drawn to guide the eye.

Thus, although dextran B and gum arabic are both polysaccharides and have comparable molecular weights, these systems behave very differently. For the gelatin/dextran systems we investigated, phase separation results in samples that can be considered to be near-critical. This near-critical behavior indicates the presence of a diffuse interface with a thickness larger than the sizes of the biopolymers. However, the gelatin/gum arabic samples we investigated do not show near-critical behavior, which indicates an interfacial region in the order of the size of the biopolymers.

2.3.4 Distribution of molecules

For off-critical systems it is known that the distribution of molecules between the concentrated and the depleted phase shows an exponential dependence on the interfacial tension according to the following relation described by Albertsson²⁸

$$\frac{c_{rich}}{c_{poor}} = e^{\frac{4\pi R^2 \gamma}{kT}} \quad (2.5)$$

Here c_{rich} and c_{poor} are the concentrations of a polymer with radius R in the concentrated and the depleted phase respectively. Since the gelatin/gum arabic system does not show near-critical behavior for the investigated samples, we investigated the distribution of the gum arabic particles. Using equation (2.5), we expect that a plot of γ versus $\ln(c_{rich}/c_{poor})$ yields a straight line. This is indeed observed in Figure 2.8. Note that the data corresponding to the samples C₁ and C₂ deviate from this linear relation. Since these samples were close to the critical point, the concentrations of both biopolymers were difficult to determine. As a result the determined compositions of the phases do not completely correspond to the binodal (Figure 2.3). These small deviations from the binodal have a great influence on $\ln(c_{gum arabic, rich}/c_{gum arabic, poor})$, which explains the large deviations from the linear fit for these two samples. The slope of γ versus $\ln(c_{rich}/c_{poor})$ equals $kT/4\pi R^2$. Using this relation and the experimentally obtained value of $4.9 \cdot 10^{-6}$ for the slope, R is determined as 8 nm, which is indeed the same order of magnitude as the radius of gyration of gum arabic (15.4 nm).

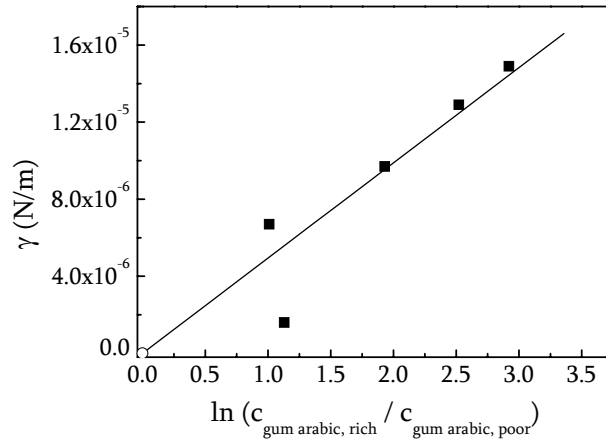


Figure 2.8 Interfacial tension of the gelatin/gum arabic system as a function of $\ln(c_{\text{gum arabic, rich}} / c_{\text{gum arabic, poor}})$. The data correspond to the points C₁ to C₅ as indicated in Figure 2.3. The line is the best linear fit through the points, with the open circle as a theoretical point.

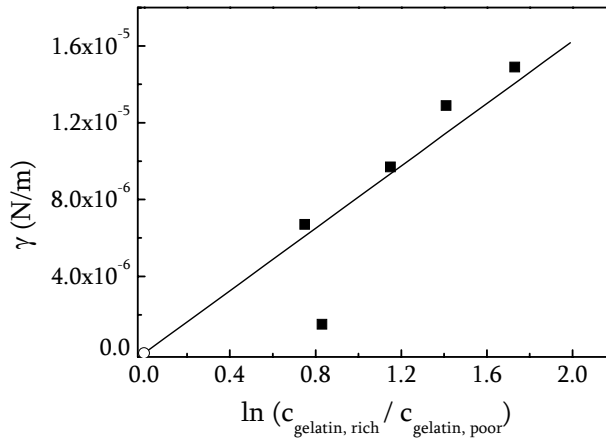


Figure 2.9 Interfacial tension of the gelatin/gum arabic system as a function of $\ln(c_{\text{gelatin, rich}} / c_{\text{gelatin, poor}})$. The data correspond to the points C₁ to C₅ as indicated in Figure 2.3. The line is the best linear fit through the points, with the open circle as a theoretical point.

The distribution of the gelatin molecules in this gelatin/gum arabic system shows similar results. Figure 2.9 shows γ versus $\ln(c_{\text{gelatin, rich}} / c_{\text{gelatin, poor}})$, from which R was determined as 6 nm, in agreement with the radius of gyration of gelatin (7 nm).

Using the same procedure for the gelatin/dextran systems, we did not observe a linear relation between γ and $\ln(c_{rich}/c_{poor})$ (not shown).

2.4 Conclusion

Using optical rotation measurements, we constructed the phase diagrams of a phase-separated gelatin/dextran and gelatin/gum arabic system, where both polysaccharides had the same molecular weight. For samples with varying polysaccharide concentrations, the interfacial tension was measured with a spinning drop apparatus. The interfacial tension was studied as a function of the density difference between the two phases, and as a function of the concentration difference of the polysaccharide with respect to the concentration at the critical point. From these relations, we could determine whether the systems gave the critical scaling exponents predicted by mean-field theory. For the investigated gelatin/dextran system, the critical exponents were in reasonable agreement with mean-field values. However, the gelatin/gum arabic system did not give these critical exponents. Instead, the interfacial tension versus the density difference showed a linear relation. For this gelatin/gum arabic system, the distribution of the gum arabic molecules turned out to be exponentially dependent of interfacial tension. The Boltzmann factor of this distribution is dependent of the molecular size of the gum arabic. This size, as obtained from the experimentally determined Boltzmann factor, was found to be of the same order of magnitude as the radius of gyration of gum arabic. Also, for the distribution of the gelatin particles, the accompanying Boltzmann factor yields a molecular size in agreement with the size of the radius of gyration of gelatin.

Acknowledgements

We thank H. Tromp and M. Edelman (NIZO Food Research, Ede, The Netherlands) for stimulating and helpful discussions, and H.N.W. Lekkerkerker (Utrecht University, The Netherlands) for his kind hospitality and allowing us to use the spinning drop apparatus in his laboratory.

References

- (1) Tolstoguzov, V. *Nahrung* **2000**, *44*, 299-308.
- (2) Doublier, J. L.; Garnier, C.; Renard, D. and Sanchez, C. *Curr. Opin. Colloid Interface Sci.* **2000**, *5*, 202-214.
- (3) Grinberg, V. Y. and Tolstoguzov, V. B. *Food Hydrocolloids* **1997**, *11*, 145-158.
- (4) Durrani, C. M.; Prystupa, D.A.; Donald, A.M. and Clark, A. *Macromolecules* **1993**, *26*, 981-987.
- (5) Jenkins, P. and Snowden, M. *Adv. Colloid Interface Sci.* **1996**, *68*, 57-96.
- (6) van Puyvelde, P.; Antonov, Y. A. and Moldenaers, P. *Food Hydrocolloids* **2002**, *16*, 395-402.
- (7) Heinrich, M. and Wolf, B. A. *Polymer* **1992**, *33*, 1926-1931.
- (8) de Gennes, P. G. *Scaling Concepts in Polymer Physics*; Cornell University Press: New York, 1979.
- (9) Rowlinson, J. S. and Widom, B. *Molecular Theory of Capillarity*; Clarendon Press: Oxford, 1984.
- (10) Brader, J. M. and Evans, R. *Europhys. Lett.* **2000**, *49*, 678.
- (11) Schneider, A. and Wolf, B. A. *Polymer* **2000**, *41*, 4089-4097.
- (12) Wunch, M. and Wolf, B. A. *Polymer* **2002**, *43*, 5027-5034.
- (13) Enders, S.; Huber, A. and Wolf, B. A. *Polymer* **1994**, *35*, 5743-5747.
- (14) Enders, S.; Wolf, B. A. and Binder, K. *J. Chem. Phys.* **1995**, *103*, 3809-3819.
- (15) Scholten, E.; Tuinier, R.; Tromp, R. H. and Lekkerkerker, H. N. W. *Langmuir* **2002**, *18*, 2234-2238.
- (16) Ding, P.; Wolf, B.; Frith, W. J.; Clark, A. H.; Norton, I. T. and Pacek, A. W. *J. Colloid Interface Sci.* **2002**, *253*, 367-376.
- (17) Glicksman, M. *Food Hydrocolloids*; CRC Press: New York, 1982.
- (18) Normand, V.; Muller, S.; Ravey, J.-C. and Parker, A. *Macromolecules* **2000**, *33*, 1063-1071.
- (19) Dickinson, E. *Food Hydrocolloids* **2003**, *17*, 25-39.
- (20) Connolly, S.; Fenyo, J. C. and Vandeveld, M. C. *Food Hydrocolloids* **1988**, *13*, 23-32.
- (21) Menzies, A. R.; Osman, M. E.; Malik, A. A. and Baldwin, T. C. *Food Addit. Contam.* **1996**, *13*, 991-999.
- (22) Freire, J. J.; Rey, A. and de la Torre, J. G. *Macromolecules* **1986**, *19*, 457-462.

- (23) Edelman, M. W.; van der Linden, E.; de Hoog, E. and Tromp, R. H. *Biomacromolecules* **2001**, *2*, 1148-1154.
- (24) de Hoog, E. H. A. and Lekkerkerker, H. N. W. *J. Phys. Chem. B* **1999**, *103*, 5274-5279.
- (25) Princen, H. M.; Zia, I. Y. Z. and Mason, S. G. *J. Colloid Interface Sci.* **1967**, *23*, 99.
- (26) Vonnegut, N. *Rev. Sci. Instrum.* **1930**, *13*, 99.
- (27) Coucoulas, L. M. *J. Colloid Interface Sci.* **1983**, *93*, 281-284.
- (28) Albertsson, P. A. *Partition of Cell Particles and Macromolecules*, second edition, John Wiley & Sons Inc.: Stockholm, 1971.

Chapter 3

Bending rigidity of interfaces in aqueous phase-separated biopolymer mixtures

Bending rigidity of interfaces in aqueous phase-separated biopolymer mixtures

Abstract

Using equations for the interfacial properties for a two-phase multicomponent system, we present a new model for the interfacial tension and bending rigidity for liquid-liquid interfaces between semi-dilute polymer phases. Using this model, we calculate the interfacial thickness and the bending rigidity for two different gelatin/dextran systems and a gelatin/gum arabic system, using experimentally determined values for the interfacial tension. The bending rigidity of such systems has been inaccessible experimentally until now. For the gelatin/dextran systems, which are both near-critical, the interfacial thickness is very large (1000 nm) close to the critical point, where the interfacial tension is very low. Further from the critical point the interfacial thickness decreases to a value in the order of the size of the biopolymers (100 nm). For the gelatin/gum arabic system, which is off-critical, we found the interfacial thickness to be constant, in the order of the size of the biopolymers. For the gelatin/dextran systems the scaling relation between the interfacial tension and the interfacial thickness was investigated. The exponents were found to be approximately 1.7 for the two systems, which is in agreement with the exponent 2 of the scaling relation $\gamma \propto 1/\xi^2$. The accompanying bending rigidities for these near-critical gelatin/dextran systems were found to be approximately constant, with a value of $500 k_b T$. The bending rigidity for the gelatin/gum arabic system, which is off-critical, was in the order of $25 k_b T$. These high values for both the interfacial thickness and the bending rigidity for the near-critical systems may be of significance for interfacial-related phenomena in aqueous phase-separated biopolymer mixtures, in particular in cases where the bending contributions dominate the stretching contributions to the interfacial energy.

3.1 Introduction

The interfacial tension of phase-separated aqueous (bio)polymer systems (water-in-water emulsions) is often very low, in the order of $1 \mu\text{N}/\text{m}$,¹ as was already discussed in chapter 2. The interfacial tension of these water-in-water emulsions is much lower than the interfacial tension of water/oil emulsions, which are normally in the order of mN/m . In systems where the interfacial tension is low, the bending rigidity becomes important, and may even dominate the behavior of the interface. Although the bending rigidity has been studied for vesicles and bilayers, for interfaces between aqueous phase-separated biopolymer systems this property has received little attention, nor has the interfacial thickness. Only for a colloid-polymer mixture interfacial parameters have been investigated. De Hoog et. al.² reported interfacial tensions of a silica/poly(dimethylsiloxane) mixture, which are of the same order of magnitude as those of (bio)polymer mixtures. They also performed an ellipsometric study of the interface of this mixture, and from the results they found the interfacial thickness to be of the order of the size of the colloids.³ Although these results are reasonable, they reported some experimental difficulties.³ In general, measuring the ellipticity of phase-separated colloid-polymer or (bio)polymer systems is not easy. Since the interfacial tension is very low, the interfaces are very sensitive to small variations in temperature, mechanical vibrations, and fluctuations in pressure. Especially for samples that are close to the critical point, these variations can be of such significance that only a crude estimation of the order of magnitude for the interfacial thickness can be obtained. Although bending rigidities have been widely studied for microemulsion systems, for aqueous biopolymer interfaces, neither experimental data nor a theoretical model has been available. The experimental determination of rigidities for these mixtures following methods successful in microemulsions (i.e. light scattering or ellipsometry) has been unsuccessful until now since it is hampered by the fact that there is a small optical contrast between the two phases.

The main objective of this chapter was to determine the bending rigidity and interfacial thickness for various aqueous phase-separated biopolymer systems, using experimental values of the (more easily accessible) interfacial tension as the only input

variable. The procedure described, circumvents the unresolved experimental difficulties of determining the bending rigidities, and instead relies on using a combination of theory and experimental determination of the interfacial tension.

3.2 Theory

In the past decade, a large number of theories regarding interfacial properties have been published.⁴⁻¹³ Here we will use the Van der Waals theory, which introduces an intrinsic density profile across the interface that interpolates between the densities of the bulk phase. The usual approach in the Van der Waals theory is to expand the free energy of the interface in terms of its curvature. From this expansion we find that the surface tension up to the second order in curvature is given by¹⁴

$$\gamma(J, K) = \gamma_0 - kC_0J + \frac{1}{2}kJ^2 + \bar{k}K \quad (3.1)$$

where γ_0 is the interfacial tension of the flat interface, k is the bending rigidity, C_0 is the spontaneous curvature of the interface, and \bar{k} is the rigidity constant associated with the Gaussian curvature. J and K are the mean curvature and Gaussian curvature respectively. The first term signifies the stretching contribution to the interfacial energy, while the other terms relate to the bending contribution. The validity of this expression is limited to small curvature (i.e. for radii of curvature larger than the important length scales or interfacial thickness). Investigating the change in grand potential under local deformations for spherical and cylindrical cones, the following equations for γ_0 and k for a two-component system have been obtained^{8,13}

$$\gamma_0 = \frac{1}{4} \sum_{\alpha, \beta} \int dz_1 \int d\mathbf{r}_{12} u'_{\alpha\beta}(r) r (1 - 3s^2) \rho_0^{\alpha\beta} \quad (3.2)$$

$$k = -\frac{1}{4} \sum_{\alpha, \beta} \int dz_1 \int d\mathbf{r}_{12} u'_{\alpha\beta}(r) r \left[\frac{1}{2} z_1 z_2 (1 - 3s^2) \rho_0^{\alpha\beta} + \frac{1}{16} r^2 (1 + 6s^2 - 15s^4) \rho_o^{\alpha\beta} + (z_1 + z_2) (s^2 - \sin^2 \varphi_{12} (1 - s^2)) \rho_{1c}^{\alpha\beta} \right] \quad (3.3)$$

where $u'_{\alpha\beta}$ is the derivative of the interaction potential between component α and β . Equation (3.3) is known as the Kirkwood-Buff formula,¹⁵ and Groenewold and Bedeaux¹³ extended this theory to obtain the result for γ_0 and k for a multicomponent system. ρ_0 , and ρ_{1c} , refer to the first, and second term in the

expansion of the pair density of a cylindrical interface. If we assume that $\rho_{c1}^{\alpha\beta}$ is independent of φ_{12} , equation (3.3) can be rewritten in the following form

$$k = \frac{1}{8} \sum_{\alpha, \beta} \int dz_1 \int dr_{12} u'_{\alpha\beta}(r) r \left[(1 - 3s^2) z_1^2 - \frac{1}{8} r^2 (1 + 6s^2 - 15s^4) \right] \rho_0^{\alpha\beta}(z_1, z_2, r) \quad (3.4)$$

To use equations (3.2) and (3.4) for the calculation of γ_0 and k we need to assume a model for the pair density of the flat interface ($\rho_0^{\alpha\beta}$) and the pair potential ($u_{\alpha\beta}(r)$). For the pair density of a flat interface we use the following approximate form:

$$\rho_0^{\alpha\beta}(z_1, z_2, r) = \rho^\alpha(z_1) \rho^\beta(z_2) g(r) \quad (3.5)$$

where $g(r)$ is the pair correlation function in a uniform liquid, and $\rho^\alpha(z_1)$ and $\rho^\beta(z_2)$ are the density profiles in the interfacial region. For the density profile we assume the classical Van der Waals profile

$$\rho^\alpha(z) = \rho_c^\alpha - \frac{1}{2} \Delta\rho^\alpha \tanh(z/2\xi) \quad (3.6)$$

where ρ_c^α is the average of the densities of component α in the two bulk phases, $\Delta\rho^\alpha \equiv (\rho_{upper\ phase}^\alpha - \rho_{lower\ phase}^\alpha)$, and ξ is the interfacial thickness. Inserting equations (3.5) and (3.6) in equations (3.2) and (3.4), and integrating over z_1 gives

$$\gamma_0 = \frac{1}{4} \pi \sum_{\alpha, \beta} \int_{-1}^1 ds \int_0^\infty dr r^4 g(r) u'_{\alpha\beta}(r) (3s^3 - s) \cotanh(sr/2\xi) \Delta\rho^\alpha \Delta\rho^\beta \quad (3.7)$$

$$k = \frac{1}{24} \pi \sum_{\alpha, \beta} \int_{-1}^1 ds \int_0^\infty dr r^4 g(r) u'_{\alpha\beta}(r) \left(\pi^2 \xi^2 (3s^3 - s) + \frac{1}{8} r^2 s (3 + 10s^2 - 21s^4) \right) \times \cotanh(sr/2\xi) \Delta\rho^\alpha \Delta\rho^\beta \quad (3.8)$$

For a single component ($\alpha = \beta = 1$), these equations reduce to the expressions for γ_0 and k derived by Blokhuis and Bedeaux.⁸ In the case of a two-component aqueous phase-separated system, α and β can both be either 1 or 2, which leads to four terms that contribute to the value of k .

For the interaction potential in equations (3.7) and (3.8) we take a potential that has been derived from smoothed density theory,¹⁶ where the distribution function of the distance of a segment from the center of mass of a molecule is used to derive the following equation

$$\frac{u_{12}(r)}{k_b T} = \nu \int \rho_1(R) \rho_2(R-r) dR \quad (3.9)$$

in which ν represents the excluded volume of a single monomer and $\rho_i(R)$ is the average segment density at distance R from the center of mass of isolated unperturbed chain i . The integral may be regarded as the effective volume excluded to one molecule by the presence of another. The segment densities $\rho_i(R)$ for the case of random chains are assumed to be Gaussian¹⁶

$$\rho_i(r) = N_i \left(\frac{3}{2\pi R_{g,i}^2} \right)^{3/2} \exp \left(-\frac{3r_i^2}{2R_{g,i}^2} \right) \quad (3.10)$$

where N_i is the total amount of monomers, $R_{g,i}$ represents the radius of gyration of the polymers and r_i is the distance of the volume element from the respective center of gravity. Substituting the Gaussian distribution (equation (3.10)) in the expression for the interaction potential (equation (3.9)), gives the interaction potential for a system with two polymers, with radius of gyration $R_{g,i}$

$$u_{12}(r) = k_b T \nu N_1 N_2 \left(\frac{1}{2\pi} \right)^{3/2} \left(\frac{3}{(R_{g,1}^2 + R_{g,2}^2)} \right)^{3/2} \exp \left(\frac{-3r^2}{2(R_{g,1}^2 + R_{g,2}^2)} \right) \quad (3.11)$$

In this equation k_b is the Boltzmann constant, T is the temperature, ν is the excluded volume of a monomer and N_i is the amount of monomers of biopolymer 1 or 2, respectively. This interaction potential is also known as the Flory-Krigbaum potential,¹⁷ which was derived for a dilute solution of heterogeneous polymers in 1950.

We used this model to predict the interfacial thickness and the bending rigidity for phase-separated protein/polysaccharide mixtures. Phase separation in such mixtures results in an upper phase, enriched in protein, and a lower phase concentrated in polysaccharide. Due to the distribution of polymers, the protein concentration in the lower phase will be below the overlap concentration (c^*). In the upper phase,

however, the concentration is above c^* , and the solution is in the semi-dilute regime. While being in the dilute regime in the upper phase, the polysaccharide is present in the semi-dilute regime in the lower phase. In a semi-dilute solution, a network with a certain blob size (ζ) is formed, which can be calculated using¹⁸

$$\zeta = R_g \left(\frac{c^*}{c} \right)^{3/4} \quad (3.12)$$

The overlap concentration (c^*) is given by

$$c^* = \frac{3M}{4\pi R_g^3 N_{av}} \quad (3.13)$$

where M is the molecular weight of the polymer and N_{av} Avogadro's number. For each polymer, two different length scales are important; the radius of gyration in the dilute phase and the blob size (ζ), in the semi-dilute phase. To simplify the integrations in equations (3.7) and (3.8) we take the average length scale of both phases ($\tilde{\zeta}$) defined by

$$\tilde{\zeta} = \left(\frac{R_g + \zeta}{2} \right) \quad (3.14)$$

This can be considered an average blob size of the system. Inserting $\tilde{\zeta}$ into equation (3.11), the interaction potential for a two-component two-phase system becomes

$$u_{\alpha\beta}(r) = k_b T \nu N_{blob}^\alpha N_{blob}^\beta \left(\frac{1}{2\pi} \right)^{3/2} \left(\frac{3}{(\tilde{\zeta}_\alpha^2 + \tilde{\zeta}_\beta^2)} \right)^{3/2} \exp \left(\frac{-3r^2}{2(\tilde{\zeta}_\alpha^2 + \tilde{\zeta}_\beta^2)} \right) \quad (3.15)$$

For the excluded volume ν we take the size of a cylinder $\nu = \pi b^3$, in which b is the Kuhn segment length. For b , we take the average Kuhn length of the biopolymers, which can be calculated from the radius of gyration, using $b = \sqrt{6R_g^2/N}$.¹⁹ The number of monomers in a blob ($N_{blob}^{\alpha,\beta}$), is calculated using $N_{blob}^{\alpha,\beta} = 6\tilde{\zeta}_{\alpha,\beta}^2/b^2$.

3.3 Materials

To obtain phase-separated biopolymer mixtures, we used gelatin as a protein mixed with either dextran or gum arabic, which are both polysaccharides. Gelatin was mixed with dextran A in a 1 M NaI solution at pH 6. In a 0.5 M NaI solution at pH 8.5, gelatin was mixed with either dextran B or gum arabic. Details of these systems can be found in chapter 2. Table 3.1 gives an overview of the properties of these biopolymers in the different solutions, as described in paragraph 2.3.2.

Table 3.1 Molecular weight, M , radius of gyration, R_g , monomer weight of the biopolymers, M_{mon} , and the Kuhn length of the monomers, b .

Biopolymer	Solvent	M (kg/mol)	R_g (nm)	M_{mon} (g/mol)	b (nm)
Gelatin	1 M NaI, pH 6	41	6.7	100	0.81
	0.5 M NaI, pH 8.5	41	7.0		0.85
Dextran A	1 M NaI, pH 6	387	17.5	180	0.92
Dextran B	0.5 M NaI, pH 8.5	579	19.4	180	0.84
Gum arabic	0.5 M NaI, pH 8.5	580	15.4	180	0.66

The phase diagrams of these phase-separated biopolymer mixtures have been determined previously, and can be found in chapter 2. The interfacial tension of the gelatin/dextran B and gelatin/gum arabic system can be found in chapter 2, Tables 2.1 and 2.2. The interfacial tension of the gelatin/dextran A system can be found elsewhere.¹ The interfacial tensions were measured using the spinning drop technique, in which deformation of a macroscopically large droplet (mm) is measured. The phase diagrams were constructed by determining the concentrations of the biopolymers in both phases using polarimetry as described in paragraph 2.2.2.3. Using these concentrations and the properties of the biopolymers, we determined the different length scales of the biopolymers in both the upper and lower phase, and from these calculations we determined the average blob size ($\tilde{\zeta}$) and the number of monomers (N_{blob}). An overview can be found in Tables 3.2-3.4.

Table 3.2 Density difference of gelatin, $\Delta\rho_{gel}$, density difference of dextran, $\Delta\rho_{dex}$, average blob size of gelatin, $\tilde{\zeta}_{gel}$, average blob size of dextran, $\tilde{\zeta}_{dex}$, number of gelatin monomers in a blob, $N_{blob,gel}$, and the number of dextran monomers in a blob, $N_{blob,dex}$ for the gelatin/dextran A system.

$\Delta\rho_{gel}$ (<i>molecules</i> / m^3)	$\Delta\rho_{dex}$ (<i>molecules</i> / m^3)	$\tilde{\zeta}_{gel}$ (<i>nm</i>)	$\tilde{\zeta}_{dex}$ (<i>nm</i>)	$N_{blob,gel}$ (<i>molecules</i>)	$N_{blob,dex}$ (<i>molecules</i>)
$6.31 \cdot 10^{23}$	$-6.36 \cdot 10^{22}$	5.4	14.3	266	1449
$1.14 \cdot 10^{24}$	$-9.22 \cdot 10^{22}$	5.2	13.2	247	1235
$1.52 \cdot 10^{24}$	$-1.10 \cdot 10^{23}$	4.9	12.8	219	1161
$2.47 \cdot 10^{24}$	$-1.65 \cdot 10^{23}$	4.6	11.8	193	987
$2.68 \cdot 10^{24}$	$-1.96 \cdot 10^{23}$	4.6	11.5	193	938

Table 3.3 Density difference of gelatin, $\Delta\rho_{gel}$, density difference of dextran, $\Delta\rho_{dex}$, average blob size of gelatin, $\tilde{\zeta}_{gel}$, average blob size of dextran, $\tilde{\zeta}_{dex}$, number of gelatin monomers in a blob, $N_{blob,gel}$, and the number of dextran monomers in a blob, $N_{blob,dex}$ for the gelatin/dextran B system.

$\Delta\rho_{gel}$ (<i>molecules</i> / m^3)	$\Delta\rho_{dex}$ (<i>molecules</i> / m^3)	$\tilde{\zeta}_{gel}$ (<i>nm</i>)	$\tilde{\zeta}_{dex}$ (<i>nm</i>)	$N_{blob,gel}$ (<i>molecules</i>)	$N_{blob,dex}$ (<i>molecules</i>)
$1.33 \cdot 10^{24}$	$-6.79 \cdot 10^{22}$	5.0	14.9	218	1888
$1.56 \cdot 10^{24}$	$-8.29 \cdot 10^{22}$	4.9	14.2	208	1710
$1.95 \cdot 10^{24}$	$-1.02 \cdot 10^{23}$	4.8	13.7	196	1603
$2.09 \cdot 10^{24}$	$-1.11 \cdot 10^{23}$	4.8	13.4	195	1529
$2.42 \cdot 10^{24}$	$-1.22 \cdot 10^{23}$	4.7	13.2	187	1481

Table 3.4 Density difference of gelatin, $\Delta\rho_{gel}$, density difference of gum arabic, $\Delta\rho_{gum}$, average blob size of gelatin, $\tilde{\zeta}_{gel}$, average blob size of gum arabic, $\tilde{\zeta}_{ara}$, number of gelatin monomers in a blob, $N_{blob,gel}$, and the number of gum arabic monomers in a blob, $N_{blob,ara}$ for the gelatin/gum arabic system.

$\Delta\rho_{gel}$ (<i>molecules</i> / <i>m</i> ³)	$\Delta\rho_{ara}$ (<i>molecules</i> / <i>m</i> ³)	$\tilde{\zeta}_{gel}$ (<i>nm</i>)	$\tilde{\zeta}_{ara}$ (<i>nm</i>)	$N_{blob,gel}$ (<i>molecules</i>)	$N_{blob,ara}$ (<i>molecules</i>)
$7.83 \cdot 10^{23}$	$-4.54 \cdot 10^{22}$	5.6	15.3	265	3209
$6.75 \cdot 10^{23}$	$-5.41 \cdot 10^{22}$	5.7	14.0	279	2707
$1.11 \cdot 10^{24}$	$-8.93 \cdot 10^{22}$	5.4	13.1	244	2370
$1.39 \cdot 10^{24}$	$-1.20 \cdot 10^{23}$	5.2	12.3	228	2072
$1.74 \cdot 10^{24}$	$-1.50 \cdot 10^{23}$	5.0	11.6	214	1867

3.4 Results and discussion

The values for the average blob size of the biopolymers, the amount of monomers present in this blob size, and the excluded volume were inserted into equation (3.15) to obtain the interaction potential for the different systems. Since the interfacial tension of these systems is known, we could substitute this value for the interaction potential into equation (3.7) and estimate the interfacial thickness. For the pair correlation function we assumed $g(r)=1$, the correlation function for an ideal fluid. The values for the interfacial thickness were substituted in equation (3.8) to obtain the bending rigidity. The results of these calculations are presented in Tables 3.5 (gelatin/dextran A), 3.6 (gelatin/dextran B) and 3.7 (gelatin/gum arabic).

Table 3.5 Interfacial tension γ , interfacial thickness ξ , and bending rigidity k for the system gelatin/dextran A.

Interfacial tension ($\mu N/m$)	Interfacial thickness ^a (nm)	Bending rigidity ^{a,b} ($k_b T$)
0.5 ± 0.1	956 ± 239	418 ± 98
2.4 ± 0.3	408 ± 58	369 ± 49
5.9 ± 0.5	214 ± 19	241 ± 22
15.7 ± 0.7	117 ± 5	192 ± 10
19.3 ± 0.8	108 ± 5	202 ± 10

^a ξ and k are calculated according to the model. Only γ is measured experimentally.¹^b the temperature T is taken as 293 K.**Table 3.6** Interfacial tension γ , interfacial thickness ξ , and bending rigidity k for the system gelatin/dextran B.

Interfacial tension ($\mu N/m$)	Interfacial thickness ^a (nm)	Bending rigidity ^{a,b} ($k_b T$)
0.6 ± 0.1	1190 ± 610	763 ± 394
1.9 ± 0.3	760 ± 140	985 ± 175
3.4 ± 0.3	470 ± 45	665 ± 73
5.3 ± 0.4	386 ± 31	714 ± 49
7.1 ± 0.4	300 ± 18	566 ± 49
9.1 ± 0.6	273 ± 19	615 ± 49

^a ξ and k are calculated according to the model. Only γ is measured experimentally.

(Values are taken from chapter 2)

^b the temperature T is taken as 293 K.

Table 3.7 Interfacial tension γ , interfacial thickness ξ , and bending rigidity k for the system gelatin/gum arabic.

Sample number	Interfacial tension ($\mu\text{N}/\text{m}$)	Interfacial thickness ^a (nm)	Bending rigidity ^{a,b} ($k_b T$)
C ₁	1.5 ± 0.2	362 ± 56	180 ± 28
C ₂	6.7 ± 1.2	43 ± 9	12 ± 3
C ₃	9.7 ± 1.5	52 ± 10	25 ± 5
C ₄	12.9 ± 1.9	47 ± 7	26 ± 4
C ₅	14.9 ± 2.4	53 ± 9	33 ± 6

^a ξ and k are calculated according to the model. Only γ is measured experimentally.

(Values are taken from chapter 2)

^b the temperature T is taken as 293 K.

3.4.1 Interfacial thickness, scaling behavior

The interfacial tension can be estimated from the scaling relation $\gamma \propto (kT/\xi^2)^{18,20}$. To confirm whether this relation is observed for these different protein/polysaccharide systems, the interfacial tension is plotted against the interfacial thickness, and fitted with $\gamma = a/\xi^b$.

Figure 3.1 shows this relation for both gelatin/dextran systems. For the gelatin/dextran A system (squares), $b = 1.7 \pm 0.1$ gave the best fit. For the gelatin/dextran B system (triangles), b was found to be 1.7 ± 0.2 . The exponent b for both systems is in line with a theoretically expected value of 2. The thickness of the interfacial region for both systems is very large close to the critical point where the interfacial tension is very low. Further from the critical point, where the interfacial tension increases, the interfacial thickness decreases to a value in the order of the size of the polymers (100 nm).

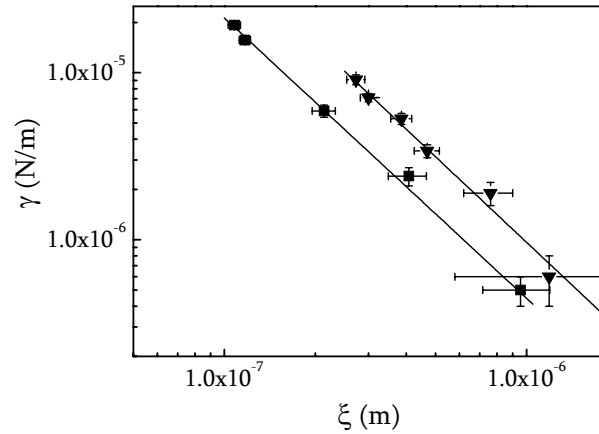


Figure 3.1 Interfacial tension γ versus interfacial thickness ξ for the gelatin/dextran A system (squares) and the gelatin/dextran B system (triangles). The phase diagram can be found in Figure 2.1 for the gelatin/dextran A system, and in Figure 2.2 for the gelatin/dextran B system.

The gelatin/gum arabic system, however, does not show this scaling relation. As can be seen in Figure 3.2, the thickness of the interfacial region is approximately constant within the statistical error and is found to be $\pm 50 \text{ nm}$, which is of the order of the size of the biopolymers. Only the interfacial thickness for sample C₁ deviates from this value. Since this sample was close to the critical point, the compositions of this sample were difficult to determine, and as a result, they do not coincide with the determined binodal (explanation can also be found in paragraph 2.3.4). These small deviations from the binodal have a large influence on the determination of the interfacial thickness.

From interfacial tension measurements and scaling behavior, we conclude that the gelatin/dextran systems are both near-critical, and that the gelatin/gum arabic system is off-critical in the investigated concentration regime, as described in chapter 2. Since the interfacial thickness in the critical point diverges, this indicates that mixtures that are near-critical should have diffuse interfacial regions that increase as the critical point is approached. For both gelatin/dextran systems this is indeed the case, and can thus be considered to be near-critical. Going further from the critical point, the interfacial thickness decreases and the system becomes off-critical. Since the

gelatin/gum arabic has a constant value for the interfacial thickness for all investigated samples, this system can be considered to be off-critical.

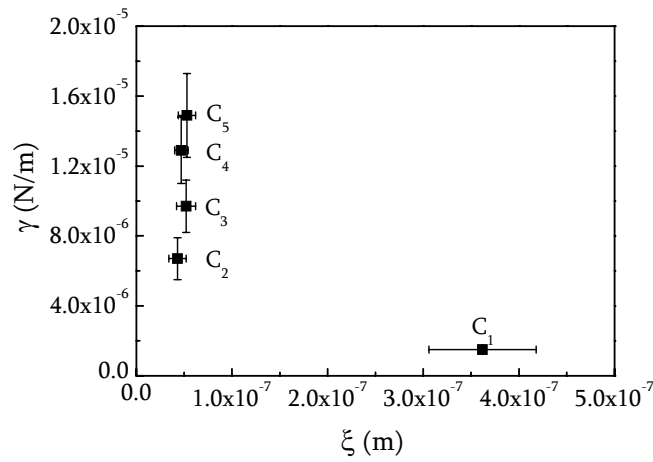


Figure 3.2 Interfacial tension γ versus interfacial thickness ξ for the gelatin/gum arabic system. The phase diagram is given in Figure 2.3.

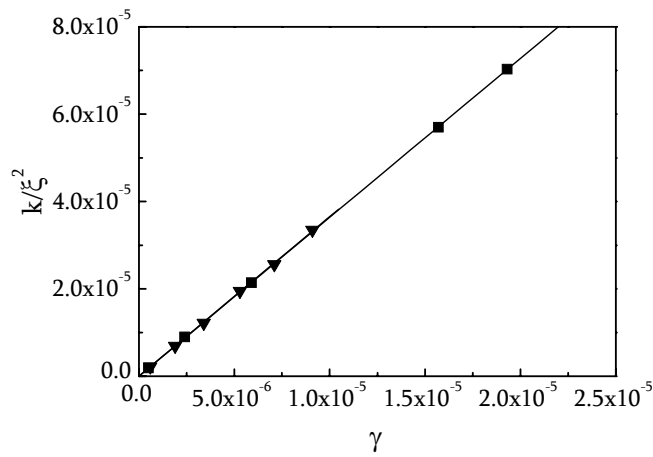


Figure 3.3 k/ξ^2 versus interfacial tension γ for the gelatin/dextran A system (squares) and the gelatin/dextran B system (triangles).

3.4.2 Bending rigidity, scaling behavior

In Tables 3.5 and 3.6 we see that the bending rigidity is approximately constant within the statistical errors for the near-critical gelatin/dextran systems, and is of the order of 200-1000 $k_b T$. For the off-critical gelatin/gum arabic system (Table 3.7), the bending rigidity is approximately 25 $k_b T$. Because of the uncertainty in the interfacial thickness for sample C₁, we attach little importance to the value of the bending rigidity of this particular sample.

According to Blokhuis and Bedeaux⁸ the bending rigidity close to the critical point, where $\xi \rightarrow \infty$, is given by

$$k = \left(\frac{1}{6}\pi^2 + 2\right)\gamma\xi^2 = 3.64\gamma\xi^2 \quad (3.16)$$

Since both gelatin/dextran systems are near-critical, these systems should obey this relation. As can be seen in Figure 3.3, this linear relationship is indeed obtained for both systems, with a slope of 3.65, in correspondence with the pre-factor in equation (3.16). For off-critical systems ($\xi \rightarrow 0$), Blokhuis and Bedeaux did not find such a relationship.

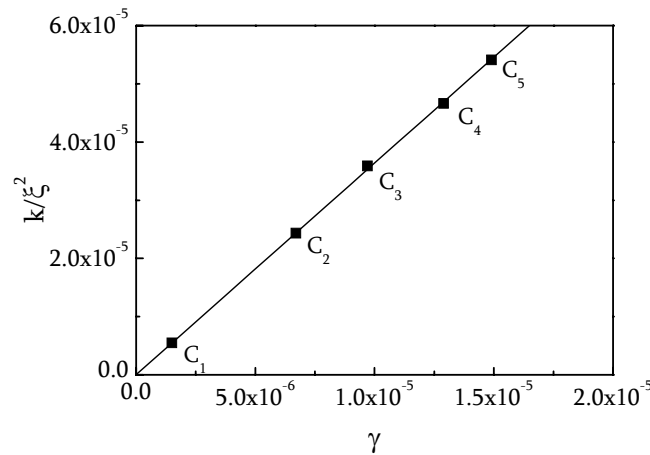


Figure 3.4 k/ξ^2 versus interfacial tension γ for the gelatin/gum arabic system.

However, when we plot k/ξ^2 versus γ for the off-critical gelatin/gum arabic system, we again observe a linear relationship (Figure 3.4), for which the slope corresponds with the pre-factor, 3.64, of equation (3.16). This linear relationship holds for all investigated protein/polysaccharide systems, and the bending rigidity can thus be determined for both near-critical and off-critical systems according to equation (3.16).

Since this equation is satisfied for all our investigated systems we can simply invert it to find $\gamma = k/3.64\xi^2$. We see that in the near-critical gelatin/dextran systems, in which the relation $\gamma \propto 1/\xi^2$ holds, k is a constant that can be determined from the slope of γ versus $1/\xi^2$. Using this relation for the near-critical systems, the bending rigidity was determined to be $200 k_b T$ for the gelatin/dextran A system and $615 k_b T$ for the gelatin/dextran B system. Contradictory to the near-critical samples, the off-critical gelatin/gum arabic system shows a constant interfacial thickness for the investigated concentration regime. Since equation (3.16) is also satisfied for this system, the bending rigidity is not expected to be constant but should increase with increasing interfacial tension (as the interfacial thickness is constant). Analogous to the procedure of calculating the bending rigidity from the interfacial thickness in near-critical systems, we can determine the interfacial thickness from the bending rigidity in off-critical systems. The relation $k = 3.64\gamma\xi^2$ shows that plotting the bending rigidity (k) versus the interfacial tension (γ) gives the interfacial thickness from the slope. Using this relation for the gelatin/gum arabic system we obtain an interfacial thickness of 50 nm .

Thus, even though for all systems the interfacial tension increases as the distance from the critical point increases, we find different scaling for the two other interfacial properties. In the case of near-critical systems, we find a decreasing interfacial thickness with increasing distance from the critical point and a constant bending rigidity. In the case of off-critical systems, we find a constant interfacial thickness, and the bending rigidity increases slightly with increasing distance from the critical point.

3.4.3 Influence of bending rigidity

The bending rigidities of the investigated off-critical gelatin/gum arabic system are comparable to those found in microemulsions and vesicle systems. However, the bending rigidities of the near-critical gelatin/dextran systems are much larger. Although the bending rigidities of vesicles and bilayers are normally of the order of $10 k_b T$, Bermudez et.al.²¹ recently reported for vesicles formed from OB18 (PEO₈₀-PBD₁₂₅), with a membrane thickness of 14.8 nm , bending rigidities of $460 k_b T$, which are comparable to the values we found for the near-critical systems. Since the interfacial tension of these systems is very low, the bending contribution to the interfacial energy may become dominant over the stretching contribution for several interfacial-related phenomena. For instance, relaxation times in bending-dominated systems will exhibit a different scaling with the droplet radius (R) compared to when the stretching contribution would be dominant (difference of a factor R^2). This may for instance apply to situations where deformation relaxation of a droplet interface occurs upon change in volume, while maintaining a constant area (thus making the stretching contribution irrelevant). Such a droplet deformation may in particular apply to aqueous phase-separated systems, where water exchange between the bulk phases is possible. Another situation where bending may dominate over stretching may occur at a droplet size where the bending energy, which is independent of the surface area, becomes larger than the stretching energy, which is dependent of the surface area of a droplet. Thus, there exists a particular crossover length scale (R_c) below which bending dominates over stretching. A rough estimate of this crossover length scale can be given by considering the two contributions to the interfacial energy to be equal. The interfacial free energy can be given as an integral over the surface as

$$F = \int \left(\gamma_0 + \frac{2k}{R^2} \right) dA \quad (3.17)$$

in which the first term signifies the stretching term, and the second term signifies the bending term. Integrating over the surface yields for the stretching term $4\pi\gamma_0 R^2$, and for the bending term $8\pi k$. Equating these two terms gives $R_c = \sqrt{2k/\gamma_0}$, the critical radius below which bending dominates stretching. Using $\gamma \approx O(10^{-6}) N/m$, and

$k \approx O(100) k_b T$, we find $R_c \approx O(1000) nm$. Since the interfacial tension can also be given in terms of the bending rigidity, $\gamma = k/3.64\xi^2$, we find that $R_c = 2.7\xi$ (i.e. thus the critical radius is of the same order of magnitude as the interfacial thickness). We stress that, since R_c becomes comparable to the interfacial thickness in these systems, the curvature cannot be considered to be small and equations (3.1) and (3.6) might not be valid in this limit. In this limit one has to take into account higher order terms in curvature and density profile. Thus, R_c can be considered as a rough estimate only. Using this estimation we find that for droplet radii smaller than 1 micron the contribution of the bending energy is expected to become important for these systems. This length scale is relevant to many practical circumstances (e.g. to shear-induced phase-separation and shear-induced droplet morphologies). It is also expected to be of relevance to the kinetics of phase separation in aqueous biopolymer systems, during stages where the domain size is smaller than R_c . The phase separation process will be discussed in the next chapter.

3.5 Conclusion

In this chapter we presented a model to calculate the interfacial thickness and bending rigidity for aqueous phase-separated biopolymer mixtures on the basis of the experimentally accessible interfacial tension. We determined these interfacial properties for three different protein/polysaccharide systems: two gelatin/dextran systems and one gelatin/gum arabic system. For the gelatin/dextran systems, the interfacial thickness was large for samples close to the critical point (1000 nm), and decreased for samples further from the critical point. The presence of the diffuse interfacial region indicated that the systems could be considered to be near-critical. For the gelatin/gum arabic system, the interfacial region was found to be constant and of the order of the size of the biopolymers (50 nm), which indicates that this system is off-critical. Using the calculated interfacial thickness we determined the bending rigidities of the systems. For the gelatin/dextran systems, the bending rigidity was found to be in the order of 500 $k_b T$ and for the gelatin/gum arabic system we found values of approximately 25 $k_b T$. The values for the interfacial thickness and the bending rigidity of the near-critical systems are much higher than those found in microemulsion systems, and may be important when the bending contribution to the

interfacial energy dominates the stretching contribution. This might be of relevance in several interfacial phenomena, such as droplet relaxation, (shear-induced) phase separation and shear-induced droplet morphologies.

Acknowledgements

We thank E. Blokhuis and H. Schaink for stimulating and helpful discussions.

References

- (1) Scholten, E.; Tuinier, R.; Tromp, R. H. and Lekkerkerker, H. N. W. *Langmuir* **2002**, *18*, 2234-2238.
- (2) de Hoog, E. H. A. and Lekkerkerker, H. N. W. *J. Phys. Chem. B* **1999**, *103*, 5274-5279.
- (3) de Hoog, E.; Lekkerkerker, H. N. W.; Schulz, J. and Findenegg, G. H. *J. Phys. Chem. B* **1999**, *103*, 10657-10660.
- (4) Milchev, A. and Binder, K. *Europhys. Lett.* **2002**, *59*, 81-86.
- (5) Mecke, K. R. and Dietrich, S. *Phys. Rev. E* **1999**, *59*, 6766-6784.
- (6) Blokhuis, E. M. and Bedeaux, D. *HCR advanced - educational review* **1994**, 55-68.
- (7) Blokhuis, E. M. and Bedeaux, D. *J. Chem. Phys.* **1991**, *95*, 6986-6988.
- (8) Blokhuis, E. M. and Bedeaux, D. *Physica A* **1992**, *184*, 42-70.
- (9) van Giessen, A. E. and Blokhuis, E. M. *J. Chem. Phys.* **2002**, *116*, 302-310.
- (10) Oversteegen, S. M. and Blokhuis, E. M. *J. Chem. Phys.* **2000**, *112*, 2980-2986.
- (11) Segovia-Lopez, J. G. and Romero-Rochin, V. *Phys. Rev. Lett.* **2001**, *86*, 2369-2372.
- (12) Varea, C. and Robledo, A. *Physica A* **1995**, *220*, 33-47.
- (13) Groenewold, J. and Bedeaux, D. *Physica A* **1995**, *214*, 356-378.
- (14) Helfrich, W. *Z. Naturforsch.* **1973**, *28c*, 693.
- (15) Kirkwood, J. G. and Buff, F. P. *J. Chem. Phys.* **1949**, *17*, 338-343.
- (16) Yamakawa, H. *Modern Theory of Polymer Solutions*, Harper & Row: New York, 1971.
- (17) Flory, P. J. and Krigbaum, W.R. *J. Chem. Phys.* **1950**, *18*, 1086-1094.
- (18) de Gennes, P. G. *Scaling Concepts in Polymer Physics*, Cornell University Press: New York, 1979.
- (19) Doi, M. and Edwards, S. F. *The Theory of Polymer Dynamics*, Clarendon Press: Oxford, 1999.
- (20) Rowlinson, J. S. and Widom, B. *Molecular Theory of Capillarity*, Clarendon Press: Oxford, 1984.
- (21) Bermudez, H.; Hammer, D. A. and Discher, D. E. *Langmuir* **2004**, *20*, 540-543.

Chapter 4

Coarsening rates of bicontinuous structures in
polymer mixtures

Coarsening rates of bicontinuous structures in polymer mixtures

Abstract

We discuss the coarsening of domains in bicontinuous structures of aqueous polymer mixtures, driven by hydrodynamic flow. Taking into account the bending energy as a contribution to the interfacial energy, we derive a general expression for the coarsening rate in these mixtures. Examining the limiting behavior of small and large length scales, we find two regimes. For small length scales, the size of the domains (Λ) scales with time (t) as $\Lambda \propto t^{1/3}$, while at large length scales, the domain size scales with time as $\Lambda \propto t$. The crossover between the two regimes occurs at a particular length scale, the critical radius R_c , which is dependent on the bending rigidity k , and the interfacial tension of a flat interface γ_0 ($R_c = \sqrt{2k/\gamma_0}$). In the case of aqueous biopolymer mixtures, we predict this particular length scale to be in the micron range. This new general expression for the coarsening of domains in aqueous polymer mixtures can explain experimental results [Lorén et al. *Macromolecules* **2001**, *34*, 8117], which show the two regimes of coarsening with a crossover at 4 microns.

4.1 Introduction

The kinetics of phase separation has received a lot of attention over the years, both experimentally and theoretically. Although a lot of mechanisms that have been proposed contribute to a better view of the phase separation process, a full understanding is still incomplete. In this chapter we focus on the coarsening of domains due to hydrodynamic flow in bicontinuous structures. This hydrodynamic flow is induced by the interfacial energy of the system, which is in general calculated using the interfacial tension of a flat interface, neglecting any curvature dependence of the interfacial energy.¹

However, Helfrich² showed in 1973 that the interfacial tension is curvature-dependent, and that bending contributions to the interfacial energy are also of importance. In chapter 3 we have shown that in near-critical biopolymer mixtures these bending contributions are considerable. To give a full description of the interfacial energy of a curved interface in biopolymer systems, the bending rigidity of the interface has to be taken into account. We derive a general expression for coarsening in polymer mixtures by hydrodynamic flow, by including the bending rigidity as a contribution to the interfacial energy. Examining the limiting behavior of small and large length scales, we find two regimes for the coarsening rate.

When phase separation occurs, the mixture becomes inhomogeneous by fluctuations in the concentration, which grow to equilibrium concentrations of the two coexisting phases of the mixture. The properties of the components and the kinetics of phase separation determine the morphology (droplets, bicontinuous structures) of the mixtures during phase separation. If one of the components is able to gel, a specific morphology of the mixture can be “frozen” by controlling the temperature during the phase separation. Understanding the kinetics of phase separation makes it possible to control the structure of phase-separated polymer systems, which affects both stability and macroscopic properties of those systems.

4.1.1 Phase separation

When the mixture is quenched into the metastable region, phase separation will occur through nucleation and growth. For deeper quenches, into the unstable state of the phase diagram, all concentration fluctuations will lead to a decrease in the free energy, and spinodal decomposition occurs,³ which is mainly observed for biopolymer mixtures.⁴⁻¹⁰ The time evolution in spinodal decomposition can be divided into two regimes:¹ the early stage and the late stage of phase separation. In the early stage, the system starts to develop inhomogeneities in the densities, which develop in time. In the late stage, the interfaces obtain their own interfacial characteristics. As the system favors a low interfacial free energy, the interfacial area will be decreased by the merging of domains, which will coarsen as the late stage of the phase separation continues.

4.1.2 Coarsening of domains

During the coarsening of the domains, different morphologies can evolve in time. In general, two different morphologies can be distinguished: the droplet morphology and the interconnected morphology, as depicted in Figure 4.1.

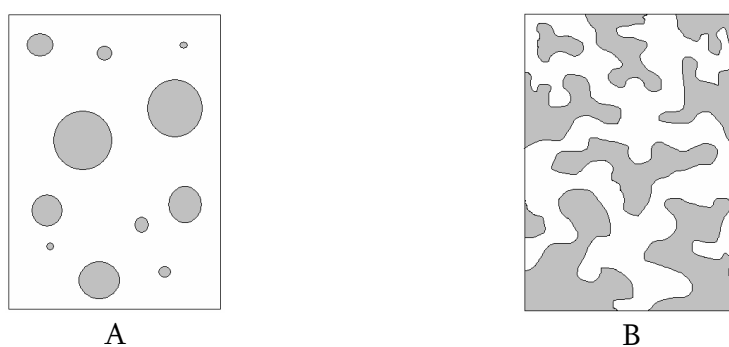


Figure 4.1. Morphologies that can be obtained during phase separation. A) droplet morphology; B) interconnected morphology.

Droplet morphologies are usually obtained for mixtures, in which the volume fraction of one of the two coexisting phases is very small. Mixtures that contain approximately equal volume fractions of both of the phases form interconnected

structures during the late stage of the phase separation. Thus, dependent of the composition of the mixture, the mixture can evolve through different morphologies, with their own characteristic length scales, Λ , which change during time.

The structure evolution during the early stage of spinodal decomposition was already described by Cahn and Hilliard in 1958.¹¹ They describe the free energy for an isotropic system of nonuniform composition or density, which is given in terms of a local density and the density gradients. This theory describes the time evolution of the density fluctuations, i.e., the stage of the phase separation during which particular wavelengths, Λ , grow in time. These growing wavelengths can be followed by light scattering by measuring the intensity at different wavevectors q . The term $\Lambda(q)$, known as the amplification factor, describes the coarsening of these fluctuations as a function of q . Plotting $\Lambda(q)/q^2$ versus q^2 , which is known as a Cahn-Hilliard plot, should yield a straight line in the early stage of phase separation. This early stage of phase separation has been studied for several (bio)polymer mixtures, but for most mixtures this linear Cahn-Hilliard plot has not been observed.^{4,6,12,13} This feature seems to be a general characteristic for polymer solutions. This indicates that the theory of Cahn and Hilliard does not describe the structure evolution of the early stage or that the early stage of phase separation is probably too short to be measured during the time frame of the experiments. Since polymers are larger than simple molecules, the interfaces between the domains in polymer mixtures are much thicker than in simple binary liquids, as described in chapter 3. The interfaces that are present in these mixtures can be viewed as interfacial regions, in which a concentration gradient for both (bio)polymers is present. Since the interfacial regions are relatively large and the gradients are relatively small, only small density fluctuations are needed to obtain these regions. Therefore, the formation of interfacial regions may be too fast to be measured with light scattering. This might explain why this regime is not observed by light scattering. As soon as the interfaces are formed, mass transport starts playing a role, which is a characteristic for the late stage of spinodal decomposition. This late stage is the more important regime for phase separating (bio)polymer mixtures.

4.1.3 Coarsening mechanisms

Late stage coarsening of the domains is characterized by a power law dependence of the domain size, $\Lambda \propto t^\alpha$, where α is an exponent, determined by the type of mass transport. In general, three different mechanisms are known:

(i) The evaporation-condensation mechanism (EC), or Ostwald ripening. In this mechanism, the bigger droplets grow at the expense of smaller ones by diffusion of material through the continuous phase into the larger droplets. This mechanism was described by Lifshitz and Slyozov in 1959.¹⁴

(ii) The Brownian-coagulation mechanism (BC), where the droplets move freely due to the Brownian motion and coalesce upon collision with another droplet. This mechanism was first described by Binder and Stauffer in 1974.¹⁵

(iii) Coarsening due to hydrodynamic flow (HF). In this mechanism, described by Siggia,¹ the flow in bicontinuous regions is driven by the gradient in the capillary pressure.

The driving force for phase separation for the first two mechanisms is the diffusion of material (EC) or droplets (BC). The coarsening of the domains with time for both mechanisms is described by $\Lambda \propto t^{1/3}$.^{14,15} For the HF-mechanism, the coarsening of the domains is driven by capillary forces. The coarsening of the domains is described by $\Lambda \propto t$.¹

The BC mechanism assumes the droplets move freely by Brownian motion and collide with another droplet. The EC-mechanism ignores the interactions between droplets. Because of these assumptions, both mechanisms are valid only in the limit of small volume fraction. Coarsening through diffusion is obtained only for phase separating mixtures that evolve through a droplet-type morphology. When the volume fraction of the dispersed phase becomes higher, hydrodynamic flow fields start playing an important role. For these higher volume fractions, the HF mechanism is the more appropriate one. Coarsening via hydrodynamic flow is thus obtained in phase separation mixtures that evolve through interconnected patterns (volume fraction close to 0.5). Since the volume fraction, and thus the domain geometry, determines the coarsening of phase separation, one would expect one dominating exponent for a specific volume fraction; either 1/3 for diffusive growth in droplet morphologies, or 1

due to hydrodynamic flow for interconnected structures. However, literature reports several crossover regimes from one exponent to the other.^{6,8,12,16,17} During the past decade, several explanations for these crossover regimes have been proposed.

Nikolayev et al.^{18,19} explain a crossover from $1/3$ to 1 in off-critical mixtures by coalescence limited by hydrodynamics. For high volume fractions, elongated structures may be obtained, where the hydrodynamics play an important role. Tanaka^{20,21} describes a similar mechanism for the crossover from $1/3$ to 1 in off-critical mixtures. He states that droplets experiencing a collision have a much higher probability of a subsequent collision with a third neighboring droplet. This mechanism is called collision-induced collision. He also mentions a second mechanism that might be important at higher volume fractions, which is known as the interface quench effect. Contrary to a crossover from $1/3$ to 1 , a crossover from 1 to $1/3$ has also been observed experimentally.^{22,23} This reduction in the growth rate has been explained by “pinning”.^{24,25} Pinning occurs when a bicontinuous microstructure is transformed into a droplet type pattern due to the breakup of the interconnected structures. When the structures break up into discrete droplets due to Rayleigh instabilities, the diffusion process might dominate over the hydrodynamic flows, and causes the growth rate to decrease (from an exponent of 1 to an exponent of $1/3$). These coarsening mechanisms can explain a crossover from $1/3$ to 1 for mixtures that evolve through droplet morphologies, and a crossover from 1 to $1/3$ for mixtures with interconnected patterns.

4.2 Comparison with experimental data

Recently, Lorén et al.²⁶ studied the late stage phase separation of a gelatin/maltodextrin sample of different concentrations and different quenches. For a 4% (w/w) gelatin and 7.3% (w/w) maltodextrin mixture, they report CLSM pictures taken during the entire process. The pictures show interconnected structures, in which the interfacial region continues to be very large throughout the entire phase separation process (micron range). They measured the growth rate for the coarsening patterns and found an exponent of $1/3$ for small length scales, and an exponent of 1 for larger length scales. The crossover from $1/3$ to 1 was observed at approximately 4 microns. The authors conclude that the first part of the evolution is governed by

diffusion. However, the diffusion mechanisms are valid only for small volume fractions, i.e., droplet morphologies. Because interconnected structures are observed throughout the entire process, the volume fraction exceeds the volume fraction still applicable for the diffusion process. Therefore, the exponent $1/3$ (and subsequently the crossover from $1/3$ to 1) cannot simply be explained by the diffusion mechanisms or other mechanisms such as the collision-induced-collision mechanism, the interface quench effect, or pinning.

In the next section, we will propose an alternative explanation for this crossover between $1/3$ and 1 in bicontinuous structures by using hydrodynamic flow. We derive a new expression for the hydrodynamic flow, by taking the bending rigidity of the interfaces as a contribution to the interfacial energy. As a result, we obtain two regimes with a crossover at a particular length scale R_c .

4.3 Contribution of bending rigidity to hydrodynamic flow

Interfacial tension measurements show that biopolymer mixtures show near-critical behavior in a large concentration regime.²⁷⁻²⁹ Depending on the concentration quench into the phase diagram, and subsequently the location of the mixture on the tie-line, these mixtures can evolve via droplet or interconnected morphologies. When the system is situated in the middle of the tie-line, one obtains near-critical systems that evolve through interconnected structures. For this type of morphology, the coarsening rate is determined by the capillary instability of the domains. The interfacial energy induces a flow field in the domains, described by the Navier-Stokes equation

$$\rho \frac{\partial \vec{v}}{\partial t} + \rho (\vec{v} \cdot \vec{\nabla} \vec{v}) = -\vec{\nabla} P + \rho \vec{g} + \eta \nabla^2 \vec{v} \quad (4.1)$$

in which \vec{v} is the flow velocity, ρ the density of the fluid, P the thermodynamic pressure, \vec{g} the gravitational constant and η the viscosity of the fluid. For biopolymer mixtures in steady flow (i.e., $\frac{\partial \vec{v}}{\partial t} = 0$), the $(\vec{v} \cdot \vec{\nabla} \vec{v})$ term and the gravitational term ($\rho \vec{g}$) can be neglected. The Reynolds number, Re , can be estimated by $\rho \cdot \Lambda \bar{v} / \eta$. Assuming Poiseuille flow in the bicontinuous structures¹ of length l , we can write $Re = \rho \cdot \Lambda^2 \gamma / \eta^2 l$. Using $\eta \approx O(10^{-2}) Pa s$, $\rho \approx O(10^3)$, $\Lambda \approx O(10^{-6})$, $\gamma \approx O(10^{-6})$, and

$l \approx O(10^{-5})$, we find that $\text{Re} \approx O(10^{-5})$, i.e., viscous effects dominate inertial effects. Using the above, the equation of motion can be written in the following form

$$0 = -\bar{\nabla} P + \eta \nabla^2 \vec{v} \quad (4.2)$$

Since both the pressure and the velocity depend on the curvature of the domains, and the curvatures are related to the size of the domains (Λ), as the only relevant length scale, we approximate the pressure gradient by $\Delta P/\Lambda$. Here, ΔP denotes the difference in pressure over a distance Λ (the background pressure is taken constant and its gradient 0). The Laplacian of the velocity can be approximated by v/Λ^2 . Substituting this into equation (4.2) one arrives at

$$\eta \frac{v}{\Lambda^2} \approx \frac{\Delta P}{\Lambda} \quad (4.3)$$

In this equation, the velocity is the time derivative of the domain size ($v = d\Lambda/dt$). The difference in pressure (ΔP) is determined by the interfacial tension, γ , and Λ ($\Delta P \propto \gamma/\Lambda$). Since the interfaces of the domains are not flat but curved, we express the interfacial tension in terms of its curvature as

$$\gamma(J, K) = \gamma_0 + kC_0 J + \frac{1}{2} kJ^2 + \bar{k}K \quad (4.4)$$

Assuming that the spontaneous curvature is zero, neglecting $\bar{k}K$, and substituting $J = -2/\Lambda$, the interfacial tension can be given by

$$\gamma(\Lambda) = \gamma_0 + \frac{2k}{\Lambda^2} \quad (4.5)$$

The first term signifies the stretching contribution to the interfacial energy and the second term signifies the bending contribution. Thus, the interfacial tension that causes the flow field and subsequently the coarsening of the domains can be divided in two different terms. The stretching contribution, which can be viewed upon as the interfacial tension of a flat interface, is size independent. However, the second term, which describes the bending contribution, is dependent on the curvature and thus on the size of the local curvature of the bicontinuous structures. The smaller these structures are, the larger their curvature is, and the larger the relative importance of the bending contribution is. Combining equations (4.3) and (4.5), we obtain

$$\frac{d\Lambda}{dt} \approx \frac{\gamma_0}{\eta} + \frac{2k}{\eta\Lambda^2} \quad (4.6)$$

which leads to the following expression for the coarsening of the domains of a phase-separating mixture

$$\Lambda - R_c \arctan\left(\frac{\Lambda}{R_c}\right) \approx t \frac{\gamma_0}{\eta} \quad (4.7)$$

where $R_c = (\sqrt{2k/\gamma_0})$ is the crossover length scale where the stretching and the bending terms in equation (4.5) are equal. For $\Lambda \ll R_c$, the function $\arctan(\Lambda/R_c)$ can be approximated by $\Lambda/R_c - \Lambda^3/3R_c^3$. For $\Lambda \gg R_c$, $\arctan(\Lambda/R_c)$ approaches $\pi/2$. Taking the limits of small and large length scales, we obtain two regimes for the coarsening of the domains.

$$\frac{\Lambda\eta}{\gamma_0} \propto t \quad \Lambda \gg R_c \quad (4.8a)$$

$$\frac{\Lambda^3\eta}{6k} \propto t \quad \Lambda \ll R_c \quad (4.8b)$$

So, in the limit of $\Lambda \gg R_c$, the domain size scales with time as $\Lambda \propto t$, which is equivalent to the scaling of the HF-mechanism, in which only the curvature-independent interfacial tension is taken into account. Since we included the bending rigidity, we obtain a different expression in the limit of $\Lambda \ll R_c$, for which the coarsening scales as $\Lambda \propto t^{1/3}$. At length scales where the stretching term dominates, the coarsening exponent will be 1, while at length scales where the bending contribution dominates the coarsening exponent will be 1/3. The crossover between the regimes occurs at $\Lambda \approx R_c$. The larger the bending rigidity and the smaller the interfacial tension of the interfaces between the separating domains, the larger this crossover length scale is.

In chapter 3 we have shown that for near-critical phase-separated biopolymer mixtures, the bending rigidity is relatively large ($500 k_b T$).³⁰ Since the interfacial tension of these mixtures is very low, and the bending rigidity is large, the length scales for which the bending contribution dominates increases significantly compared to other systems. A scaling relation (as discussed in paragraph 3.4.3) showed that for these near-critical systems the crossover length scale, for which the bending dominates the stretching energy, is of the order of a micron. So, taking into account

the bending rigidity of the curved interfaces, for near-critical biopolymer systems we expect to find a crossover from a coarsening exponent of $1/3$ to an exponent of 1 at a length scale in the order of a micron.

From the results of Lorén et al.²⁶ we can conclude that the phase separation of the gelatin/maltodextrin mixtures evolves through interconnected structures throughout the whole process. For this morphology, the process is driven by the hydrodynamic flow in the domains, but the HF-mechanism cannot explain the crossover. However, our description of the hydrodynamic flow including the bending rigidity *does* explain a crossover between the exponents. They²⁶ found that the crossover between the exponents occurs at a length scale of approximately 4 microns, which is of the same order of magnitude as we predicted from scaling. Thus, taking into account the bending rigidity, we are able to explain these experimental results, which cannot be explained by any other described mechanism in literature.

4.4 Conclusion

We have shown that for near-critical biopolymer systems the scaling of the domain size with time during the late stage of phase separating mixtures changes with time. For mixtures that contain a high volume fraction of the dispersed phase, hydrodynamic flow determines the coarsening of the domains in the phase separation process. We derived a general expression for the hydrodynamic flow that includes the bending rigidity of the interface and obtained a new description for the coarsening of the domains. Taking the limits $\Lambda \gg R_c$ and $\Lambda \ll R_c$, we found that the domain size with time scales as $\Lambda \propto t^{1/3}$ for small length scales and as $\Lambda \propto t$ for larger length scales. The crossover between these two exponents occurs when the stretching contribution to the interfacial energy equals the bending contribution. The crossover length scale, R_c , is equal to $\sqrt{2k/\gamma_0}$, which in the case of biopolymer mixtures can be expected to be in the micron range. This new description for coarsening by hydrodynamic flow can explain the crossover that is observed for mixtures that evolve through interconnected structures throughout the entire phase separation process.

References

- (1) Siggia, E. D. *Phys. Rev. A* **1979**, *20*, 595-605.
- (2) Helfrich, W. *Z. Naturforsch.* **1973**, *28c*, 693.
- (3) Dhont, J. K. G. *An Introduction to Dynamics of Colloids*; Elsevier Science B.V.: Amsterdam, 1996.
- (4) Anderson, V. J. and Jones, R. A. L. *Polymer* **2001**, *42*, 9601-9610.
- (5) Butler, M. F. and Heppenstall-Butler, M. *Biomacromolecules* **2003**, *4*, 928-936.
- (6) Verhaegh, N. A. M.; van Duijneveldt, J. S.; Dhont, J. K. G. and Lekkerkerker, H. N. W. *Physica A* **1996**, *230*, 409-436.
- (7) Butler, M. F. and Heppenstall-Butler, M. *Food Hydrocolloids* **2003**, *17*, 815-830.
- (8) Tuinier, R.; Dhont, J. K. G. and de Kruif, C. G. *Langmuir* **2000**, *16*, 1497-1507.
- (9) de Hoog, E. H. A. and Tromp, R. H. *Colloid Surf. A-Physicochem. Eng. Asp.* **2003**, *213*, 221-234.
- (10) Williams, M. A. K.; Fabri, D.; Hubbard, C. D.; Lundin, L.; Foster, T. J.; Clark, A. H.; Norton, I. T.; Lorén, N. and Hermansson, A.-M. *Langmuir* **2001**, *17*, 3412-3418.
- (11) Cahn, J. W. and Hilliard, J. E. *J. Chem. Phys.* **1958**, *28*, 258-267.
- (12) Tromp, R. H.; Rennie, A. R. and Jones, R. A. L. *Macromolecules* **1995**, *28*, 4129-4138.
- (13) Rojanapitayakorn, P.; Thongyai, S. and Covavisaruch, S. *J. Polym. Sci. Pt. B-Polym. Phys.* **2003**, *42*, 871-885.
- (14) Lifshitz, I. M. and Slyozov, V. V. *J. Phys. Chem. Solids* **1961**, *19*, 35-50.
- (15) Binder, K. and Stauffer, D. *Phys. Rev. Lett.* **1974**, *33*, 1006-1009.
- (16) Butler, M. F. and Heppenstall-Butler, M. *Biomacromolecules* **2001**, *2*, 812-823.
- (17) Butler, M. F. *Biomacromolecules* **2002**, *3*, 1208-1216.
- (18) Nikolayev, V. S.; Beysens, D. and Guenoun, P. *Phys. Rev. Lett.* **1996**, *76*, 3144-3147.
- (19) Nikolayev, V. S. and Beysens, D. A. *Phys. Fluids* **1997**, *9*, 3227-3234.
- (20) Tanaka, H. *Phys. Rev. Lett.* **1994**, *72*, 1702-1705.
- (21) Tanaka, H. *J. Chem. Phys.* **1995**, *103*, 2361-2364.
- (22) Cabral, J. T.; Higgins, J. S.; Yerina, N. A. and Magonov, S. N. *Macromolecules* **2002**, *35*, 1941-1950.
- (23) Takeno, H. and Hashimoto, T. *J. Chem. Phys.* **1997**, *107*, 1634-1644.
- (24) Crist, B. *Macromolecules* **1996**, *29*, 7276-7279.
- (25) Chen, H. and Chakrabati, A. *J. Chem. Phys.* **1998**, *108*, 6006-6013.

- (26) Lorén, N.; Altskär, A. and Hermansson, A.-M. *Macromolecules* **2001**, *34*, 8117-8128.
- (27) Antonov, Y. A.; van Puyvelde, P. and Moldenaers, P. *Int. J. Biol. Macromol.* **2004**, *34*, 29-35.
- (28) Scholten, E.; Tuinier, R.; Tromp, R. H. and Lekkerkerker, H. N. W. *Langmuir* **2002**, *18*, 2234-2238.
- (29) Scholten, E.; Visser, J. E.; Sagis, L. M. C. and van der Linden, E. *Langmuir* **2004**, *20*, 2292-2297.
- (30) Scholten, E.; Sagis, L. M. C. and van der Linden, E. *J. Phys. Chem. B* **2004**, *108*, 12164-12169.

Chapter 5

Effect of permeability on aqueous biopolymer
interfaces in spinning drop experiments

Effect of permeability on aqueous biopolymer interfaces in spinning drop experiments

Abstract

We show that interfaces in aqueous phase-separated biopolymer mixtures are permeable for all components present in the system. In spinning drop experiments, droplets of the low-density phase decreased up to 90% in volume over a time span of days to weeks, when inserted in a matrix of the high-density phase. We propose an expression for this change of volume in time in terms of the diffusion coefficients of the components. From the magnitude of these coefficients, we conclude that the transfer of gelatin from inside the droplet to the outer phase was the rate determining step in this process. Since the interfaces are permeable to all components, the properties of the system change in time. Therefore, this technique is not an accurate method for the measurement of the exact value for the interfacial tension for these aqueous phase-separated systems.

5.1 Introduction

Interfacial tension plays a role in many interfacial phenomena, and is of importance in a large variety of applications. The interfacial tension is the driving force for phase separation, a process used for the isolation of water-soluble ingredients, such as proteins, nucleic acids, viruses and cells.¹ It also plays a role in the oil tertiary recovery process.^{2,3} Since the interfacial tension plays a role in the phase separation process, it is also of importance in the formation of morphologies in aqueous phase-separated mixtures. These aqueous (biopolymer) mixtures are often used to create a large diversity of products and materials with unique properties (e.g. food, pharmaceuticals and cosmetics). It is therefore of practical interest to gain a better knowledge of the values for the interfacial tension in these mixtures.

There are different techniques that can be used to measure the interfacial tension, which can basically be classified into three groups:

- a) Techniques that use the balance between interfacial forces and gravitational forces, such as the Wilhelmy plate and the pendant drop technique.
- b) Techniques that use the equilibrium shape and size of dispersed droplets, such as the spinning drop method,^{4,5} and deformation of droplets in a flow field.^{6,7}
- c) Techniques based on the dynamics of dispersed droplets, such as the breaking thread method,⁸ and the relaxation behavior of deformed drops after the cessation of an applied flow field.⁹

Since the techniques of class a) depend on gravitational forces, they cannot be used to measure very low interfacial tensions encountered in aqueous phase-separated systems. For these systems, the interfacial tension can be measured only by techniques of class b) and c). These two methods use the same approach; the interfacial forces determined by the interfacial tension, are balanced by some other force, which is obtained by an applied force field.

These techniques are accepted as reliable methods and are therefore widely used to measure interfacial tensions in (aqueous) phase-separated (bio)polymer systems. Although these methods seem to be easy and to give good results, some difficulties and peculiarities were observed in the past. Guido et. al.¹⁰ reported measurements of Na-

caseinate and Na-alginate mixtures for which they measured the interfacial tension by applying the droplet deformation technique. They found that when one phase was injected into the other phase, the size of the droplets decreased in rest. They attributed this effect to temperature effects and non-equilibrium effects. Van Puyvelde et. al.¹¹ measured the interfacial tension of aqueous gelatin/dextran mixtures. They used light scattering to follow the deformation of the dispersed droplets, which were placed in a shear cell. After subjecting the droplets to a flow field, they observed homogenization of the immersed droplets into the other phase. As a result, they found a shear rate dependent phase diagram of these ternary mixtures. Ding et. al.¹² also measured gelatin/dextran mixtures and observed a difference in interfacial tension with different shear rates. Chan et. al.¹³ observed a similar effect for spinning drop measurements on silicone oil/water and water/air systems. For increasing rotation speeds they found an increase in the interfacial tension for both systems. They investigated several possible causes, such as the effect of capillary width, lack of gyrostatic equilibrium, lagging of the drop diameter behind the rotation speed, pressure effects in the capillary and heat effects of the bearing house, but neither one of these effects seem to be able to explain the observed phenomenon. They concluded that this effect might be attributed to flow patterns in the tube, and that these secondary flows might effect the equilibrium shape of the droplet. Guido et. al.¹⁴ studied diffusion effects in a polymer blend, and showed droplet shrinkage from 67 to 51 micrometer in a few days as a result of the solubility of PIB in PDMS.

Although a lot of these peculiarities have been discussed in literature for different systems, a good and clear explanation has never been given. In this chapter, we want to address the problem of the size and shape change of droplets for aqueous phase-separated biopolymer systems, also known as water-in-water emulsions. In these systems, both coexisting phases consist of about 90% water. Since the water does not have any specific preference to stay in either the upper or lower phase, water can diffuse through the interface depending on the forces that act on the system. These interfaces can thus be compared with permeable membranes. In this chapter, we want to investigate whether or not and to what extent this permeability plays a role in the change in size and shape of dispersed droplets.

5.2 Experimental section

We performed spinning drop measurements on mixtures with different compositions. The advantage of the spinning drop method is that only one droplet of the low-density phase is inserted in a matrix of the high-density phase, so the droplet is not influenced by interactions of neighboring droplets, as could be the case in techniques based on deformation and relaxation measurements. All effects observed can be attributed to one droplet and the surrounding medium. With this technique it is reasonably easy to measure different properties (such as shape, volume and interfacial tension) of the droplet in a long time frame, so time effects can be tracked easily. To perform these experiments we have used several aqueous fish gelatin/dextran mixtures at different concentrations, and with compositions in the two-phase region. These systems become inhomogeneous upon mixing and phase separate in time. No centrifugation technique was used to speed up the process of phase separation, since a real thermodynamic equilibrium is needed to be able to dismiss possible non-equilibrium effects in the experiments. Centrifugation might slightly change the phase behavior, as in a similar way shear does.¹¹

5.2.1 Materials

The high molecular weight fish gelatin was kindly provided by Norland Products Incorporated, Cranbury, US. The molar mass, M_w , of the gelatin is 102 *kDa*. Fish gelatin is known for its low gelling temperature, and therefore all mixtures remain liquid-like in a large concentration range, which is a prerequisite to be able to use the spinning drop method. The dextran was purchased from Sigma-Aldrich and has a molar mass, M_w , of 511 *kDa*.

5.2.2 Methods

5.2.2.1 Preparation of the biopolymer mixtures

Gelatin and dextran were dissolved simultaneously in a 0.05 M NaI solution. This small amount of salt was used to increase the solubility of the gelatin. Sodiumazide (0.02%) was added as an antimicrobial agent. The mixtures were left overnight to soak

the biopolymers, after which they were dissolved easily by heating them at approximately 40°C for about 30 minutes and frequent shaking. All mixtures became opaque, and phase separation was allowed to take place to obtain two distinct clear phases. The two phases were removed from each other using a syringe. After the separation, both phases were clear without the presence of small immiscible droplets of the other phase.

5.2.2.2 Determination of the concentration of biopolymers in both phases

The concentration of the biopolymers in the phases was determined by measuring the optical rotation of the phases with a Perkin-Elmer polarimeter. The optical rotation was measured at 80°C since at this temperature, the optical rotation of the mixture was found to be a simple addition of the contribution of each biopolymer. The details about this analysis can be found in paragraph 2.2.2.3.

5.2.2.3 Determination of the densities of both phases

The spinning drop method is a fairly easy technique to measure the interfacial tension. The only disadvantage is that the precise density difference between the two phases is needed in order to calculate the interfacial tension. Since in phase-separated biopolymer mixtures both phases consist mainly of water, the density difference is very small (especially for samples close to the critical point). The viscosities of the mixtures were very high and direct density measurements on the solutions were hampered. Therefore, we calculated the densities of the phases using the densities of the pure components rather than measuring them. The densities of the dry components were determined from calibration curves, for which the densities of solutions with different concentrations were measured with an Anton Paar DMA 5000 density meter.

5.2.2.4 Spinning drop measurements

We have used the SVT20, a spinning drop tensiometer from Dataphysics, Germany. This apparatus consists of a capillary that is mounted on a tilting table. The capillary is surrounded by an oil bath, which regulates the temperature of the capillary. Because the temperature of the capillary can be controlled well, heating effects did not play a role in the measurements that were performed. The capillary was filled with the high-density phase of the phase-separated mixtures with the use of a syringe. As the

viscosity of these solutions was substantial, the solutions were rotated overnight at high rotational speed to collect possible air bubbles, which could disturb the shape of the droplets and might induce flow effects. Before a droplet of the low-density phase was inserted with a microsyringe, the high-density solution was checked for air bubbles. The position of the table was adjusted in order to prevent the droplet from wandering to either side of the tube. The apparatus is equipped with a light source, for which the intensity can be varied. A camera is placed in front of the capillary and has a zoom function that allows measuring the size of the droplets at different magnifications. The camera is connected to a computer with a frame grabber and software to calculate the interfacial tension with the appropriate method (Vonnegut⁴ or Cayias-Schechter-Wade¹⁵). Using a template that can be placed around the droplet, the shape and size of the droplet was determined, from which the volume and the interfacial tension were calculated.

5.3 Results and discussion

5.3.1 Phase diagram and coexisting phases

For the spinning drop experiments, different samples were prepared that differ in concentration. The samples were allowed to phase separate after which the concentration of both phases was determined with the use of polarimetry. From the calculated concentrations, the phase diagram was determined. Figure 5.1 shows this phase diagram, in which the open circles represent the overall concentration of the mixtures. As can be seen, the gelatin concentration was kept constant, while the concentration of dextran was varied.

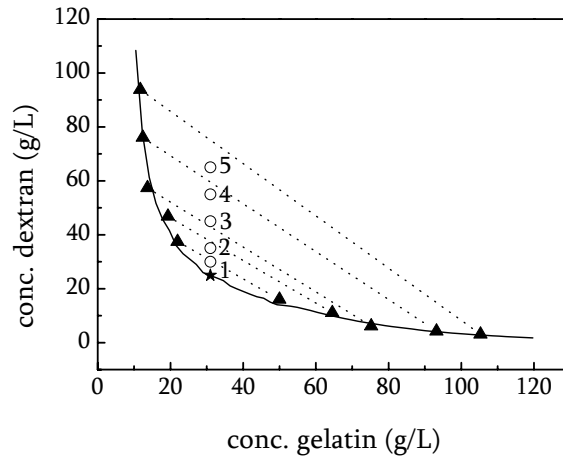


Figure 5.1 Phase diagram of the gelatin/dextran mixtures. The star denotes the critical point. The open circles refer to the overall concentrations of the mixtures that have been prepared. The triangles refer to the compositions of the upper and the lower phase after the mixtures were phase-separated. The solid line is the binodal, which connects the compositions of the phases after phase separation.

5.3.2 Densities of the phases

The densities of the separate components were determined to be 1.367 g/mL for the dry fish gelatin, 1.603 g/mL for the dry dextran, and 1.005 g/mL for the 0.05 M NaI solution. Using these densities, the densities of both phases of all samples were calculated. In addition, the difference in density between the two phases, $\Delta\rho$, was calculated, and was used by the software of the SVT20 to calculate the interfacial tension.

5.3.3 Spinning drop experiments

In order to compare the results of the spinning drop measurements, we performed all measurements at the same speed, which was 1000 rpm . Higher rotational speeds were not possible, since the elongation of the droplets would be of such extent that the droplets disappear partially out of sight. As a consequence, the volume of the droplets

cannot be measured. A lower rotational speed is undesirable, since a certain minimum deformation of the droplets is needed to be able to measure the interfacial tension accurately. Therefore, the range of rotational speeds that could be used was rather narrow.

5.3.3.1 Droplet volume measurements

To be able to compare the effects between different samples, we tried to control the volume of the droplet that was inserted, which was approximately $2.5 \mu\text{L}$. The samples were inserted into the capillary and the rotational speed was set at 1000 rpm. As soon as the droplet was located in the middle of the capillary and did not appear to change shape, the volume of the droplet was determined. This value was taken as the initial volume of the droplet. Figure 5.2 shows an example of a droplet at different times during the experiment. The left picture shows the volume at the beginning of the experiment ($t=0$) and the right side shows the volume after a few days.

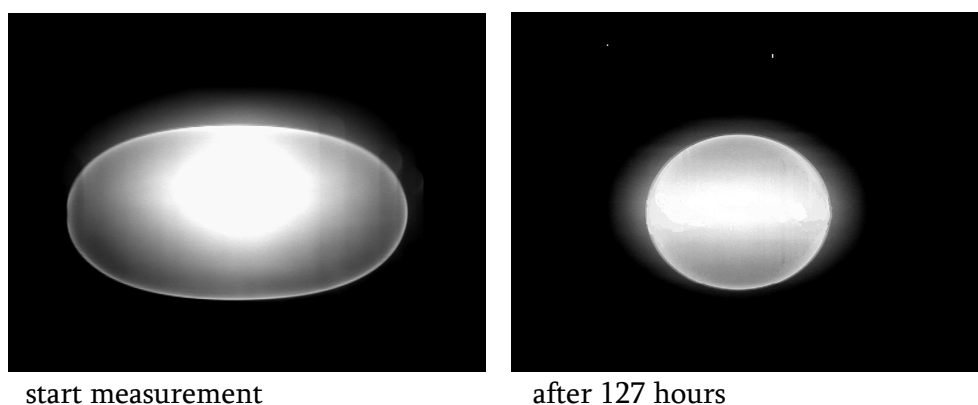


Figure 5.2 Shape and size evolution of a droplet during the spinning drop experiments. The magnification of the frames is the same. The pictures were taken from sample 3, for which the overall concentration is denoted by the open circle in Figure 5.1 and the composition of the phases by the triangles.

These results show that the droplets become smaller in time, which indicates that the interface is permeable to certain components. But to which components is the interface permeable? There are three components present in this system: the biopolymers gelatin and dextran and the solvent water. Since water molecules are

much smaller than the biopolymers and smaller than the mesh size of the phases, water should be able to diffuse through the interface with ease. The biopolymers are normally present in the semi-dilute regime in either one of the phases and due to their entanglements, the biopolymers will exhibit hindered diffusion. So, one might expect that only the water would diffuse through the interface. However, if water is the only component that diffuses through the interface, the concentrations of the biopolymers within the droplets would increase to such extent that the density within the droplet would exceed the density of the outer phase. In that case, the droplet would not have stayed in the middle of the capillary, since the low-density phase is pushed to the middle by the centrifugal forces. This indicates that the density of the droplet is always lower than the surrounding medium, for which the density remains effectively unchanged since its volume is approximately 3 orders of magnitude larger. This indicates that also biopolymers should be expelled from the droplet in order to keep the droplet density lower than the density of the surrounding medium.

We can explain this phenomenon by a shift in the binodal under the influence of the applied force field. Puyvelde et. al.¹¹ showed that for a gelatin/dextran mixture subjected to high shear rates, the phase behavior is different compared to the phase behavior at rest. They reported the phase diagram, with accompanying binodal, and showed that under shear the binodal shifts as depicted in Figure 5.3. This means that when dispersed droplet of these mixtures are subjected to a force field, the binodal shifts and therefore the equilibrium composition of the coexisting phases belonging to the overall composition will change. As can be seen in Figure 5.3, the equilibrium composition of the upper phase (number 1) has shifted towards a lower concentration of gelatin, while the equilibrium composition of the lower phase (number 2) has shifted to a higher concentration of gelatin. Therefore, the droplet will expel gelatin in order to lower its concentration, while the outer phase will take up gelatin from the droplet in order to increase the gelatin concentration. However, the concentration of the outer phase remains effectively unchanged since the volume of the outer phase is about 3 orders of magnitude higher than the droplet phase. Therefore, the outer phase continues to take up gelatin from the droplet, which results in a large decrease of its concentration in the droplet. Consequently, the droplet will start to expel water in order to keep the gelatin concentration at the desired value for the composition of the gelatin-rich phase (number 1). Dextran will either enter or leave the droplet

depending on its overall concentration. Since the composition of the outer phase will never change sufficiently, the system will never reach a stage with two equilibrium coexisting phases, so the system keeps transferring both biopolymers and water until eventually the droplet will disappear.

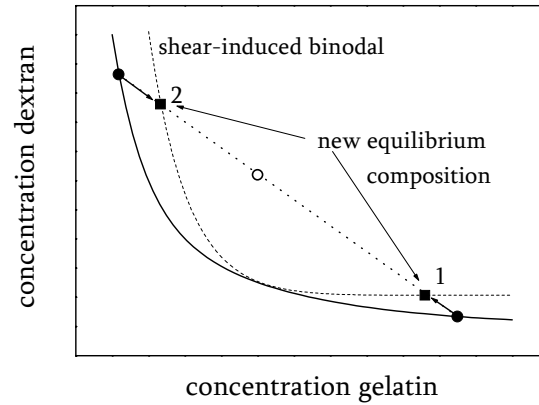


Figure 5.3 Schematic picture of the composition of the droplet in the capillary during the spinning drop experiment based on the phase diagram provided by van Puvelde et. al.¹¹ The solid line refers to the binodal in rest. The dashed line refers to the shear-induced binodal. The new equilibrium compositions of any overall composition (open circle) on the tie-line (dotted line) are denoted by the squares. The old equilibrium compositions in rest are denoted by the circles. The droplet phase is referred to as number 1 and the surrounding medium as number 2.

Figure 5.4 shows the volume of these droplets in time, normalized by the initial size of the droplet. From the explanation described above, the droplets should disappear, as the composition of the droplet approaches the composition of the surrounding phase. However, in our experiments we do not observe the disappearance of the droplets, since at a certain size its position starts to deviate from the middle of the capillary. At this point, the centrifugal force ($\propto \Delta\rho\omega^2r$, where $\Delta\rho$ is the density difference between the two phases, ω is the rotation speed and r is the distance from the middle of the capillary) equals the gravitational force ($\propto \Delta\rho g$, where g is the gravitational constant). When the droplets become even smaller, the centrifugal force is not sufficient to exceed the gravitational force and the droplet is pulled up by gravity.

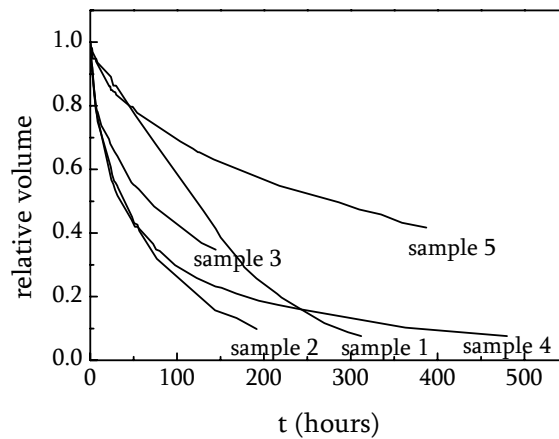


Figure 5.4 Volume change of all samples during time.

We see from these results that samples 1, 2 and 4 reduce in size by almost 90 %. At that size, the droplets started to move from the middle of the capillary. For sample 3 and 5 the measurement was stopped at 60% decrease. During the experiments, we noticed that when the droplet is elongated, the short axis of the droplet does not change significantly; only the long axis of the droplets. When the droplets become smaller and approach a more spherical shape, the width of the droplets starts to reduce as well. This might be explained by the fact that due to the larger curvature in the caps of the elongated droplets, the pressure in the caps is larger than in the middle of the droplet. Therefore, the diffusion of components might be more pronounced in the caps.

The rate at which the components diffuse through the interface depends on several parameters that can enhance or hinder the diffusion, such as the viscosity, the density difference, the size of the biopolymers and the mesh size of the entangled polymer solutions. Due to the distribution of the components, dextran is concentrated in the lower phase and gelatin is concentrated in the upper phase. Therefore, the dextran concentration inside the droplets and the gelatin concentration outside the droplet are in the dilute regime. In this regime, the biopolymers are present as random coils, and the characteristic length scale is the radius of gyration. The dextran concentration outside the droplet and the gelatin concentration inside the droplet are in the semi-dilute regime. So inside the droplet, there is an entangled network with a certain mesh

size of gelatin, and outside the droplet, there is an entangled network with a mesh size of dextran. The mesh size of the network and the size of the biopolymers diffusing through the network will influence the diffusion rate.

Comparing for example sample 1 and 5, we see that the gelatin concentration inside the droplet differs with a factor of 2. Sample 1 has a concentration of about 50 mg/mL and sample 5 has a concentration of more than 100 mg/mL . Since the concentration is related to the mesh size, we can say that the mesh size of the network of sample 5 is much smaller than in sample 1. Since the network of sample 5 is much more compact, the diffusion of the biopolymers will be hindered more. In a similar way, we also see that the dextran concentration for sample 5 in the surrounding medium is higher than for sample 1. Thus, besides having a much denser gelatin network in the droplet, it also has a network of dextran with a smaller mesh size in the surrounding medium. The denser the network, the more hindered is the diffusion of the components.

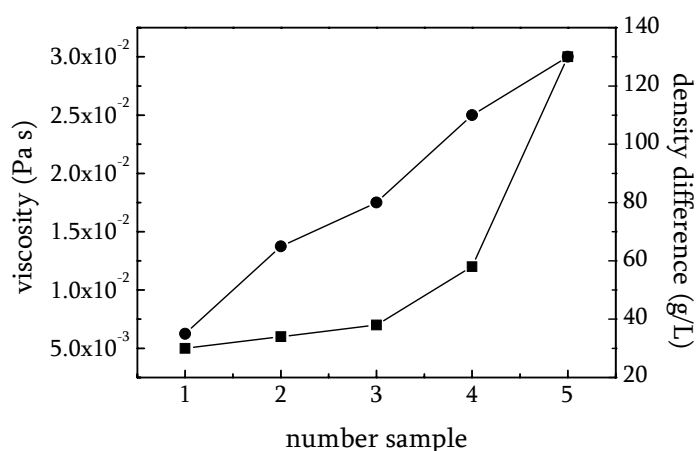


Figure 5.5 The average viscosity (●) of the system and the difference in density (■) between the two phases at the beginning of the experiment.

Figure 5.5 shows the viscosity and the density difference between the two phases at the beginning of the experiment. The density difference can be viewed upon as a driving force for diffusion, since this is related to the length of the tie-lines and thus also to the difference between the composition of the original phases and the new

equilibrium composition on the shear-sensitive binodal. The viscosity of the solution slows down the diffusion of the biopolymers.

All these variables determine the rate of the diffusion for the components. From Figure 5.4 we can see that there is no straightforward relation between the change of volume of the droplet and any of the variables, which indicates that apparently all variables are important in the diffusion process. For example, for sample 1, the density difference is very small, so there is a small driving force for the diffusion. On the other hand, the viscosity is small and the mesh size of the network is large, so this will increase the rate of the diffusion process. Looking at the properties of sample 5 we see that the density difference is much higher so there is a larger driving force for diffusion. However, the viscosity is also much higher, which hinders the diffusion. Also the mesh size of the gelatin network inside the droplet and the dextran network outside the droplet is much smaller, which also hinders the diffusion. The balance between these different parameters eventually determines the overall rate of the diffusion process.

The diffusion process is considered to be Fickian and we assume the total diffusion to be a linear addition of contributions from the diffusion of both the biopolymers and the water. The differential equation for the total change in volume in time can be described as¹⁶

$$\frac{dV_{total}}{dt} = f(V_{\infty} - V_t) \quad (5.1)$$

where f is the rate constant for the change in volume, V_{∞} is the volume at the end of the process and V_t is the volume of the droplet at time t . Integration of this equation leads to

$$V_{total,t} = V_{\infty} + A \cdot \exp(-ft) \quad (5.2)$$

where A is a constant. Since we assume that the diffusion process is a combination of the diffusion of the separate components, i , we describe the total change in volume as

$$V_{total,t} = V_{total,\infty} + \sum_i A_i \cdot \exp(-f_i t) \quad (5.3)$$

The rate constant f_i , is related to a diffusion coefficient, D_i , and the diameter of the droplet, d , as¹⁶

$$f_i = \frac{4\pi^2 D_i}{d^2} \quad (5.4)$$

Table 5.1 shows the results of the fits of equation (5.3) through the data points from Figure 5.4, which gives three diffusion coefficients with the use of equation (5.4); a clear identification of those coefficients in terms of the three components cannot be made, since the diffusion of the components is coupled. For the value of the diameter of the droplet, we have taken the initial diameter at the beginning of the experiment.

Table 5.1 Diffusion coefficients for the three components.

Sample	$D_1 \text{ (m}^2/\text{s)}$	$D_2 \text{ (m}^2/\text{s)}$	$D_3 \text{ (m}^2/\text{s)}$
1	--	--	--
2	$3.2 \cdot 10^{-12}$	$3.2 \cdot 10^{-12}$	$2.2 \cdot 10^{-13}$
3	$3.9 \cdot 10^{-12}$	$3.9 \cdot 10^{-12}$	$2.2 \cdot 10^{-13}$
4	$2.6 \cdot 10^{-12}$	$3.9 \cdot 10^{-13}$	$7.2 \cdot 10^{-14}$
5	$1.3 \cdot 10^{-12}$	$1.6 \cdot 10^{-14}$	$1.6 \cdot 10^{-14}$

For sample 1, no satisfactory results were obtained for the fits. For all other samples, we find three diffusion coefficients, which are related to the diffusion of the three components.

In order to determine which process is the rate determining step that eventually determines the total time for the reduction of the droplets volume, we compare these values to the self-diffusion coefficients of the components. The self-diffusion coefficient of the components can be estimated from the following relation

$$D_{self} = \frac{k_b T}{6\pi\eta R_h} \quad (5.5)$$

in which k_b is the Boltzmann constant, T is the temperature, η is the viscosity and R_h is the hydrodynamic radius of the component. Taking the hydrodynamic radius as 8.4 nm (as determined by viscosity measurements) we find self-diffusion coefficients for gelatin ranging from $2.5 \cdot 10^{-12} \text{ m}^2/\text{s}$ for sample 1 to $8.4 \cdot 10^{-13} \text{ m}^2/\text{s}$ for sample 5. The values for dextran are of the same order of magnitude, since the radius of dextran

is comparable to that of gelatin. The self-diffusion coefficient for water is equal to $2.3 \cdot 10^{-9} \text{ m}^2/\text{s}$, 3 orders of magnitude larger than the diffusion coefficient of gelatin. We see that the diffusion coefficients deduced from the fits are comparable to the self-diffusion coefficient of the biopolymers. From this we can conclude that the rate of the diffusion process is not dominated by the diffusion of water, which can diffuse most easily through the samples due to its small size. As described before, the droplet will try to decrease its concentration in gelatin and to increase its concentration in dextran. Since the droplets decrease in volume, the diffusion of gelatin to the outer phase appears to be more pronounced than the diffusion of the dextran. Therefore, we assume that the diffusion of the gelatin is the rate determining step. The rate of the other diffusion processes is constrained by the diffusion of the gelatin.

5.3.3.2 Interfacial tension measurements

Due to the permeability of the interface in these aqueous ternary mixtures, the properties of the interface change during time as all components can transfer through the interface. The change in composition of the droplet phase depends on the shift in the binodal and the rate of the diffusion of the different components. As a result, the density of the droplet will change and subsequently a difference in density between the two phases will change as well. Since the exact density difference is needed in order to calculate the interfacial tension, an error will be present in these calculations. Besides a change in the bulk properties of the samples, the properties of the interface also change. As the composition of the phases changes, the concentration profile in the interfacial region of both gelatin and dextran will differ from its original profile. This results in a change of the thickness of the interfacial region, ξ . This interfacial region is related to the interfacial tension as $\gamma \propto 1/\xi^2$,¹⁷ so a change in composition will result in a change in interfacial thickness and subsequently a change in interfacial tension. So, on the one hand, there is an error in the calculations of the interfacial tension since the density of the droplet changes, and on the other hand, the interfacial tension changes due to the change in concentration profile. Thus, during spinning drop experiments, the interfacial tension is not constant but will change in time, and no equilibrium interfacial tension can be determined with this method. Figure 5.6 shows an example of the change in interfacial tension in time. (The measurements for the other samples are not shown, but give similar results.) The interfacial tensions

were calculated using the initial value of the density difference between the two phases.

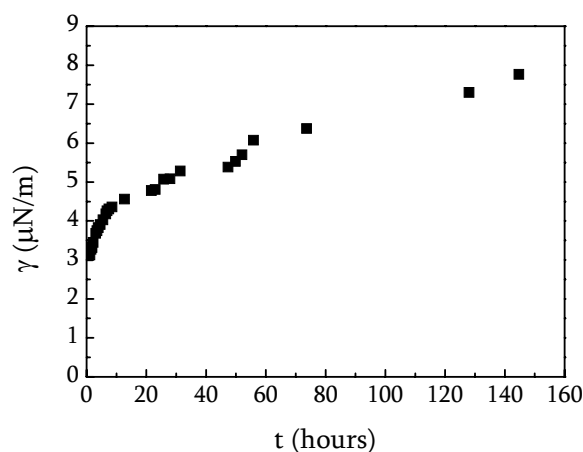


Figure 5.6 Interfacial tension versus time for sample 3 (31/45 *mg / ml* gel/dex)

Taking into account the permeability of the interfaces in phase-separated biopolymer mixtures, we can conclude that measuring the interfacial tension at equilibrium for these systems is not possible with the spinning drop technique. At the moment a force is applied on the droplet, the binodal of the system will change, and therefore the coexisting phases in the spinning drop tensiometer are not in equilibrium. Due to this non-equilibrium state, all components in the sample will start diffusing in order to reach a new equilibrium state, which will never be reached. This causes a change in composition and therefore a change in properties of the bulk phase as well as the interface. To what extent the properties will be different than their equilibrium values in rest, partly depends on the shift in the binodal for the shear-induced phase diagram. The larger the shift in the binodal is, the larger is the deviation from the properties in the bulk and the interface compared to their properties in rest, and the larger is the error in the interfacial tension. For phase-separated biopolymer mixtures, one should use another method in order to measure the exact value for the interfacial tension. The spinning drop method is not accurate enough to determine the exact value for the interfacial tension, but can only be used to obtain an estimate of the magnitude of the interfacial tension.

5.4 Conclusion

We have performed spinning drop experiments to investigate the possible effect of interfacial permeability on the value for the interfacial tension in phase-separated aqueous biopolymer mixtures. These systems consist of two coexisting phases, both with 90% water. Low-density phase droplets were inserted in a high-density matrix, and the droplets decreased in size by about 90% over a time span of several days when the droplets were rotated around their horizontal axis. The results indicate that the interfaces of these droplets are permeable to all components in the system: water and the biopolymers gelatin and dextran. The rate of volume change depends on several parameters of the system, such as the viscosity, the density difference, and the length scales in the system. We suggest a relation for the change in volume in time, which is related to the separate contributions of the components. From this relation, we obtain three different diffusion coefficients, which range from approximately $1.6 \cdot 10^{-14} \text{ m}^2/\text{s}$ to $3.9 \cdot 10^{-12} \text{ m}^2/\text{s}$. These values are comparable to the self-diffusion coefficient of gelatin and dextran, from which we conclude that the diffusion of gelatin is the rate determining step in the process. Due to the diffusion of the components, the composition of the phases changes in time and as a result the properties of the bulk phases and the interface change. This means that for these aqueous phase-separated biopolymer systems, the spinning drop method is not accurate enough to measure the exact value for the interfacial tension.

References

- (1) Hoebe, M. A.; van der Lans, R. G. J. M.; van der Wielen, L. A. M. and Kwant, G. *AIChE J.* **2004**, *50*, 1156-1168.
- (2) Bi, Z.; Liao, W. and Qi, L. *Colloid Surf. A-Physicochem. Eng. Asp.* **2005**, *256*, 117-121.
- (3) Liu, Q.; Dong, M.; Zhou, W.; Ayub, M.; Zhang, Y. P. and Huang, S. *J. Pet. Sci. Eng.* **2004**, *43*, 75-86.
- (4) Vonnegut, N. *Rev. Sci. Instrum.* **1930**, *13*, 99.
- (5) Princen, H. M.; Zia, I. Y. Z. and Mason, S. G. *J. Colloid Interface Sci.* **1967**, *23*, 99.
- (6) Taylor, G. I. *Proc. Roy. Soc. A* **1932**, *138*, 41-48.
- (7) Taylor, G. I. *Proc. Roy. Soc. A* **1934**, *146*, 501-523.
- (8) Lekkerkerker, H. N. W. and de Hoog, E.H.A. *Physica A* **2001**, *298*, 69-74.
- (9) Mellema, J.; Blom, C. and Beekwilder, J. *Rheol. Acta* **1987**, *26*, 418-427.
- (10) Guido, S.; Simeone, M. and Alfani, A. *Carbohydr. Polym.* **2002**, *48*, 143-152.
- (11) van Puyvelde, P.; Antonov, Y. A. and Moldenaers, P. *Korea-Aust. Rheol. J.* **2002**, *14*, 115-119.
- (12) Ding, P.; Wolf, B.; Frith, W. J.; Clark, A. H.; Norton, I. T. and Pacek, A. W. *J. Colloid Interface Sci.* **2002**, *253*, 367-376.
- (13) Chan, C. C. V.; Elliott, J. A. W. and Williams, M. C. *J. Colloid Interface Sci.* **2003**, *260*, 211-218.
- (14) Guido, S.; Simeone, M. and Villone, M. *Rheol. Acta* **1999**, *38*, 287-296.
- (15) Cayias, J. L.; Schechter, R. S. and Wade, W. H. *The measurement of low interfacial tension via the spinning drop technique*, Adsorption at interfaces, in: ACS Symposium Series, Mittal, K. L. **1975**, *8*, 234-247.
- (16) Berens, A. R. and Hopfenberg, H. B. *Polymer* **1978**, *19*, 489-496.
- (17) Rowlinson, J. S. and Widom, B. *Molecular Theory of Capillarity*, Clarendon Press: Oxford, 1984.

Chapter 6

Effect of interfacial permeability on droplet relaxation
in biopolymer-based water-in-water emulsions

Effect of interfacial permeability on droplet relaxation in biopolymer-based water-in-water emulsions

Abstract

In this chapter we show that for aqueous phase-separated biopolymer mixtures (water-in-water emulsions) both interfacial tension and permeability of the interface are important for the relaxation process of deformed droplets. We give an expression for the characteristic relaxation time that contains both contributions. With this description, the interfacial tension and the permeability can be deduced from cessation-of-flow experiments. The results show that for samples that are very close to the critical point the interfacial tension, calculated without taking into account the permeability, are overestimated significantly. For samples close to the critical point, the permeability has to be taken into account in the description for the relaxation time to get a reliable estimation of the interfacial tension. Our experiments show that for these systems the effective permeability is inversely proportional to the interfacial tension, $\lambda_{eff} \propto 1/\gamma$, and proportional to the square of the interfacial thickness, $\lambda_{eff} \propto \xi^2$. We find that the permeability is related to an effective diffusion coefficient as $D_{eff} \propto \gamma \lambda_{eff}$. From this relation, we find that the diffusion coefficient is equal to $0.9 \cdot 10^{-9} \text{ m}^2/\text{s}$, which is close to the self-diffusion coefficient of water; $D_w^0 = 2.3 \cdot 10^{-9} \text{ m}^2/\text{s}$. This indicates that only water diffuses through the interface and the diffusion coefficient is independent of the composition of the system for the concentration regime that is used.

6.1 Introduction

Phase separation is a common phenomenon that often occurs in polymer or biopolymer mixtures. Phase separation results in the formation of an interface, separating two bulk phases, and the interfacial properties are interesting from both a fundamental and an applied point of view. Many industries (food, pharmaceutical, plastics, personal care) make use of this phenomenon to create a diversity of products, and the properties of these products, such as stability, shelf life, and sensorial perception, are strongly influenced by the morphologies (droplets dispersed in a matrix, bicontinuous phases) formed after phase separation has occurred. In the plastic industry, mixtures of immiscible synthetic polymers are used to create a large variety of soft and hard composites. In the food industry, phase separation is used in the production of low-calorie products as a substitute for fatty products. To obtain the right sensory perception, such as mouth-feel, the morphology of the structures is a critical parameter. During the fabrication process, these products are exposed to flow fields, which influence their morphology (deformation, breakup, coalescence). The interplay between viscous forces and interfacial forces (such as interfacial tension) determines the magnitude of the changes in the morphology. Understanding the phase separation process and the resulting interfacial properties are key ingredients to influence and control product properties.

In the past decade, extensive research has been performed on polymer blends¹⁻⁹ and biopolymer mixtures.¹⁰⁻¹⁶ In most of these investigations, dispersions of droplets of one phase in a matrix of the other phase are subjected to different types of flow, and the effects on the morphology are investigated with methods such as the deformed drop retraction^{1,2,6} or droplet deformation method.^{5,7,10-13,15,16} The deformation of droplets in both methods can be followed by microscopic observations, small angle light scattering (SALS) or rheo-optics. Because of the applied shear flow, the droplets are deformed and form ellipsoidal droplets. At steady-state deformation, the viscous forces that act on the droplet are balanced by the interfacial forces. Assuming that the interfacial tension is the only parameter that contributes to the interfacial forces, one can determine the interfacial tension from the viscous forces that are applied.¹⁷ However, we will show that in the case of biopolymer mixtures the interfacial tension is not the only parameter that contributes to the deformation and relaxation behavior.

Biopolymer mixtures exist of more than 90% water. When these mixtures phase separate, the main ingredient of both coexisting phases is water. These systems can thus be considered as water-in-water emulsions. Since the solvent (water) does not have any specific preference to stay in either the upper or lower phase, water can diffuse through the interface depending on the forces that act on the system. These interfaces can thus be compared with membranes that have a permeability.¹⁸ This permeability can contribute to the deformation and relaxation behavior and can therefore influence the morphologies of the systems.

In chapter 5 we have shown that the permeability of the interface is of importance in aqueous biopolymer mixtures. In this chapter we will focus on the effect of this permeability on the relaxation of droplets after cessation of shear flow.

6.2 Experimental section

6.2.1 Materials and Methods

To obtain aqueous phase-separated biopolymer mixtures, we have mixed gelatin with dextran in water. At low concentrations these mixtures phase separate into two clear phases, with the lower phase enriched in dextran and the upper phase enriched in gelatin. All experiments are performed at room temperature (25°C). We have used a high molecular weight fish gelatin (instead of mammalian gelatin), with a low gelling temperature, to ensure that all mixtures stay liquid at room temperatures. The high molecular weight gelatin was kindly provided by Norland Products Incorporated, Cranbury, U.S. The molecular weight, M_w , of the gelatin is 102 *kDa*. The dextran was purchased from Sigma-Aldrich and has a molecular weight, M_w , of 511 *kDa*.

6.2.1.1 Preparation of the biopolymer mixtures

The mixtures of gelatin and dextran were prepared by dissolving these biopolymers simultaneously in a 0.05 M NaI solution. This low molar salt solution was used to enhance the solubility of the gelatin. Sodiumazide (0.02%) was added as an antimicrobial agent. The mixtures were allowed to stand overnight, after which they were heated at 40°C for about 30 minutes and shaken frequently to obtain

homogeneous mixtures. After they were cooled to room temperature, they were allowed to stand in order for the separation to complete. For the concentrated mixtures, this could take a few days/weeks. A faster method to obtain two separated phases would be to centrifuge at high speeds. However, centrifugation might influence the phase behavior of the system, since the interfaces are permeable. This could induce a non-equilibrium state of the mixture, and therefore, we chose not to follow this procedure. After the mixtures were completely separated, the upper phase was removed from the lower phase.

6.2.1.2 Determination of concentrations of biopolymers in both phases

The concentration of biopolymers in mixtures was determined by measuring the optical rotation with a Perkin-Elmer polarimeter. Before the mixtures were measured, they were diluted 20-50 times. The details of this analysis technique can be found in paragraph 2.2.2.3.

6.2.1.3 Determination of viscosity of both coexisting phases

To determine the viscous forces that act on the droplets, the viscosities of both the lower phase and the upper phase were determined. Here, we make use of the intrinsic viscosities of both biopolymers. The viscosity of a polymer solution can be described by¹⁹

$$\eta_{rel} = 1 + [\eta_0] \cdot c + \frac{1}{25} ([\eta_0] \cdot c)^{7/2} \quad (6.1)$$

in which η_{rel} is the relative viscosity of the solution, η_0 the intrinsic viscosity, and c the concentration of the biopolymer. The intrinsic viscosity is a specific property of a biopolymer. When two different biopolymers are mixed, we assume that the intrinsic viscosity of the mixtures can be described as a function of the separate intrinsic viscosities as

$$[\eta_0]_{mix} = [\eta_0]_1 \cdot f_1 + [\eta_0]_2 \cdot f_2 \quad (6.2)$$

where f_i is the mass fraction of polymer i . By inserting this intrinsic viscosity of the mixtures in equation (6.1) and taking c as the total biopolymer concentration, the relative viscosity of the biopolymer solution can be calculated. The relative viscosity of seven samples of both gelatin and dextran, with concentrations ranging from 1 to 100 mg/mL, were measured with Ubbelohdes at room temperature (25°C). From

these measurements, the intrinsic viscosities of gelatin and dextran were deduced and used to calculate the intrinsic viscosity of mixtures. Equation (6.2) is valid only when the intrinsic viscosity of a mixture is a simple addition of the separate contributions. To test whether this relation holds for the concentration regime of the experiments, the viscosity of mixtures of gelatin and polysaccharides were measured and compared to the determined viscosity according to equation (6.2). The calculated values were in good agreement with the experimental values (within 5% deviation).

6.2.1.4 Relaxation experiment

To be able to tell whether the permeability contributes to the relaxation of deformed droplets in cessation-of-flow experiments, we have performed relaxation measurements. When droplets are subjected to a shear flow $\dot{\gamma}$, the droplets will deform because of the viscous forces that act on the droplet. After cessation of the flow, the interfacial forces will induce a retraction of the droplet to the energetically more favorable spherical shape. For these experiments, six samples were used with different concentrations of the polysaccharide and a fixed concentration of gelatin. After the separation of the phases, the upper phase was redispersed into the lower phase with a ratio of 0.075 (volume-based). The dispersions were poured into a parallel plate shear cell (Linkam Scientific Instruments, type CCS 450), with a rotating lower plate and a fixed upper plate. The shear cell is mounted on a microscope (Zeiss Axioskop 2 plus) equipped with a CCD camera (Hitachi CCD color camera). A shear rate was chosen in the range from 0.01 to 0.2 s^{-1} . (The relaxation time of the droplets is assumed to be independent of the shear rate). The gap size between the plates was adjusted to at least 4 times the droplet size, to exclude possible wall effects. The dispersions were subjected to a shear flow until an equilibrium size was obtained, and then the shear flow was stopped. The retraction of the droplet after the cessation of flow was recorded with a speed of 5 frames per second. By analyzing the different frames, the deformation of the droplets can be followed in time.

The deformation is determined using the approach as used by e.g. Mellema et. al.²⁰ A weakly deformed sphere with an initial radius R_0 can be described in spherical coordinates by²¹

$$R(\theta, \varphi) = R_0 + s(\theta, \varphi) \quad (6.3)$$

The function $s(\theta, \varphi)$ can be expanded in spherical harmonics. Here we approximate $s(\theta, \varphi)$ by the second-order Legendre polynomial $s = \frac{1}{2} s_2 (3 \cos^2 \theta - 1)$, where s_2 is the amplitude of the deformation, equal to $\frac{2}{3}(a - b)$. The parameters a and b are the major axis and minor axis of the deformed droplet. The time evolution of the amplitude of deformation can be expressed as

$$s_2 = s_0 \exp\left(\frac{-t}{\tau}\right) \quad (6.4)$$

in which s_0 is an unknown parameter, t is time, and τ is the characteristic relaxation time for the given system. The deformation of the droplet in time gives the system-specific relaxation parameter τ . Expressions that link this parameter to the viscosity of the phases and interfacial properties are discussed in the next section.

6.3 Results and discussion

6.3.1 Phase behavior and distribution of biopolymers

We have studied six samples with varying composition and varying distance from the critical point. The concentration of gelatin was kept constant, while the concentration of dextran varied. The samples were allowed to phase separate, after which the phases were separated from each other with a syringe. The optical rotation of both phases was determined with the use of polarimetry, as described in paragraph 2.2.2.3, from which the concentrations of both biopolymers in both phases could be determined. The phase diagram is given in Figure 6.1. The overall concentrations and the distribution in both the upper and lower phase are given in Table 6.1.

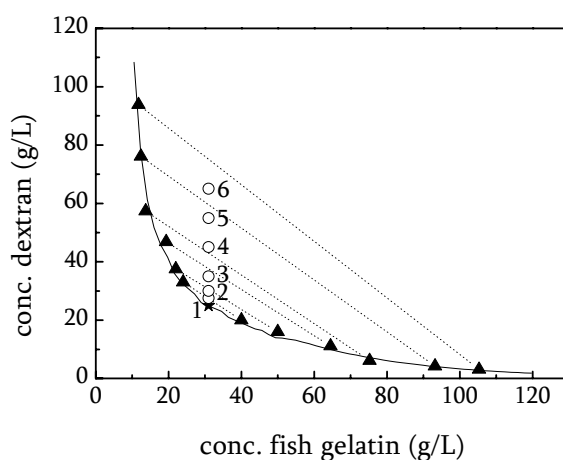


Figure 6.1 Phase diagram of the gelatin/dextran system. The open circles refer to the overall compositions, the star denotes the critical point, and the triangles refer to the compositions of the coexisting phases.

Table 6.1 Overall concentrations and distribution of both biopolymers.

Sample	Overall Conc. Fish Gelatin (g / L)*	Overall conc. Dextran (g / L)*	Upper phase		Lower phase	
			Conc. gelatin	Conc. Dextran	Conc. gelatin	Conc. dextran
1	31	30	40.0	21.5	32.0	27.5
2	31	35	50.0	16.0	22.0	37.5
3	31	40	64.5	11.1	19.3	46.8
4	31	45	75.2	6.1	13.7	57.4
5	31	55	93.2	4.2	12.4	76.1
6	31	65	105.3	3.1	11.7	93.8

* solvent that was used is a 0.05 M NaI solution.

Table 6.2 Viscosities of upper and lower phase of used samples given in Table 6.1.

Sample	phase	$[\eta_0]_{mix}$ (L / g)	η_{rel}	η ($mPa \cdot s$)
1	upper	0.059	8.23	7.3
	lower	0.061	7.59	6.8
2	upper	0.058	9.19	8.2
	lower	0.061	8.37	7.4
3	upper	0.057	12.01	10.7
	lower	0.062	10.69	9.5
4	upper	0.056	13.85	12.3
	lower	0.063	13.05	11.6
5	upper	0.056	21.78	19.4
	lower	0.063	23.32	20.8
6	upper	0.056	29.16	26.0
	lower	0.063	39.10	34.8

6.3.2 Phase behavior and viscosities of separated phases

The intrinsic viscosity, $[\eta_0]$, of gelatin was determined to be $0.0558 L / g$, and the intrinsic viscosity of dextran was determined to be $0.0646 L / g$. With equation (6.2), the intrinsic viscosities of any mixture with different fractions of gelatin and dextran could be calculated. Inserting this intrinsic viscosity into equation (6.1) gives the relative viscosity of the mixtures. By using the viscosity of the water at 25°C ($\eta = 0.89 mPa \cdot s$), these relative viscosities can be converted to the viscosities of the phases, as summarized in Table 6.2.

6.3.3 Relaxation behavior

To perform the relaxation experiments, a small fraction of the upper phase was redispersed into the lower phase. A shear rate was applied to break up the droplets to a final size between 20 and $70 \mu\text{m}$ (experimental size limit). Figure 6.2 shows an example of the retraction of droplets. Only droplets that have no contact with any

other droplet were taken into account, to avoid interaction effects between the droplets.

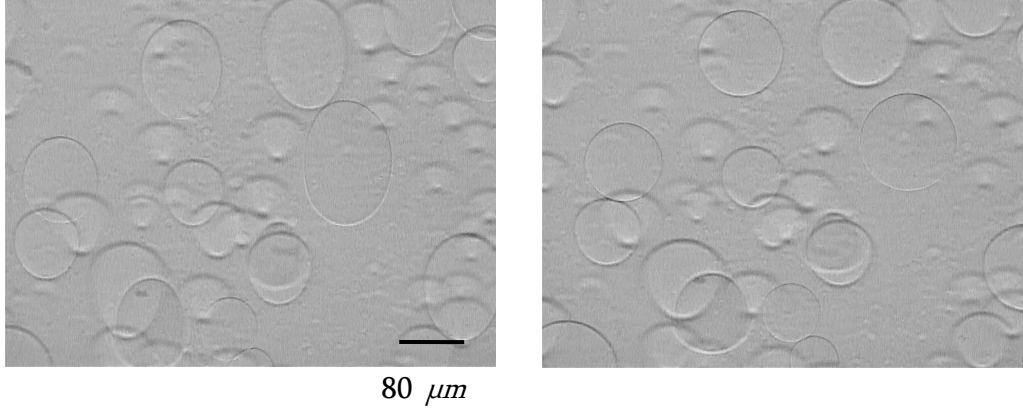


Figure 6.2 Retraction of droplets after cessation of flow: dispersed droplets of sample 2. The left picture shows the deformation before cessation of the flow field. The right picture shows the droplets at the end of the retraction where they regain their spherical shape. The droplets elongate in the direction of the flow field.

The deformation amplitude, s_2 , was determined at different times from the pictures that were taken with the camera. Plotting this deformation factor versus time, and using equation (6.4), the characteristic relaxation times, τ , for the retraction of different droplets were determined for all six samples. Oldroyd¹⁷ showed that for viscous liquids this characteristic relaxation time is given by

$$\tau = \frac{\eta R_0}{\gamma} \left[\frac{(19E + 16)(2E + 3)}{40(E + 1)} \right] \quad (6.5)$$

in which η is the viscosity of the continuous phase, R_0 is the size of the droplet after retraction, γ is the interfacial tension, and E is the viscosity ratio of the dispersed and continuous phases. This expression has been used for polymer blends² and biopolymer solutions,^{10-12,16} using known values for the viscosities of the phases and measured values of the characteristic relaxation time of a single droplet of size R_0 . However, determination of the interfacial tension from just one droplet size is not very accurate, and precision can be improved by measuring the relaxation as a function of R_0 . Plotting τ versus R_0 should yield a straight line, from which the

interfacial tension can be determined. Figure 6.3 (A-F) gives an overview of these plots for samples 1-6.

A straight line was fitted through the data points of each sample, and the slope was used to calculate the interfacial tension, using equation (6.5), and the data from Table 6.2. The calculated interfacial tensions are given in Table 6.3.

Table 6.3 Interfacial tension for the gelatin/dextran samples given in Table 6.1.

Sample	γ ($\mu\text{N} / \text{m}$)
1	0.15 ± 0.01
2	0.3 ± 0.1
3	1.2 ± 0.2
4	2.4 ± 0.3
5	5.1 ± 0.9
6	9.2 ± 1.9

From these data, we can see that the interfacial tension increases with an increase in dextran concentration. The order of magnitude is comparable to values that have been measured before for gelatin/dextran systems.^{22,23} In Figure 6.3, the lines through the data points show a non-zero intercept on the y-axis. Equation (6.5) predicts that these lines should go through the origin. This is clearly not the case for any of the systems, and therefore, equation (6.5) is not an adequate representation of our data. The existence of an intercept indicates that the interfacial tension and the viscosities of the phases are not the only parameters that play a role in the retraction of droplets after cessation of a flow field.

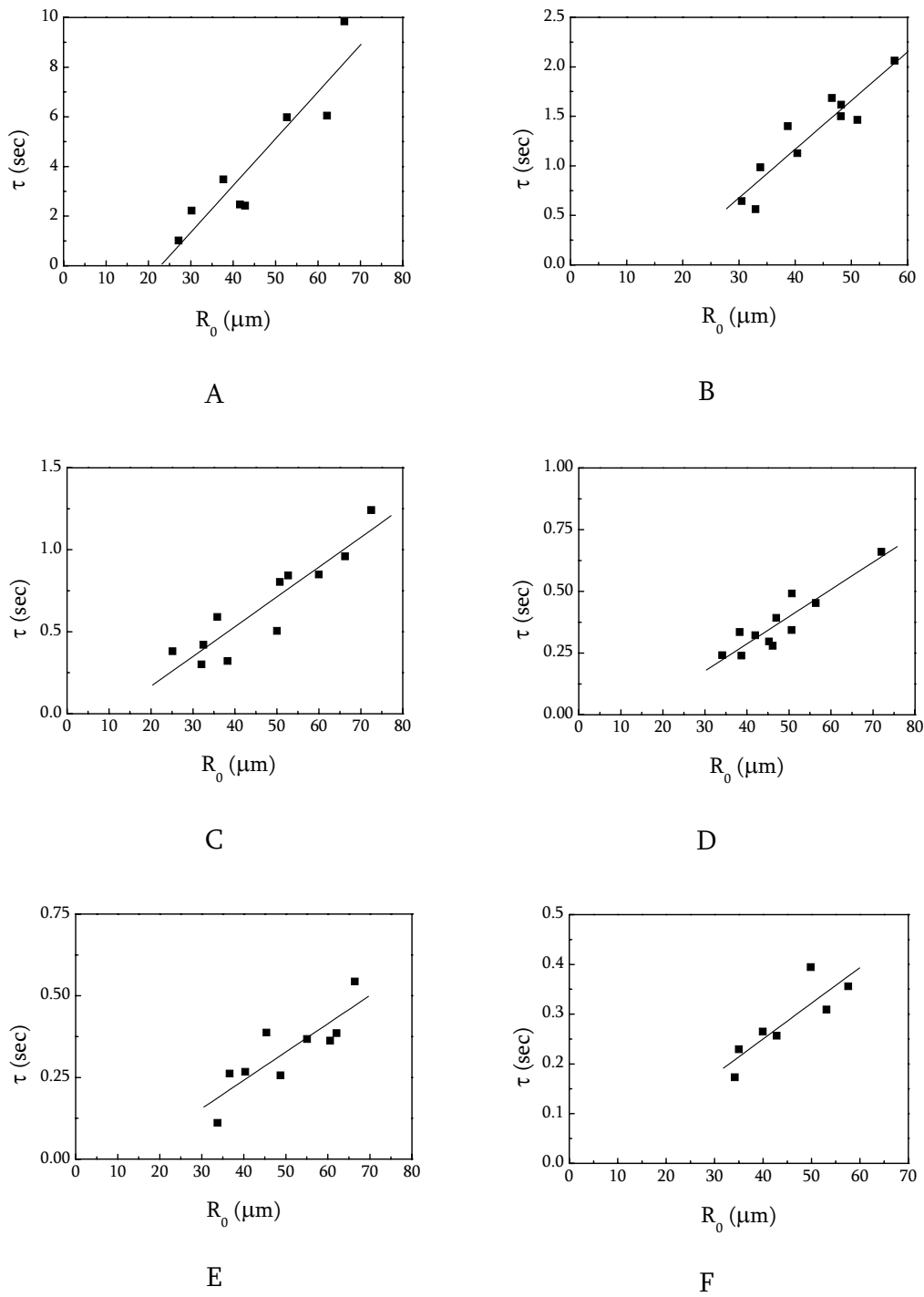


Figure 6.3 Characteristic relaxation time, τ , plotted versus the radius of the deformed droplet, R_0 . A) sample 1, B) sample 2, C) sample 3, D) sample 4, E) sample 5, F) sample 6. For compositions of these samples see Table 6.1. The line is a linear fit through the data points, from which the interfacial tension is determined.

In chapter 3 we have discussed the importance of the bending rigidity in these biopolymer systems with a very low interfacial tension. These bending rigidities might become important and could play a role in various interfacial phenomena,²⁴ and might also play a role in the retraction of droplets. The bending rigidity might have to be taken into account in the description of the interfacial forces. From previous calculations in chapter 3, the bending rigidities were estimated to be a few hundred $k_b T$ for near-critical systems with a very large interfacial thickness.²⁵ These calculations showed that bending rigidities become important at droplet sizes smaller than a certain critical radius, R_c , which was estimated to be of the order of a micron. However, for the relaxation measurements, we used droplets with radii between 20 and 80 micron, which is much larger than the critical radius below which the bending rigidity has to be taken into account. The contribution from the bending rigidity to the interfacial energy should be negligible for the droplet sizes that were used and should not give a large effect in the relaxation time of the retracting droplets. Therefore, the intercept in Figure 6.3 cannot be attributed to the bending rigidity.

Shi et. al.²⁶ published results on interfacial tension measurements of polydisperse immiscible polymers (PDMS and PIB). They measured the interfacial tension with the pendant drop technique and observed that it decreases with time (minutes to hours). They ascribe this effect to the polydispersity of the polymers. Since the interfacial tension depends on the size of the components at the interface, the smaller components migrate to the interface, thus lowering the energy of the system. Although they show this effect in the pendant drop method only, they expect this migration to occur also in shear experiments, but at times scales much shorter than for the pendant drop technique. Since our biopolymers are polydisperse (dextran has a polydispersity of 1.5 and fish gelatin of 2.7), this effect might occur in our experiments as well. When the migration time is of the same order of magnitude as the relaxation time, this effect might influence the value of the relaxation time, since the diffusion of low molecular weight components would change the interfacial tension during the measurement. This effect would be different for various droplet sizes, since the relaxation time of the droplets is different. However, Shi et al.²⁶ expect the migration time for shear experiments to be much shorter than the time scale in our experiments, which means that no effect of migration will be observed. Even if the migration time is of the same order of magnitude, the migration effect does not seem to explain our

experimental results. From their results, with polymers that have a similar degree of polydispersity as ours, they see that the interfacial tension decreases up to 15% only, which could never explain the large deviation from the origin in our plots.

The results from Figure 6.3 show that besides the interfacial tension other interfacial properties may be involved in the relaxation of droplets. One of the parameters that could play a role is the permeability of the interfaces. The results described in chapter 5 show that the interfaces in aqueous phase-separated biopolymer mixtures are indeed permeable. All ingredients can diffuse easily through the interface from one bulk phase into the other. The spinning drop experiments showed that the gelatin-rich droplets show a decrease in volume of about 90% in days to weeks. This time scale is much longer than in the relaxation experiments, but the permeability may also play a role at shorter time scales.

By taking into account the permeability of the interface, we are including a second mechanism for droplet relaxation. Apart from the retraction driven by interfacial tension forces we are allowing the deformed droplets to relax by transferring mass across the interface. The volume flux of mass, j (m/s), across the interface is proportional to $\lambda \cdot \Delta P \propto \lambda \gamma / R_0$, where λ is the permeability of the interface and ΔP is the Laplace pressure of a sphere. The volume flux is also proportional to R_0 / τ . Hence, by accounting for mass transfer across the interface we introduce an additional relaxation mechanism with a characteristic time $\tau \propto R_0^2 / \lambda \gamma$. If we assume that both relaxation mechanisms act in parallel, then the expression for the overall relaxation time of the system is given by

$$\frac{1}{\tau} = A \frac{\gamma}{\eta R_0} + B \frac{\lambda \gamma}{R_0^2} \quad (6.6)$$

In this equation, A and B are prefactors. This equation resembles a relation suggested by Prost et. al.,¹⁸ who studied the fluctuations of membranes as a function of porosity. The values for A and B could be deduced from the exact profiles of the flow inside and around the droplets. We will assume that, since in the limit of zero permeability, equation (6.6) should reduce to equation (6.5), the prefactor A is equal to $\frac{40(E+1)}{(19E+16)(2E+3)}$. Prefactor B is unknown, so for reasons of simplicity, we exchange $B\lambda$

by an effective permeability, λ_{eff} , where we expect B to be of the order of 1 for biopolymer systems (since $E \approx 1$).

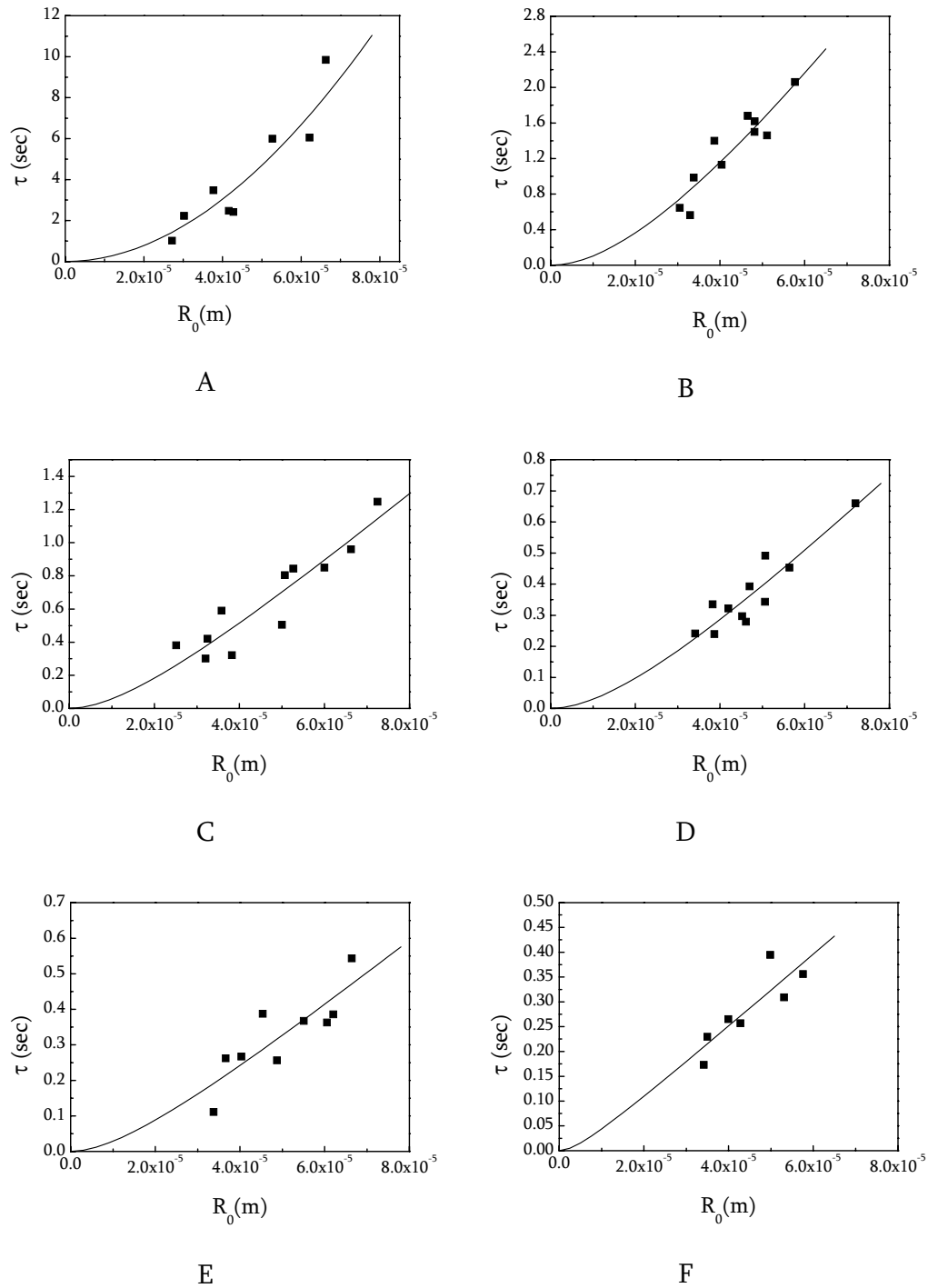


Figure 6.4 Characteristic relaxation time, τ , plotted versus the radius of the deformed droplet, R_0 . A) sample 1, B) sample 2, C) sample 3, D) sample 4, E) sample 5, F) sample 6. The line is the best fit to equation (6.6), from which the interfacial tension and the permeability are calculated.

Rewriting equation (6.6) gives the following expression for the relaxation time

$$\tau = \frac{\eta R_0}{\gamma} \left(\frac{1}{A + \frac{\lambda_{eff} \eta}{R_0}} \right) \quad (6.7)$$

which we have used to fit the experimental data (given as squares in Figure 6.4) to see whether the permeability plays a role in the relaxation experiments. The best fits through the data points are given as the solid lines. As can be seen, the fitted lines go through the data points as well as the origin, which was not the case when using equation (6.5). This shows that indeed the permeability of the interface has to be taken into account for a full description of the relaxation of deformed droplets. If this permeability is not taken into account, the interfacial tension will be overestimated, especially when the interfacial tension is deduced from the relaxation time of only *one* droplet size.

Table 6.4 gives the results for γ and λ_{eff} from the fits through the data points. For sample 1 we were not able to get a good fit. When the interfacial tension is very low and the permeability very high, the second term in equation (6.6) is dominant. Since both the interfacial tension and the permeability are present in the numerator of this term, it is difficult to fit both λ_{eff} and γ independently. For values larger than $1 \cdot 10^{-8} \text{ N/m}$, a satisfactory fit through the data points could not be found. For any value smaller than this, any combination of γ and λ_{eff} gave a good fit. This indicates that the interfacial tension must be smaller than $1 \cdot 10^{-8} \text{ N/m}$. Consequently, the value for the permeability should be larger than approximately $5 \cdot 10^{-2} \text{ m}^3/\text{N} \cdot \text{s}$, since below this value a fit through the data points is not in agreement with the experimental data.

Table 6.4 Interfacial tension (γ) calculated with equation (6.7), the interfacial tension (γ) calculated with equation (6.5), and the permeability, λ_{eff} , of samples 1 to 6.

sample	γ ($\mu N / m$)	γ ($\mu N / m$)	λ_{eff} ($m^3 / N \cdot s$)
1	≤ 0.01	0.15 ± 0.01	$\geq 5 \cdot 10^{-2}$
2	0.2 ± 0.1	0.3 ± 0.1	$3.4 \cdot 10^{-3} \pm 1.1 \cdot 10^{-3}$
3	1.0 ± 0.3	1.2 ± 0.2	$1.3 \cdot 10^{-3} \pm 0.6 \cdot 10^{-3}$
4	1.9 ± 0.6	2.4 ± 0.3	$1.4 \cdot 10^{-3} \pm 0.5 \cdot 10^{-3}$
5	4.6 ± 2.2	5.1 ± 0.9	$5.3 \cdot 10^{-4} \pm 5.2 \cdot 10^{-4}$
6	9.2 ± 3.2	9.2 ± 1.9	$9.0 \cdot 10^{-5} \pm 2.2 \cdot 10^{-4}$

The error margins in both the interfacial tension and the permeability are substantial. This can be explained by the fact that the data points from the experiments show a fairly large scatter, which is a result of the method that we use. Since we have only one rotating plate, it is not possible to measure the same droplet several times so the relaxation time can only be measured once for different droplet sizes. The relaxation process is recorded with a frame grabber with a speed of 5 frames per second. The amount of data points to deduce the specific relaxation time τ is therefore limited to the speed of the frame grabber. The faster the relaxation process, the less accurate is the determination of the relaxation time. These experimental limitations cause the scatter in the data points, which has its influence on the error margins of the interfacial properties. This explains the large error margins in the permeability of samples 5 and 6. The results could be improved by using a shear cell with two rotating plates in opposite direction. This would allow multiple measurement of a single droplet, from which an average could be taken. The use of a faster frame grabber would improve the determination of the relaxation time τ .

To show that the permeability indeed plays a role, we plot $\frac{1/\tau - A\gamma/\eta R_0}{\lambda_{eff}\gamma}$ versus $\frac{1}{R_0^2}$, using the values from the fit of equation (6.5) (Table 6.4). This should give a master curve with a slope equal to 1 when the permeability plays a role in the relaxation process. Figure 6.5 shows that the data of all samples are located around a

line with a slope of 1, which indicates that the permeability indeed has to be included for a full description for the relaxation process.

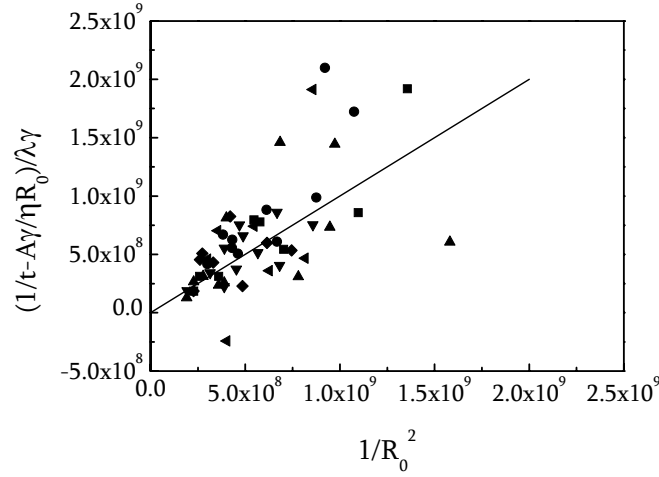


Figure 6.5 $\frac{1/\tau - A\gamma/\eta R_0}{\lambda_{eff} \gamma}$ plotted as a function of $1/R_0^2$ for sample 1 (■), sample 2 (●), sample 3 (▲), sample 4 (▼), sample 5 (►), and sample 6 (◄). The line has a slope equal to one.

From Table 6.4 we see that the interfacial tension for sample 1 is at the most $1 \cdot 10^{-8}$ N/m , while the value was $1.5 \cdot 10^{-7}$ when calculated without taking the permeability into account. This is a difference of about 90%. With increasing interfacial tension, the difference in the interfacial tension (with or without the contribution of the permeability) decreases. Since the distance from the critical point increases when going from sample 1 to 6 (going further into the two-phase state in the phase diagram), we can conclude that the deviation in the interfacial tension becomes large for samples close to the critical point and diminishes when going further from the critical point. For samples far from the critical point, the interfacial tension as deduced from equation (6.5) will give satisfactory results. However, when systems are close to the critical point and the interfacial tension is very low, the interfacial tension as determined from equation (6.5) is overestimated. For these systems, the permeability has to be taken into account for a full description of the relaxation time, and the interfacial tension must be determined using equation (6.7).

Table 6.4 also shows the effective permeability of the interfaces (when prefactor B is known, these values can be converted to exact values for the permeability). Looking at the trend of the permeability of the interfaces, we see that the permeability increases with a decrease in interfacial tension. Thus, for a lower interfacial tension, the permeability plays a more important role, which explains the large difference in interfacial tension for sample 1. The higher the interfacial tension, the less important the permeability is.

From these results, we can see that indeed these interfaces are very permeable to the ingredients in the system. The smaller the interfacial tension is, the higher the permeability is. When the interfacial tension is small (close to the critical point), the composition of both phases is alike, and the water can diffuse easily through the interface. For systems further from the critical point (with larger interfacial tension), the composition of the phases differ more, and this results in a lower permeability (more pressure is needed to push the water through the interface). The interfacial tension, and subsequently the distance from the critical point, can be related to the thickness of the interface as $\gamma \propto 1/\xi^2$.^{27,28} Since the permeability decreases with increasing interfacial tension, the permeability should increase with increasing interfacial thickness. To see whether this is true, we have calculated the interfacial thickness as described in chapter 3. Table 6.5 shows the interfacial tension, the permeability of the system and the interfacial thickness. We will leave the values for sample 1 out of consideration, since the best values for the fit are not known. From the data, we indeed see that the permeability increases with increasing interfacial thickness.

To investigate the scaling relation between the permeability of the interface with other interfacial properties, we have plotted the permeability versus the interfacial tension and the interfacial thickness. Figure 6.6 shows the permeability versus the interfacial tension. The data were fitted to the relation $\lambda_{eff} \propto \gamma^a$, for which the exponent $a = -0.9$ gave the best fit. Figure 6.7 shows the permeability versus the interfacial thickness, for which the data was fitted to the relation $\lambda_{eff} \propto \xi^b$. The best fit gave an exponent $b = 2.0$.

Thus, the permeability seems to be inversely related to the interfacial tension $\lambda_{eff} \propto 1/\gamma$, and related to the square of the interfacial thickness, $\lambda_{eff} \propto \xi^2$. This is what we would expect, since the interfacial tension is related to the interfacial thickness as $\gamma \propto 1/\xi^2$.

Table 6.5 γ , λ_{eff} , and the interfacial thickness, ξ , for samples 2 to 6.

sample	γ ($\mu\text{N} / \text{m}$)	λ_{eff} ($\text{m}^3 / \text{N} \cdot \text{s}$)	ξ (nm)
2	0.2	$3.4 \cdot 10^{-3}$	340
3	1.0	$1.3 \cdot 10^{-3}$	215
4	1.9	$1.4 \cdot 10^{-3}$	220
5	4.6	$5.3 \cdot 10^{-4}$	105
6	9.2	$1.0 \cdot 10^{-4}$	53

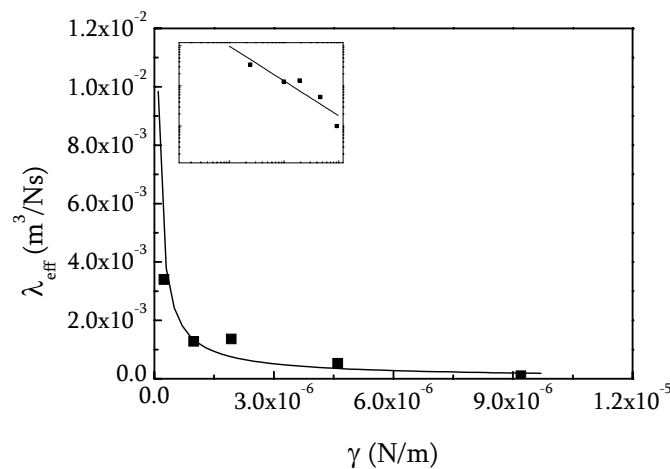


Figure 6.6 Permeability, λ_{eff} , plotted versus the interfacial tension, γ . The squares refer to the experimental data points. The solid line is the scaling relation $\lambda_{eff} \propto \gamma^{-0.9}$.

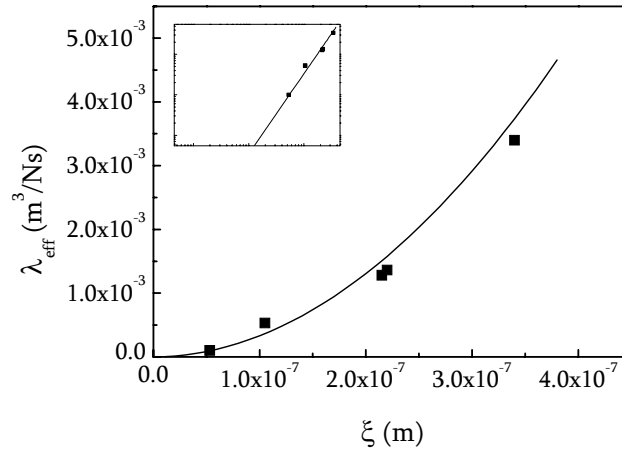


Figure 6.7 Permeability, λ_{eff} , plotted versus the interfacial thickness, ξ , as given in Table 6.5. The squares are the experimental data points. The solid line is the scaling relation $\lambda_{eff} \propto \xi^{2.0}$.

Since the interfaces of these water-in-water emulsions are permeable, all components could be able to diffuse through the interface in the relaxation process. The self-diffusion coefficient ($D_{self-diffusion} = k_b T / 6\pi\eta R_h$, where R_h is the hydrodynamic radius) of the biopolymers is much smaller than that of water because of the large difference in the hydrodynamic radius. Taking into account the short time scale of the experiments, we assume that only the water diffuses through the interface in these relaxation experiments. For ordinary diffusion over a distance R_0 the scaling relation for the relaxation time is given by

$$\tau \propto \frac{R_0^2}{D} \quad (6.8)$$

where D is the diffusion coefficient. Comparing equation (6.8) with the second term of equation (6.6), we see that the product of the interfacial tension and the permeability represents an effective diffusion coefficient, $D_{eff} \propto \lambda_{eff} \cdot \gamma$. Rewriting this expression leads to the following relation for the permeability of the interface, $\lambda_{eff} \propto D_{eff} / \gamma$. Since the permeability is inversely proportional to the interfacial tension ($\lambda_{eff} \propto 1/\gamma$), the diffusion coefficient should be constant. Thus, the diffusion coefficient is independent of the concentration of the ingredients that are present in the concentration regime of these systems. Since the water molecules are much

smaller (\AA) than the mesh size of the biopolymer solutions, which are normally of the order of nanometers, the water molecules are probably not slowed by the polymer network, but diffuse through the network with ease. Using the relation for the interfacial tension and the interfacial thickness, $\gamma \propto 1/\xi^2$, we see that the permeability is also proportional to $\lambda_{eff} \propto D_{eff}\xi^2$. From this relation, we see that the permeability is dependent only of the diffusion coefficient of the water molecules and the thickness of the interface.

Using $\lambda_{eff} \propto D_{eff}/\gamma$, we can determine the diffusion coefficient from the plot of λ_{eff} versus $1/\gamma$, which is given as Figure 6.8. The slope of the fit through the data points is equal to $0.9 \cdot 10^{-9} \text{ m}^2/\text{s}$. This is comparable to values found by Yapel et. al.,²⁹ who measured the self-diffusion of water through gelatin gels with different water content by puls-gradient NMR spectroscopy. They found values ranging from $1 \cdot 10^{-10}$ to $2.5 \cdot 10^{-9} \text{ m}^2/\text{s}$ depending on the concentration of the gelatin present in the systems. It is also close to the self-diffusion coefficient of water, D_w^0 , which is equal to $2.3 \cdot 10^{-9} \text{ m}^2/\text{s}$. This indicates that indeed only the water diffuses through the interface.

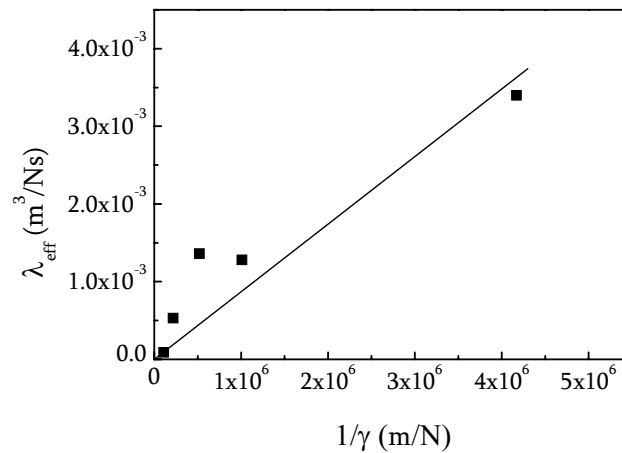


Figure 6.8 λ_{eff} versus $1/\gamma$. The line is the linear fit through the points, with the origin as a theoretical point.

6.4 Conclusion

We have performed relaxation experiments on deformed droplets of phase-separated biopolymer mixtures. Our experiments indicate that the permeability of the interface plays an important role in the relaxation of deformed droplets after cessation of flow. These phase-separated mixtures can be regarded as water-in-water emulsions with two coexisting phases that mainly consist of water (for about 90%). The water does not have more affinity to be in either one of the phases, and therefore, the water can diffuse through the interface. From our experiments, we see that, without taking this permeability into account, the interfacial tension is overestimated for samples very close to the critical point, with very low interfacial tensions. For these samples, where the phases are almost alike and the interfacial thickness is very large, the permeability is very high. The permeability decreases for increasing interfacial tension (going further from the critical point). From scaling relation we found that the permeability is inversely proportional to the interfacial tension ($\lambda_{eff} \propto 1/\gamma$) and related to the square of the interfacial thickness ($\lambda_{eff} \propto \xi^2$). The effective diffusion coefficient was determined from $\lambda_{eff} \propto D_{eff}/\gamma$, and was found to be close to the value of the self-diffusion coefficient of water. This indicates that only the water diffuses through the interface. From the results we see that the diffusion coefficient is independent of the composition of the mixtures and the concentration regime that is used. Since the size of the water molecules is much smaller than the mesh size of the polymer networks, the water molecules are assumed to diffuse through the networks without any hindrance of the biopolymers.

Acknowledgements

We thank J. Prost (Institut Curie, Paris, France) for helpful discussions.

References

- (1) Son, Y. and Yoon, J. T. *Polymer* **2001**, *42*, 7209-7213.
- (2) Son, Y. and Migler, K. *Polymer* **2002**, *43*, 3001-3006.
- (3) Guido, S.; Simeone, M. and Villone, M. *Rheol. Acta* **1999**, *38*, 287-296.
- (4) Cavallo, R.; Guido, S. and Simeone, M. *Rheol. Acta* **2003**, *42*, 1-9.
- (5) Guido, S. and Villone, M. *J. Rheol.* **1998**, *42*, 395-415.
- (6) van Puyvelde, P.; Moldenaers, P. and Mewis, J. *Phys. Chem. Chem. Phys.* **1999**, *1*, 2505-2511.
- (7) Tassiere, M.; Grizzuti, N. and Greco, F. *Macromol. Symp.* **2003**, *198*, 53-67.
- (8) Vermant, J.; van Puyvelde, P.; Moldenaers, P. and Mewis, J. *Langmuir* **1998**, *14*, 1612-1617.
- (9) Ziegler, V. E. and Wolf, B. A. *Langmuir* **2004**, *20*, 5826-5833.
- (10) Pacek, A. W.; Ding, P. and Nienow, A. W. *Chem. Eng. Sci.* **2001**, *56*, 3247-3255.
- (11) Simeone, M.; Alfani, A. and Guido, S. *Food Hydrocolloids* **2004**, *18*, 463-470.
- (12) Ding, P.; Wolf, B.; Frith, W. J.; Clark, A. H.; Norton, I. T. and Pacek, A. W. *J. Colloid Interface Sci.* **2002**, *253*, 367-376.
- (13) van Puyvelde, P.; Antonov, Y. A. and Moldenaers, P. *Food Hydrocolloids* **2003**, *17*, 327-332.
- (14) van Puyvelde, P.; Antonov, Y. A. and Moldenaers, P. *Korea-Aust. Rheol. J.* **2002**, *14*, 115-119.
- (15) Lundell, C.; Walkenström, P.; Lorén, N. and Hermansson, A.-M. *Food Hydrocolloids* **2004**, 805-815.
- (16) Guido, S.; Simeone, M. and Alfani, A. *Carbohydr. Polym.* **2002**, *48*, 143-152.
- (17) Oldroyd, J. G. *Proc. Royal Soc. London* **1953**, *218*, 122-132.
- (18) Prost, J.; Manneville, J.-B. and Bruinsma, R. *Eur. Phys. J. B.* **1998**, *1*, 465-480.
- (19) Tuinier, R. *An exocellular polysaccharide and its interactions with proteins*, PhD Thesis, Wageningen, 1999.
- (20) Mellema, J.; Blom, C. and Beekwilder, J. *Rheol. Acta* **1987**, *26*, 418-427.
- (21) Winterhalter, M. and Helfrich, W. *J. Colloid Interface Sci.* **1987**, *122*, 583-586.
- (22) Scholten, E.; Visser, J. E.; Sagis, L. M. C. and van der Linden, E. *Langmuir* **2004**, *20*, 2292-2297.
- (23) Antonov, Y. A.; van Puyvelde, P. and Moldenaers, P. *Int. J. Biol. Macromol.* **2004**, *34*, 29-35.

- (24) Scholten, E.; Sagis, L. M. C. and van der Linden, E. *Macromolecules* **2005**, *38*, 3515-3518.
- (25) Scholten, E.; Sagis, L. M. C. and van der Linden, E. *J. Phys. Chem. B* **2004**, *108*, 12164-12169.
- (26) Shi, T.; Ziegler, V. E.; Welge, I. C.; An, L. and Wolf, B. A. *Macromolecules* **2004**, *37*, 1591-1599.
- (27) de Gennes, P. G. *Scaling Concepts in Polymer Physics*; Cornell University Press: New York, 1979.
- (28) Rowlinson, J. S. and Widom, B. *Molecular Theory of Capillarity*; Clarendon Press: Oxford, 1984.
- (29) Yapel, R. A.; Duda, J. L.; Lin, X. and van Meervall, E. D. *Polymer* **1994**, *35*, 2411-2416.

Chapter 7

Discussion

7.1 Biopolymer mixtures in daily life

Biopolymer mixtures are very common in daily life, since they are used by many industries, such as food industry, pharmaceutical industry and cosmetics for the manufacture of a variety of products. In the food industry protein-polysaccharide mixtures as discussed in this thesis are used in ice-cream production¹ and as zero-fat spreads.^{2,3} These protein-polysaccharide mixtures are often used when demixed into two coexisting phases.⁴ As both immiscible phases are water-based, these systems are often referred to as water-in-water emulsions. By controlling properties such as gelling behavior, viscosity and network formation of both phases, these systems can be used as a substitute for oil/water emulsions. The specific properties of these oil/water emulsions, such as the creaminess of mayonnaise and desserts, are controlled by for example the size of the dispersed droplets. To be able to mimic the properties of oil/water emulsions, one should be able to control the size, shape and structure in the water-in-water emulsions, since they influence the sensorial perception of products, such as mouthfeel.⁵ Using ingredients that have gelling properties, these water-in-water emulsions could also be used as delivery vehicles for flavor molecules and other functional ingredients. Upon melting of the delivery vehicles, one can control for example flavor release in products such as ice-cream and desserts.

In order to control and predict properties of food products based on water-in-water emulsions, one needs knowledge of the relation between structures (size, shape and morphology) and sensorial perception. Knowledge about the parameters that influence the structures in the systems is also essential. In this thesis we have focused on the parameters that influence the structures in these water-in-water emulsions, leading to a better understanding of the dynamic behavior of this type of emulsion. The results of this work may be used to better control the macroscopic properties of food products, or to develop novel food products.

7.1.1 Relevance of interfacial properties

In the formation of morphologies and structures, interfacial parameters play an important role.^{6,7} Therefore, knowledge of the interfacial properties is desirable in order to gain insight in their relation with structural design. Normally, one assumes

that the interfacial tension is the only important parameter regarding the interfacial forces. This interfacial tension is studied extensively, as well as the morphologies of these systems. However, little attention has been given to other interfacial properties such as interfacial thickness, bending rigidity and interfacial permeability.

The interfaces of these water-based emulsions are different than normal oil/water emulsions. For example, the interfacial tension for water-water interfaces is of the order of $\mu\text{N}/\text{m}$, while the interfacial tension for oil/water emulsions is of the order of mN/m . Since the interfacial tension of these water-water interfaces is much lower, the bending rigidity becomes more important, and may even dominate the behavior of the interface. In oil/water emulsions, the bending rigidity is low, and bending contribution to the interfacial energy is negligible. Another large difference between these two emulsions is the fact that in water-in-water emulsions both phases exist of more than 90% water. Since water does not favor one of the phases, water can diffuse through the interface to the other bulk phase, depending on the forces that are exerted on the systems, such as shear or rotational flow. Interfaces of water-based systems can thus be permeable to water and other ingredients in the systems.

Since the bending rigidity and the interfacial permeability may be of importance in these emulsions, we have focused on the relevance of these properties. We have investigated the effect of the interfacial permeability on interfacial tension measurements using the spinning drop and the droplets relaxation method. Since experimental determination of bending rigidity is rather difficult, we have calculated this interfacial property using a model. Further, we have addressed the combined effects of interfacial tension, bending rigidity and interfacial permeability on the dynamics of these water-in-water emulsions.

7.2 Permeability

To investigate whether transfer of ingredients indeed occurs in these systems, we have performed experiments with the spinning drop method and the droplet relaxation method. Both methods are widely accepted as reliable methods for the

determination of the interfacial tension. In both techniques, an external force field is applied in order to achieve deformation of the dispersed droplets.

In the spinning drop experiments as described in chapter 5, we observed that the volume of the dispersed droplets decreased in time. Over a period of a few days to weeks, the volume decreased up to 90% for most samples. From these results we could conclude that the interfaces are permeable to all components in the system. At the moment a force is applied on the system, the phase behavior is different than the phase behavior at rest, and the binodal shifts. The coexisting phases are therefore not in equilibrium with each other since the new equilibrium values will be on the new shear-induced binodal. The system will try to reach this new equilibrium state by diffusion of components from one phase to the other. As the phases will never reach their new equilibrium composition, the diffusion of all three components will continue till the droplet disappears.

In chapter 5, we give a description for the volume change in time in terms of three diffusion coefficients. The determined diffusion coefficients are comparable to the self-diffusion coefficients of the biopolymers. From this, we could conclude that the diffusion of the biopolymers determine the rate of the volume change. Since these biopolymers are rather large, and their diffusion coefficient is rather high, the diffusion process is slow. The decrease in volume of the droplets in the spinning drop experiments takes up to three weeks, depending on their composition. In the droplet relaxation method, as discussed in chapter 6, the time scale of the experiments is a few seconds only. This time scale is much shorter than in the case of the spinning drop experiments: it differs by as much as five orders of magnitude. One might expect that for these short time scales, the interfacial permeability is not important and that the relaxation behavior is dominated by the interfacial tension only. However, from the results discussed in chapter 6, we see that the interfacial permeability apparently does play a role in the process of retraction. Accounting for the interfacial tension and an effective permeability, we give a new description for the relaxation time of the droplet. From scaling relations, we could relate this permeability to an effective diffusion coefficient, which was found to be comparable to the self-diffusion coefficient of water. This indicates that water is the only component that diffuses through the interface. So, although the time scale in these experiments is rather short,

diffusion of the water molecules is still important in the relaxation behavior of deformed droplets. The time scale is too short for the biopolymers to diffuse through the interface, since their diffusion coefficient is about three orders of magnitude smaller than that of water.

For both methods, we see that it is necessary to take the permeability into account for a full description of the behavior of the interface. Since all components are able to transfer through the interface, the properties of the bulk phase (concentration, density) and subsequently the properties of the interface (thickness, interfacial tension) will change in time. This makes the spinning drop method not an accurate method for the determination of the equilibrium interfacial tension. This method can only be used to obtain the right order of magnitude but not to measure the exact value for the interfacial tension. However, the interfacial tension *can* be determined from relaxation measurements, as long as the contribution of the permeability is taken into account. Using the new description for the relaxation process given in chapter 6, the interfacial tension and the interfacial permeability can be deduced simultaneously.

For biopolymer systems, an alternative method for the determination of the interfacial tension would be a method that does not rely on a force field that is applied on the droplets, and induces a pressure difference across the interface. An example of such a method is described by Wijting et. al,⁸ who determined the interfacial tension of a colloidal liquid-gas system using the meniscus of the interface at a fiber that is suspended in the system. The problem with this method is, however, that due to the low optical contrast and the very small sizes of the menisci, the contact angle is difficult to observe. They solved this problem by measuring dynamic contact angles by moving the fiber up and down. However, we do not know what the effect of this movement will be on the interface and to what extent the permeability of the interfaces would affect the results of such an experiment.

7.3 Bending rigidity

Since the interfacial tension for these phase-separated biopolymer mixtures is rather low, the bending rigidity might become important in the description of the interfacial energy, and might even dominate the behavior of the interface. The interfacial region

of these biopolymer systems is much larger than normal oil/water interfaces, since the thickness is determined by the concentration profile of the dissolved biopolymers. The bending rigidity is related to the thickness of this interface and the interaction between the particles in this interface. Therefore, we expected that the bending rigidity could be much higher than for normal oil/water or water/air interfaces.

These bending rigidities are very hard to determine experimentally, since due to the low interfacial tension of these interfaces, they are very sensitive to small fluctuations in temperature, pressure, vibrations etc.⁹ Till now, no measurements have been reported in literature. Therefore, we proposed a model that uses expressions for the interfacial tension and the bending rigidity, described in chapter 3. From this model we found that the interfacial thickness for near-critical systems is indeed much larger than normal water/air or water/oil interfaces. Because of the large interfacial thickness for near-critical systems, we also found that the bending rigidities for these systems are very high, in the order of $500 k_b T$. This is an order of magnitude larger than values found for micro-emulsions and vesicles, which are of the order of $10 k_b T$. Since these values for the bending rigidity are high, and the interfacial tension for these systems are very low, this bending rigidity has to be taken into account for a full description of the interfacial energy.

7.4 Effect of interfacial permeability and bending rigidity on kinetics of phase separation

One of the phenomena in which the interfacial properties play an important role is the phase separation process. During phase separation, different morphologies can be obtained with different length scales. The size of the domains and the morphology (droplet or bicontinuous) determine the macroscopic properties of the systems. When one of the components is able to gel, one could “freeze” the system in a particular morphology with domains with a particular length scale in order to control the properties of a product. Knowledge of the kinetics of the phase separation is thus desirable in order to control and predict the properties of biopolymer mixtures. The kinetics of phase separation has received a lot of attention over the years, both experimentally and theoretically.¹⁰⁻¹⁸ Although the mechanisms that have been

proposed contribute to a better insight into of the phase separation process,¹⁹⁻²⁸ a full understanding is still incomplete. In chapter 4, we already described the effect of bending rigidity on the coarsening rates in bicontinuous structures. Using the Navier-Stokes equation, we derived a new description for the hydrodynamic flow in bicontinuous structures. Including this bending rigidity into the description for the interfacial energy, we found two regimes for the coarsening, dominated by either the stretching contribution (related to interfacial tension) or the bending contribution (related to bending rigidity).

In this chapter we will show the combined effects of interfacial tension, bending rigidity and interfacial permeability on the phase separation process, and show that these three interfacial properties have to be taken into account for a full description of the hydrodynamic flow in these bicontinuous mixtures.

Starting with the Navier-Stokes equation as given in chapter 4 (equation (4.1)), neglecting the gravitational term and the inertia term and assuming steady flow, we find

$$0 = -\vec{\nabla} P + \eta \nabla^2 \vec{v} \quad (7.1)$$

Approximating the pressure gradient as $\Delta P/\Lambda$ and the Laplacian of the velocity by v/Λ^2 , one arrives at

$$\eta \frac{v}{\Lambda^2} \approx \frac{\Delta P}{\Lambda} \quad (7.2)$$

The difference in pressure (ΔP) is determined by the interfacial tension, γ , and Λ ($\Delta P \propto \gamma/\Lambda$). As discussed in chapter 4, we write the curvature-dependent interfacial tension for the description of the total interfacial energy

$$\gamma(\Lambda) = \gamma_0 + \frac{2k}{\Lambda^2} \quad (7.3)$$

where γ_0 is the interfacial tension of the flat interface, and k is the bending rigidity. The first term signifies the stretching contribution to the interfacial energy, while the second term is related to the bending contribution. Combining equation (7.2) and (7.3), we obtain

$$\frac{d\Lambda}{dt} \approx \frac{\gamma_0}{\eta} + \frac{2k}{\eta\Lambda^2} \quad (7.4)$$

From chapter 5, we have seen that the change in volume ($\propto d\Lambda^3/dt$) is not just determined by the interfacial tension, but also by the permeability of the interface. From the differential mass balance, the volume change in time is related to the permeability and the pressure on the interface as $d\Lambda/dt = \lambda \cdot \Delta P$. Using the Laplace equation and equation (7.3) we find that as a result of mass transfer across the interface

$$\frac{d\Lambda}{dt} \approx \frac{\gamma_0 \lambda_{eff}}{\Lambda} + \frac{2k\lambda_{eff}}{\Lambda^3} \quad (7.5)$$

We assume that both mechanisms work in parallel. Depending on whether the interfacial tension or the permeability is more relevant, the coarsening of domains will either be dominated by interfacial tension driven flow in the bulk phases or mass transfer across the interface.

As all four terms in equations (7.4) and (7.5) have a different scaling with respect to domain size, the relative importance of these terms will change for different curvature of the domains in the bicontinuous structures. As a result, we will observe different scaling behavior as a function of domain size.

We can estimate the length scales for which the different interfacial properties become important and may become dominant in the phase separation process. By equating both terms in equations (7.4) or (7.5), we find a critical radius, $R_c = \sqrt{2k/\gamma_0}$, the critical radius below which the bending contribution dominates the stretching contribution to the interfacial energy as already discussed in chapter 3. Equating the first terms of equations (7.4) and (7.5), we find a critical radius $R_\lambda \approx \lambda_{eff}\eta$, the radius below which the phase separation process will be dominated by the permeability of the interfaces. So, depending on the values for the different critical length scales, R_c and R_λ , the scaling of the domain size with time for bicontinuous structures should show different regimes (in the limit of small and large length scales):

i) A regime with a domain size larger than R_c and R_λ ($\Lambda \gg R_c$, $\Lambda \gg R_\lambda$). The coarsening process will then be dominated by the interfacial tension and equation (7.4) reduces to give

$$\frac{\Lambda \eta}{\gamma_0} \propto t \quad (7.6a)$$

We see that in this regime, the domain size scales with time as $\Lambda \propto t$.

ii) A regime with a domain size larger than R_c but smaller than R_λ ($\Lambda \gg R_c$, $\Lambda \ll R_\lambda$). The coarsening process will then be dominated by the interfacial tension and the permeability of the interface. The first term on the right side of equation (7.5) will be dominant, and leads to the following relation with time:

$$\frac{\Lambda^2}{\gamma \lambda_{eff}} \propto t \quad (7.6b)$$

For this regime, the domain size scales with time as $\Lambda \propto t^{1/2}$.

iii) A regime with a domain size smaller than R_c but larger than R_λ ($\Lambda \ll R_c$, $\Lambda \gg R_\lambda$). For this regime, the coarsening process is dominated by the bending rigidity and equation (7.4) reduces to

$$\frac{\Lambda^3 \eta}{2k} \propto t \quad (7.6c)$$

which gives a scaling relation $\Lambda \propto t^{1/3}$.

iv) A regime with a domain size smaller than R_c and R_λ ($\Lambda \ll R_c$, $\Lambda \ll R_\lambda$), where the second term of the right side in equation (7.5) will be most dominant and one arrives at

$$\frac{\Lambda^4}{2k \lambda_{eff}} \propto t \quad (7.6d)$$

For this regime we find that the domain size scales with time as $\Lambda \propto t^{1/4}$.

So, depending on the values of the critical sizes R_c ($\sqrt{2k/\gamma_0}$) and R_λ ($\eta \lambda_{eff}$), we find scaling exponents ranging from 1/4 to 1. We find an exponent of 1/4 for

bending- and permeability-dominated coarsening, an exponent of $1/3$ for bending-dominated coarsening, an exponent of $1/2$ for interfacial tension- and permeability-dominated coarsening and an exponent of 1 for interfacial tension-dominated coarsening in bicontinuous structures.

We can estimate the length scales R_c and R_λ by taking into account the values for the separate interfacial properties. As we have seen in chapter 6, the interfacial permeability of these interfaces is of the order of $1 \cdot 10^{-3} \text{ m}^3/N \cdot s$. Taking a value for the viscosity of a viscous fluid as $10 \cdot 10^{-3} \text{ Pa} \cdot s$, we find a critical radius R_λ of approximately 10 micron. So, below length scales of 10 micron, the permeability of the interfaces will dominate the coarsening behavior. We can estimate the other critical radius R_c from the values of the interfacial tension and the bending rigidity, which was already calculated in chapter 3. Taking a value of $1 \cdot 10^{-6}$ for the interfacial tension and a value of $500 \text{ } k_b T$ for the bending rigidity, we find a critical radius R_c of about 1 micron. Thus, for droplets smaller than a micron, bending contributions will dominate the stretching contribution to the interfacial energy. So, depending on the interfacial properties, the coarsening of the domains in bicontinuous structures will exhibit different scaling depending on the length scales in the system. As both critical length scales (R_c and R_λ) have values that are of importance in the phase separation process, the permeability and the bending rigidity of the interfaces have to be taken into account for a full description of the interface. Depending on the critical length scales and the size of the domains, the different regimes for the coarsening rate can be expected.

These results show that in the case of aqueous phase-separated biopolymer mixtures (water-in-water emulsions), the interfacial permeability and the bending rigidity cannot be ignored when discussing interfacial-related phenomena, such as phase separation, droplet morphologies, shear-induced phase separation, and droplet deformation. Normally, these interfacial properties are not taken into account, but as we have seen they can have a large effect on these biopolymer mixtures. As the interfaces are permeable to all ingredients, pressure gradients that are exerted on the interface will induce the diffusion of both water and biopolymers. So, to be able to describe the interfacial phenomena under force fields, such as shear, this permeability

has to be taken into account. Also the bending rigidity of the interfaces might be of importance. Since these bending rigidities are very high and interfacial tension is very low in these systems, this interfacial parameter has to be taken into account when dealing with large curvatures, e.g. small droplet size. Especially for phenomena such as phase separation, the kinetics of the process will be influenced by all discussed interfacial properties. Depending on the critical radii R_c and R_λ , the relative importance of the stretching contribution, bending contribution, and mass transfer will differ for different domain or droplet sizes.

7.5 Conclusion

In order to control the macroscopic properties of food products, one has to control the morphologies of the system and the shape and the size of the domains/droplets in the water-in-water emulsions. Since food products are often produced under shear, these morphologies are controlled by the phase separation process and the degree of shear flow.²⁹⁻³² With large flow forces, one could even create string-like structures.³³⁻³⁵ Controlling the gelling behavior of the dispersed phase as well as the continuous phase, one can “freeze” certain morphologies of the domains.^{3,36} So, to be able to predict and control the morphologies of immiscible biopolymer systems, knowledge of the interfacial properties is essential, since they determine the behavior of the interface, and hence the structures in the system. As we have shown in this thesis, the interfaces of phase-separated biopolymer mixtures are much more complicated than normal oil/water or water/air interface, and behave differently under flow fields. In the description of oil/water interfaces, the interfacial tension is the only parameter of importance for phenomena, such as phase separation and droplets morphologies. However, for water-water interfaces, interfacial permeability and bending rigidity are also essential for the description of the interface. Thus, to be able to understand the behavior of these water-in-water emulsions, one needs to include these interfacial properties in order to have a complete insight of their behavior. The results described in this thesis might contribute to a better understanding of these systems, and hence the development of novel food products.

References

- (1) Goff, H. D. *Int. Dairy J.* **1997**, *7*, 363-373.
- (2) Bot, A.; Mellema, M. and Reiffers-Magnani, C. K. *Industrial Proteins* **2003**, *11*, 11-13.
- (3) Kasapis, S.; Morris, E. R.; Norton, I. T. and Brown, C. R. T. *Carbohydr. Polym.* **1993**, *21*, 261-268.
- (4) Tolstoguzov, V. *Nahrung* **2000**, *44*, 299-308.
- (5) Ledward, D. A. *Trends Food Sci. Tech.* **1993**, *4*, 402-405.
- (6) Walther, B.; Hamberg, L.; Walkenstrom, P. and Hermansson, A.-M. *J. Colloid Interface Sci.* **2004**, *270*, 195-204.
- (7) Hamberg, L.; Wohlwend, M.; Walkenstrom, P. and Hermansson, A.-M. *Food Hydrocolloids* **2003**, *17*, 641-652.
- (8) Wijting, W. K.; Besseling, N. A. M. and Cohen Stuart, M. A. *J. Phys. Chem. B* **2003**, *107*, 10565-10570.
- (9) de Hoog, E.; Lekkerkerker, H. N. W.; Schulz, J. and Findenegg, G. H. *J. Phys. Chem. B* **1999**, *103*, 10657-10660.
- (10) Anderson, V. J. and Jones, R. A. L. *Polymer* **2001**, *42*, 9601-9610.
- (11) Butler, M. F. and Heppenstall-Butler, M. *Biomacromolecules* **2003**, *4*, 928-936.
- (12) Verhaegh, N. A. M.; van Duijneveldt, J. S.; Dhont, J. K. G. and Lekkerkerker, H. N. W. *Physica A* **1996**, *230*, 409-436.
- (13) Butler, M. F. and Heppenstall-Butler, M. *Food Hydrocolloids* **2003**, *17*, 815-830.
- (14) de Hoog, E. H. A. and Tromp, R. H. *Colloid Surf. A-Physicochem. Eng. Asp.* **2003**, *213*, 221-234.
- (15) Williams, M. A. K.; Fabri, D.; Hubbard, C. D.; Lundin, L.; Foster, T. J.; Clark, A. H.; Norton, I. T.; Lorén, N. and Hermansson, A.-M. *Langmuir* **2001**, *17*, 3412-3418.
- (16) Lorén, N.; Altskär, A. and Hermansson, A.-M. *Macromolecules* **2001**, *34*, 8117-8128.
- (17) Siggia, E. D. *Phys. Rev. A* **1979**, *20*, 595-605.
- (18) Dhont, J. K. G. *An Introduction to Dynamics of Colloids*; Elsevier Science B.V.: Amsterdam, 1996.
- (19) Lifshitz, I. M. and Slyozov, V. V. *J. Phys. Chem. Solids* **1961**, *19*, 35-50.
- (20) Binder, K. and Stauffer, D. *Phys. Rev. Lett.* **1974**, *33*, 1006-1009.

-
- (21) Nikolayev, V. S.; Beysens, D. and Guenoun, P. *Phys. Rev. Lett.* **1996**, *76*, 3144-3147.
 - (22) Nikolayev, V. S. and Beysens, D. A. *Phys. Fluids* **1997**, *9*, 3227-3234.
 - (23) Tanaka, H. *Phys. Rev. Lett.* **1994**, *72*, 1702-1705.
 - (24) Tanaka, H. *J. Chem. Phys.* **1995**, *103*, 2361-2364.
 - (25) Cabral, J. T.; Higgins, J. S.; Yerina, N. A. and Magonov, S. N. *Macromolecules* **2002**, *35*, 1941-1950.
 - (26) Takeno, H. and Hashimoto, T. *J. Chem. Phys.* **1997**, *107*, 1634-1644.
 - (27) Crist, B. *Macromolecules* **1996**, *29*, 7276-7279.
 - (28) Chen, H. and Chakrabati, A. *J. Chem. Phys.* **1998**, *108*, 6006-6013.
 - (29) Lundell, C.; Walkenström, P.; Lorén, N. and Hermansson, A.-M. *Food Hydrocolloids* **2004**, 805-815.
 - (30) Walkenstrom, P. and Hermansson, A.-M. *Curr. Opin. Colloid Interface Sci.* **2002**, *7*, 413-418.
 - (31) van Puyvelde, P.; Antonov, Y. A. and Moldenaers, P. *Food Hydrocolloids* **2003**, *17*, 327-332.
 - (32) Norton, I. T. and Frith, W. J. *Food Hydrocolloids* **2001**, *15*, 543-553.
 - (33) Wolf, B.; Scirocco, R.; Frith, W. J. and Norton, I. T. *Food Hydrocolloids* **2000**, *14*, 217-225.
 - (34) Wolf, B. and Frith, W. J. *J. Rheol.* **2003**, *47*, 1151-1170.
 - (35) van Puyvelde, P.; Antonov, Y. A. and Moldenaers, P. *Food Hydrocolloids* **2002**, *16*, 395-402.
 - (36) Lorén, N. and Hermansson, A.-M. *Int. J. Biol. Macromol.* **2000**, *27*, 249-262.

Summary

Summary

Samenvatting

Summary

Phase-separated protein-polysaccharide mixtures are frequently used in the food industry for the production of spreads, ice-creams and desserts. These systems are also known as water-in-water emulsions, and as their properties are comparable to normal oil/water emulsions, these systems are used as substitutes for fatty products. Controlling the morphologies and sizes of the phases, the macroscopic properties of these zero-fat water-in-water emulsions can be controlled in order to mimic the properties of fatty products. Using phase separation and applied shear flow, the size of the structures can be tuned. The size and the shape of these structures are determined by the interfacial properties of these systems. In general, one assumes that interfacial tension is the only important parameter. Since the properties of water-water interfaces differ from oil/water interfaces, the objective of this thesis was to investigate interfacial properties, such as bending rigidity and interfacial permeability, and to determine the effect of these interfacial properties on the kinetics of phase separation and the deformation behavior of emulsion droplets in shear flow.

In Chapter 2 we have investigated two protein-polysaccharide systems; a gelatin/dextran and a gelatin/gum arabic system. For both mixtures, we have measured the interfacial tension as a function of the distance to the critical point. We found the interfacial tension to be of the same order of magnitude for both systems, which was expected since the biopolymers are of similar size. However, from scaling relations, we found that the gelatin/dextran system could be considered to be near-critical while the gelatin/gum arabic system could be considered to be off-critical. This indicates that the interface of the gelatin/gum arabic system is rather narrow, while the interface of the gelatin/dextran system is diffuse.

Since the thickness of the interface is related to the bending energy of that interface, we have focused on interfacial thickness and bending rigidity in chapter 3. Experimental determination of this interfacial parameter is hampered by the fact that the interfaces of these systems are very sensitive to small fluctuations in pressure, temperature etc. Therefore we have proposed a model that calculates the interfacial thickness and the bending rigidity, using the measured interfacial tension described in chapter 2, and the interaction potential of the biopolymers in the interface. The results

show that the interfacial thickness of off-critical systems is of the size of the biopolymers. The bending rigidity for these systems is comparable to normal oil/water interfaces. For the near-critical samples we find the interfacial thickness to be much larger than for off-critical systems, as well as the accompanying bending rigidity.

In chapter 4 we have incorporated this bending rigidity into the description of the interfacial energy. This leads to a curvature-dependent interfacial energy, including a stretching contribution and a bending contribution. Using this description for the interfacial energy, we derive a new description for the coarsening of bicontinuous structures during phase separation. Since the bending energy is size independent and the stretching energy is size dependent, we find different regimes for the coarsening rate at different length scales. For small length scales we find the domain size to scale with time as $\Lambda \propto t^{1/3}$, while for large length scales, we find the domain size to scale with time as $\Lambda \propto t$. Comparing our theoretical findings with experimental data, we find that the crossover between these two regimes is indeed observed for these systems.

Chapter 5 describes the results of spinning drop experiments. Following the change in volume of a gelatin-concentrated droplet in time, we could investigate the effect of permeability on the dynamics of these water-water interfaces. After a few days to weeks, the droplets decreased in size up to 90%, from which we could conclude that all ingredients in the system diffuse through the interface. We give a description for the change in volume in terms of diffusion of the ingredients. From this description, we deduced three diffusion coefficients, comparable to the self-diffusion coefficients of the biopolymers. These results indicate that the diffusion of the biopolymers determine the rate of the overall diffusion process.

The diffusion of ingredients occurs at long time scales, as described in chapter 5. We have performed droplet relaxation experiments in order to see whether the interfacial permeability also plays a role at short time scales. From the droplet relaxation experiments, described in chapter 6, we found that the interfacial tension alone is not able to describe the relaxation behavior of the droplets, indicating that the permeability apparently does play a role. Accounting for this interfacial permeability in the description for the relaxation time, we give a new description from which the

interfacial tension and the interfacial permeability can be deduced simultaneously. From scaling relations, we find that the interfacial permeability can be related to an effective diffusion coefficient. These coefficients compare to the self-diffusion coefficient of water, indicating that water only diffuses through the interface. Thus, although the time scale in relaxation experiments is much shorter, diffusion of water still plays a role.

Chapter 7 includes a discussion of the relevance of interfacial parameters such as bending rigidity and interfacial permeability for these water-in-water emulsions at different length scales. We discuss the validity of the spinning drop and the droplet relaxation method. Since the interfaces are permeable, the spinning drop method is too inaccurate to measure the exact value for the interfacial tension. However, the droplet relaxation method can be used to measure the interfacial tension as long as the contribution of the permeability is taken into account for the description of the relaxation behavior. We have incorporated the interfacial permeability in the description for coarsening in bicontinuous structures, in a similar way as described previously in chapter 4. From this description we find two different critical length scales that determine which of the interfacial parameters are of importance. We find four different regimes for coarsening depending on whether the process is interfacial tension-, bending rigidity-, or permeability-dominated. For both critical length scales we find that they are of relevance in phase separation, and that they could be of relevance in other phenomena, such as shear-induced phase separation and droplet deformation.

To conclude, we have shown that both bending rigidity and interfacial permeability are of significant importance for demixed biopolymer systems, and need to be included to describe the dynamics of these systems.

Samenvatting

Fasegescheiden proteïne-polysaccharide mengsels worden vaak gebruikt voor de productie van levensmiddelenproducten als spreads, roomijs en toetjes. Deze systemen zijn ook wel bekend als water-in-water emulsies. Hun eigenschappen zijn vergelijkbaar met de eigenschappen van normale olie/water emulsies, waardoor deze watergebaseerde systemen ook wel gebruikt kunnen worden als vervanging voor vetrijke producten. De macroscopische eigenschappen van emulsies worden bepaald door de grootte en de vorm van de gedispergeerde fase. Door de grootte en vorm van deze fase te veranderen kan men de eigenschappen van vetrijke producten imiteren, zoals de romigheid van bijvoorbeeld mayonaise of toetjes. Deze structuren (grootte en vorm) van de gedispergeerde fase kunnen worden gereguleerd met behulp van het fasescheidingsproces en opgelegde stroming. De eigenschappen van het grensvlak tussen de twee fasen spelen een grote rol in de structuurvorming van deze systemen. Over het algemeen wordt er van uitgegaan dat grensvlakspanning de enige eigenschap is die een rol speelt bij deze structuurvorming. Water-water grensvlakken gedragen zich echter anders dan normale olie-water grensvlakken. Het doel van dit promotieonderzoek was daarom om het belang van grensvlakeigenschappen als buigingsrigiditeit en permeabiliteit (doorlaatbaarheid) te onderzoeken en het effect te bepalen van deze eigenschappen op de kinetiek van fasescheiding en het deformatiegedrag van emulsiedruppels in een stromingsveld.

In hoofdstuk 2 bespreken we twee proteïne-polysaccharide systemen; een gelatine/dextraan en een gelatine/arabische gom systeem. Voor beide systemen hebben we de grensvlakspanning bepaald als functie van de afstand tot het kritisch punt. De resultaten laten zien dat de grensvlakspanning voor beide systemen dezelfde ordegrrootte heeft. Dit was te verwachten aangezien de biopolymeren in beide systemen even groot zijn. Ondanks dat de waarden voor deze eigenschap in beide systemen bijna hetzelfde zijn, vinden we uit schalingsrelaties dat het gelatine/dextraan systeem nabij-kritisch gedrag vertoont, terwijl het gelatine/arabische gom systeem niet-kritisch gedrag vertoont. Dit wijst erop dat de grenslaag in het gelatine/arabisch gom systeem vrij dun is (van dezelfde ordegrrootte als de biopolymeren) terwijl de grenslaag in het gelatine/dextraan systeem diffuus is.

Omdat de dikte van de grenslagen gerelateerd is aan de buigingsenergie van dat grensvlak, hebben we ons gericht op de grenslaagdikte en de buigingsrigiditeit in hoofdstuk 3. De bepaling van deze parameters met experimentele methoden is bijna onmogelijk omdat deze grensvlakken erg gevoelig zijn voor kleine veranderingen in temperatuur, druk etc. Daarom presenteren we in hoofdstuk 3 een model dat de grenslaagdikte en de buigingsrigiditeit berekent aan de hand van de grensvlakspanning (uit hoofdstuk 2) en de interactiepotentiaal van de biopolymeren in de grenslaag. Uit de resultaten kunnen we concluderen dat voor het niet-kritische gelatine/arabische gom systeem de grenslaagdikte dezelfde grootte heeft als de biopolymeren. De buigingsrigiditeit van deze systemen is vergelijkbaar met die van normale olie/water emulsies. Voor de nabij-kritische gelatine/dextraan systemen vinden we dat zowel de grenslaagdikte als de bijbehorende buigingsrigiditeit veel groter is dan voor niet-kritische systemen.

In hoofdstuk 4 hebben we deze buigingsrigiditeit meegenomen in de beschrijving van de grensvlakenergie. Dit geeft een krommingafhankelijke grensvlakenergie met een contributie gerelateerd aan rek en een contributie gerelateerd aan buiging. Met deze beschrijving voor de grensvlakenergie leiden we een beschrijving af voor de vergroving van bicontinue structuren tijdens fasescheiding. Aangezien de buigingsenergie niet krommingafhankelijk is en de rekenergie wel, vinden we verschillende regimes voor de vergroavingsnelheid bij verschillende lengteschalen. Voor kleine lengteschaal vinden we dat de domeingrootte schaalt met de tijd als $\Lambda \propto t^{1/3}$, terwijl we voor grote lengteschaal vinden dat de domeingrootte schaalt met tijd als $\Lambda \propto t$. Als we deze theoretische bevindingen vergelijken met experimentele data, zien we dat overgang tussen deze twee regimes inderdaad voorkomt.

In hoofdstuk 5 behandelen we de resultaten van de roterende-druppel experimenten. In deze experimenten volgen we de volumeverandering van een druppel in de tijd, waaruit we het effect kunnen bepalen van de permeabiliteit op de dynamica van water-water grensvlakken. De druppels waren na een aantal dagen tot weken tot ongeveer 90% in volume afgenomen. Hieruit konden we concluderen dat alle ingrediënten in het systeem door het grensvlak kunnen diffunderen. In dit hoofdstuk geven we een beschrijving van de verandering van volume in de tijd in termen van de diffusie van de afzonderlijke ingrediënten. Uit deze beschrijving halen

we drie diffusiecoëfficiënten, die allen vergelijkbaar zijn met de zelfdiffusie coëfficiënten van de biopolymeren. Dit geeft aan dat de diffusie van de biopolymeren de snelheid bepaalt van het totale diffusieproces.

De diffusie van de ingrediënten zoals beschreven in hoofdstuk 5 vindt plaats op lange tijdschaal. Om te zien of grensvlakpermeabiliteit ook een rol speelt op korte tijdschaal hebben we druppel relaxatie metingen uitgevoerd. De resultaten beschreven in hoofdstuk 6 wijzen uit dat grensvlakspanning alleen niet genoeg is om het relaxatiegedrag van de druppels te verklaren en dat blijkbaar de grensvlakpermeabiliteit ook een rol speelt. We nemen deze grensvlakpermeabiliteit mee in een nieuwe beschrijving voor de relaxatietijd, waaruit de grensvlakspanning en de permeabiliteit tegelijkertijd kunnen worden bepaald. Uit schalingsrelaties vinden we dat de permeabiliteit gerelateerd kan worden aan een effectieve diffusiecoëfficiënt. Deze diffusiecoëfficiënt is vergelijkbaar met de zelfdiffusie coëfficiënt van water, wat aangeeft dat alleen water door het grensvlak diffundeert. Dus, ondanks dat de tijdschaal van de relaxatie experimenten veel korter is speelt diffusie nog steeds een rol.

In hoofdstuk 7 geven we een algemene discussie over het belang van grensvlakeigenschappen zoals buigingsrigiditeit en grensvlakpermeabiliteit voor water-in-water emulsies bij verschillende lengteschalen. We bediscussiëren het effect van de grensvlakpermeabiliteit op grensvlakspanningsmetingen en concluderen dat de roterende-druppel methode te onnauwkeurig is om de exacte waarde voor de grensvlakspanning te meten. De druppelrelaxatie methode kan wel worden gebruikt om de grensvlakspanning te meten zolang het effect van de permeabiliteit maar is meegenomen in de beschrijving van het relaxatiegedrag. We hebben de grensvlakpermeabiliteit meegenomen in de beschrijving voor de vergroving voor bicontinue structuren op een manier vergelijkbaar als beschreven in hoofdstuk 4. We vinden twee verschillende kritische lengteschalen die bepalen welke van de grensvlakeigenschappen van belang zijn in de fasescheiding. We vinden vier verschillende regimes voor de vergroving afhankelijk of het proces gedomineerd wordt door grensvlakspanning, buigingsrigiditeit of permeabiliteit. We vinden dat beide kritische lengteschalen relevant zijn tijdens fasescheiding, en dat ze relevant zouden

kunnen zijn voor andere verschijnselen als stromingsgeïnduceerde fasescheiding en druppeldeformatie.

Concluderend kunnen we zeggen dat we hebben laten zien dat zowel buigingsrigiditeit als grensvlakpermeabiliteit van significant belang is voor ontmengde biopolymeersystemen, en dat deze parameters moeten worden meegenomen in de beschrijving voor de dynamica van deze systemen.

Dankwoord

Dankwoord

Aangekomen bij het laatste onderdeel van mijn proefschrift, wat waarschijnlijk het populairste onderdeel is van velen, kan ik natuurlijk niet een lege pagina achterlaten. Ruim vier jaar geleden ben ik begonnen aan dit promotieonderzoek, waar ik altijd met veel plezier aan heb gewerkt. Het was niet altijd even makkelijk; ik heb heel wat keren vloekend door het gebouw gelopen, en vaak de neiging gehad om wat apparatuur het raam uit te gooien. Maar, uiteindelijk komt het allemaal op zijn pootjes terecht en is dit proefschrift het resultaat van vier jaar vooral hard nadenken. Als u de kافت van dit proefschrift bekijkt, lijkt het alsof ik de enige ben die met de eer kan gaan strijken, maar het tot stand komen van een proefschrift gaat niet zonder hulp van anderen. Daarom wil ik van de gelegenheid gebruik maken om verschillende mensen persoonlijk te bedanken. Allereerst natuurlijk mijn promotor Erik. Ik heb jouw enthousiasme in onderzoek en jouw creativiteit altijd erg op prijs gesteld. Steeds als ik even in de bekende AIO-dip zat of even een duwtje in de rug nodig had, kwam ik altijd weer gemotiveerd jouw kamer uit. Ik heb altijd graag met je samengewerkt. Natuurlijk wil ik ook mijn co-promotor Leonard bedanken. Jouw deur stond altijd voor mij open. Als ik wiskundig weer eens in de knoei zat, nam jij altijd de tijd om het weer eens uit te leggen. En om dan je geduld te bewaren bij zo'n koppig iemand als ik, dat kan niet altijd even gemakkelijk geweest zijn. Ik heb veel geleerd van jouw kennis in de fysica, al vond ik het soms lastig mezelf in die abstracte wereld te plaatsten. Ik waardeer het zeer dat jullie mij mijn vrijheid hebben gegeven tijdens dit onderzoek.

Ik wil ook al mijn kamergenootjes van de afgelopen vier jaar bedanken; Henny, Cecile, Suzanne, Hilde en Christopher. Ik heb altijd met erg veel plezier op kamer 306 gewerkt. Er was altijd tijd voor nuttige en zinloze discussies, waardoor het werk er soms een klein beetje bij inschoot. Henny, jou wil ik graag persoonlijk bedanken. Ook al was je geen officiële begeleider van mij, ik heb het erg op prijs gesteld dat je altijd voor me klaar stond als ik weer eens hulp nodig had met wat dan ook. Ik hoefde me maar om te draaien en help te roepen en jij had altijd tijd. Dank je! Suus, na ruim drie jaar tegenover elkaar gezeten te hebben, vind ik het erg leuk dat je mijn paranimf wilt zijn. Natuurlijk wil ik ook graag alle andere mensen van Food Physics bedanken voor de leuke sfeer in de groep en voor de vele borrels, labuitjes, kerstuitjes, AIO-etentjes, het AIO-reisje en andere evenementen.

Ook wil ik graag de mensen van PDQ bedanken voor de goede sfeer in de koffiepauzes en tijdens de lunches. Ik vond de gezamenlijke PDQ-FPH etentjes erg leuk, vooral als daar het spelletje Jenga in voor kwam. Ik wil ook graag de enige twee studenten bedanken die ik heb gehad; Jendo en Joris. Ik heb jullie inzet erg gewaardeerd en mede daardoor zijn hoofdstuk 2 en hoofdstuk 6 geworden wat ze zijn. Ik heb met veel plezier met jullie samengewerkt en vind het erg leuk dat jullie beide AIO zijn geworden.

Er zijn natuurlijk ook nog anderen geweest die op een of andere manier hebben bijgedragen aan mijn proefschrift. De mensen van de werkplaats, die altijd weer iets konden fabriceren als mijn apparaat weer niet deed wat ik wilde. Boudewijn van Veen voor alle microscoop en software problemen en de mensen van het fasescheidingsclubje voor interessante wetenschappelijke discussies.

Natuurlijk zat ik niet 24 uur per dag in het Biotechnion, en kon ik 's avonds na een dag (hard) werken weer even bijkomen op afdeling 8b (nee, dit is geen psychiatrische afdeling, al had het daar soms wel wat van weg, maar het nummer van ons studentenhuys). Ik wil graag al mijn huisgenoten bedanken voor de leuke tijd die ik op 8b in deze vier jaar heb gehad. Ik heb altijd erg genoten van onze uitgaansavonden, de uitstapjes en de vakanties.

En als laatste wil ik graag mijn familie bedanken voor de interesse die ze altijd hebben getoond. Guido, broertje, ook al zie ik je tegenwoordig niet zo heel erg veel, ik vind het fijn dat jij mijn paranimf wilt zijn. Pap, mam, bedankt dat jullie mij altijd de vrijheid hebben gegeven in de keuzes die ik heb gemaakt en dat jullie altijd achter mij stonden. En natuurlijk wil ik als laatste ook graag mezelf bedanken, want zonder mij was dit proefschrift er natuurlijk nooit geweest.

Bedankt!!

Elke

List of publications

Elke Scholten, Remco Tuinier, R. Hans Tromp, and Henk N.W. Lekkerkerker, *Interfacial tension of a decomposed biopolymer mixture*, Langmuir **2002**, *18*, 2234-2238.

Elke Scholten, Jendo E. Visser, Leonard M.C. Sagis, and Erik van der Linden, *Ultralow interfacial tensions in an aqueous phase-separated gelatin/dextran and gelatin/gum arabic system: A comparison*, Langmuir **2004**, *20*, 2292-2297. (chapter 2)

Elke Scholten, Leonard M.C. Sagis, and Erik van der Linden, *Bending rigidity of interfaces in aqueous phase-separated biopolymer mixtures*, J. Phys. Chem. B **2004**, *108*, 12164-12169. (chapter 3)

Elke Scholten, Leonard M.C. Sagis, and Erik van der Linden, *Coarsening rates of bicontinuous structures in polymer mixtures*, Macromolecules **2005**, *38*, 3515-3518. (chapter 4)

Elke Scholten, Joris Sprakel, Leonard M.C. Sagis, and Erik van der Linden, *Effect of interfacial permeability on droplet relaxation in biopolymer-based water-in-water emulsions*, Biomacromolecules **2006**, in press. (chapter 6)

Elke Scholten, Leonard M.C. Sagis, and Erik van der Linden, *Effect of permeability on aqueous biopolymer interfaces in spinning drop experiments*, submitted to Biomacromolecules. (chapter 5)

Elke Scholten, Leonard M.C. Sagis, and Erik van der Linden,
*Effect of bending rigidity and interfacial permeability on the
dynamical behavior of water-in-water emulsions*, submitted to
J. Phys. Chem. B. (chapter 7)

Elke Scholten, Leonard M.C. Sagis, and Erik van der Linden,
*Effect of interfacial permeability and bending rigidity on the
dynamics of immiscible biopolymer systems*, Proceedings of the 4th
International Symposium on Food Rheology and Structure **2006**,
Zurich, Switzerland.

Curriculum Vitae

Elke Scholten werd geboren op 17 mei 1976 te Breda. Na het behalen van haar Havo-diploma aan het Riethill college in Raamsdonksveer in 1993, begon zij aan de HLO te Etten-Leur, met een specialisatie in organische chemie. Haar stage heeft zij uitgevoerd op de Universiteit van New England in Armidale, Australië, en vervolgens heeft zij een afstudeeropdracht gedaan aan de Universiteit van West Australië in Perth. Zij behaalde in 1997 haar diploma. Vervolgens is zij in 1998 begonnen aan de studie Scheikunde aan de Universiteit van Utrecht. Haar afstudeeropdracht werd uitgevoerd op het van 't Hoff laboratorium voor Fysische en Colloidchemie. Haar studie werd afgerond in 2001. Vanaf september 2001 was zij in dienst van Wageningen Universiteit bij de leerstoelgroep Fysica en Fysische Chemie van Levensmiddelen, waar zij gedurende vier jaar dit promotieonderzoek heeft uitgevoerd. De resultaten van dit onderzoek zijn verbonden in dit proefschrift. In oktober 2004 kreeg zij een Storm van der Chijs stipendium voor haar promotieonderzoek. Dit stipendium heeft zij besteed aan een bezoek aan de groep van G. Whitesides aan de Universiteit van Harvard, Cambridge, USA en aan een bezoek aan de groep van T.A. Hatton, MIT (Massachusetts Institute of Technology), Cambridge, USA. Aan de hand van dit bezoek is een voostel geschreven voor een post-doc positie op MIT die is ingediend bij NWO voor een TALENT-beurs.

Educational activities

Discipline specific activities

- Autumn meeting on macroscopic chemistry, Schiermonnikoog, The Netherlands
- Han sur Lesse Winterschool, Belgium
- NWO meeting Liquids and Interfaces, Lunteren, The Netherlands
- Conference: Food Colloids, Wageningen, The Netherlands
- PhD trip, England
- NWO talentendagen, Zeist, The Netherlands
- Bio-Nanotechnology symposium, Wageningen, The Netherlands
- Conference: Faraday discussions 129, Cambridge, England
- Membrane emulsification symposium, Wageningen, The Netherlands
- Conference: Julich Soft Matter days, Kerkrade, The Netherlands
- Workshop Macro-ion Complexation, Wageningen, The Netherlands
- Conference: Liquid Matter 2005, Utrecht, The Netherlands
- Student conference, Biezenmortel, The Netherlands
- ECIS Conference, Geilo, Norway
- ISFRS conference on Food Rheology and Structure, Zurich, Switzerland

General courses

- Basiscursus didactiek
- Afstudeervak begeleiden
- Gespreksvaardigheden
- Interactie in communicatie
- Scientific writing
- Project planning and time management

The research described in this thesis was carried out at Wageningen University, The Netherlands. This research was part of the research program of the graduate school VLAG (Food Technology, Agro biotechnology, Nutrition & Health Sciences).

Cover: Picture of a product called Orbitz, a drink based on a water-in-water emulsion